FACULDADE DE ENGENHARIA DA UNIVERSIDADE DO PORTO

Evaluating the mechanical properties of biological soft tissues using inverse methods: application to the pelvic floor muscles

Maria Elisabete Teixeira da Silva

A thesis submitted in conformity with the requirements for the

Doctoral Degree in Biomedical Engineering

Supervisor: Prof. Dr. Marco Paulo Lages Parente

Co-supervisor: Prof. Dra. Maria Teresa da Quinta e Costa Mascarenhas Saraiva

November 2017

There are many hypotheses in science which are wrong. That's perfectly all right; they're the aperture to finding out what's right.

Carl Sagan (1934-1996)

Agradecimentos (Acknowledgements)

No decurso desta etapa felizmente pude contar com a ajuda de várias pessoas. Antes de tudo, gostaria de agradecer ao Prof. Marco Parente e ao Prof. Renato Natal Jorge, pelo o apoio contínuo, ideias, paciência, motivação e por acreditarem mais do que eu. Sem eles a minha tese não teria sido realizada. A minha profunda gratidão também se estende à Prof. Teresa Mascarenhas.

Agradeço o apoio financeiro proporcionado pela Fundação para a Ciência e a Tecnologia, através da Bolsa de Doutoramento SFRH/BD/89519/2012, bem como ao IDMEC/FEUP e depois ao INEGI, especialmente ao departamento da UCVE.

Agradeço a todos os meus colegas e amigos do INEGI/FEUP, particularmente à Carla, Daniel, Dulce, Joana, Júlia, Marcelo, Nilza, Paulo, Rita e Sofia, com quem partilhei bons momentos.

As minhas palavras de apreço à minha família, pelo apoio que me deu durante o tempo em que realizei este trabalho e estive ausente, pela paciência e pelo tempo de espera. Em especial à minha irmã, Raquel, e ao Saulo pelo incentivo.

Abstract

The female pelvic region comprises one of the most complex regions of the human anatomy, normally associated with different dysfunctions, such as urinary incontinence and pelvic organ prolapse. These dysfunctions are related to the weakness or direct injuries of the pelvic floor muscles associated with different risk factors - hormonal changes, vaginal delivery, aging, among others. In this sense, the mechanical characteristics are relevant to understand these dysfunctions and how they are related with changes in the biomechanical behaviour of these tissues. The pelvic tissues have been studied through different methods: from tensile tests using tissues from female cadavers or tissues collected at the time of a transvaginal hysterectomy procedure and imaging techniques such as ultrasound or magnetic resonance imaging. However, this region remains understudied from a biomechanical perspective, mainly the mechanical properties of the soft tissues involved in the female pelvic cavity.

In this thesis, an inverse finite element analysis, completely non-invasive, was implemented to estimate the passive and active *in vivo* biomechanical properties of the pelvic floor muscles in order to achieve passive and active biomechanical behaviour during the Valsalva manoeuvre and muscle contraction, respectively. The numerical models of the pelvic floor muscles and their surrounding structures (coccyx, obturator muscles and *symphysis pubis*) were built from magnetic resonance axial images acquired at rest. The surrounding structures are essential to accurately reproduce the female pelvic anatomy. Different groups of women, without pathology, with stress urinary incontinence and pelvic organ prolapse were recruited.

To achieve the passive behaviour of the pelvic floor muscles without pathology the Mooney-Rivlin constitutive model was applied. Additionally, the material constants of this model were estimated and displacements of the numerical model were compared with that of the magnetic resonance images. The difference in displacement was of 0.15 mm in the antero-posterior direction and 3.69 mm in the supero-inferior direction, equating to a percentage error of 7.0% and 16.9%, respectively.

The Neo-Hookean, Mooney-Rivlin and Yeoh hyperelastic constitutive models were applied to the *pubovisceralis* muscle of healthy, incontinent and prolapsed women. The

material constants were significantly higher for the asymptomatic women than for the women with stress urinary incontinence. The variation of the c_1 for asymptomatic *vs.* incontinent group was approximately 38.46% for the Neo-Hookean constitutive model, 38.46% for the Mooney-Rivlin constitutive model, and 48.39% for the Yeoh constitutive model. Hence, these results showed that the *puboviscerali*s muscle of incontinent women have a lower elasticity than asymptomatic women. Women with pelvic organ prolapse presented material constants higher than asymptomatic women, meaning that women with prolapse presented a higher stiffness.

In order to simulate the realistic behaviour of the *puboviscerali*s muscle, a quasi-incompressible transversely isotropic hyperelastic constitutive model was used. The passive and active material parameters of this model were estimated and were higher for the women with pelvic organ prolapse, meaning a higher stiffness than in asymptomatic and incontinent women. Additionally, the influence of these parameters was analysed by evaluating their stress-strain and force-displacements response. The force produced by the *puboviscerali*s muscle in women with pelvic organ prolapse was 47% and 82% higher when compared to women without pathology and with stress urinary incontinence, respectively.

The inverse finite element analysis seems to be a useful tool to estimate the *in vivo* biomechanical properties of the pelvic floor muscles for different conditions and shows promising results for subject-specific analyses.

Resumo

A região pélvica feminina compreende uma das regiões mais complexas da anatomia humana, normalmente, associada a diferentes disfunções, como incontinência urinária e prolapso dos órgãos pélvicos. Estas disfunções estão relacionadas com fraqueza ou lesões diretas dos músculos do pavimento pélvico associadas a diferentes fatores de risco - alterações hormonais, parto vaginal, envelhecimento, entre outros. Neste sentido, as características mecânicas são relevantes para entender estas disfunções, e como estão relacionadas com mudanças no comportamento biomecânico desses tecidos. Os tecidos pélvicos foram estudados através de diferentes métodos: desde ensaios de tração utilizando tecidos de cadáveres femininos ou tecidos recolhidos no momento do procedimento de histerectomia transvaginal, e técnicas de imagem como ultrassom ou imagens de ressonância magnética. No entanto, esta região permanece sub-estudada sob uma perspetiva biomecânica, principalmente as propriedades mecânicas dos tecidos moles envolvidos na cavidade pélvica feminina.

Nesta tese, uma análise inversa de elementos finitos, completamente não-invasiva, foi implementada para estimar as propriedades biomecânicas passivas e ativas *in vivo* dos músculos do pavimento pélvico, com o intuito de alcançar comportamento biomecânico passivo e ativo durante a manobra de Valsalva e contração muscular, respetivamente. Os modelos numéricos dos músculos do pavimento pélvico e as suas estruturas circundantes (cóccix, músculos obturadores e sínfise púbica) foram construídos a partir de imagens axiais de ressonância magnética adquiridas em repouso. As estruturas circundantes são essenciais para reproduzir com precisão a anatomia pélvica feminina. Diferentes grupos de mulheres, sem patologia, com incontinência urinária de esforço e prolapso de órgãos pélvicos, foram recrutados.

Para alcançar o comportamento passivo dos músculos do pavimento pélvico sem patologia, o modelo constitutivo Mooney-Rivlin foi aplicado. Adicionalmente, as constantes de material deste modelo foram estimadas e os deslocamentos do modelo numérico foram comparados com os das imagens de ressonância magnética. A diferença de deslocamento foi de 0.15 mm na direção antero-posterior e 3.69 mm na direção supero-inferior, correspondendo a uma percentagem de erro de 7.0% e 16.9%, respetivamente.

Os modelos constitutivos hiperelásticos Neo-Hookean, Mooney-Rivlin e Yeoh foram aplicados ao músculo pubovisceral de mulheres assintomáticas, incontinentes e com prolapso. As constantes de material foram significativamente maiores para as mulheres assintomáticas do que para as mulheres com incontinência urinária de esforço. A variação do c_1 para o grupo assintomático *vs.* incontinente foi de aproximadamente 38.46% para o Neo-Hookean, 38.46% para o Mooney-Rivlin e 48.39% para o Yeoh. Assim, estes resultados mostraram que o músculo pubovisceral de mulheres incontinentes tem uma elasticidade inferior ao das mulheres assintomáticas. As mulheres com prolapso dos órgãos pélvicos apresentaram constantes materiais superiores às das mulheres assintomáticas, significando que as mulheres com prolapso apresentaram maior rigidez.

Com o intuito de simular o comportamento realista do músculo pubovisceral, um modelo constitutivo hiperelástico tranversalmente isotrópico quase-incompressível foi usado. Os parâmetros passivos e ativos deste modelo foram estimados e foram maiores para as mulheres com prolapso dos órgãos pélvicos, significando maior rigidez do que em mulheres assintomáticas e incontinentes. Adicionalmente, a influência destes parâmetros foi analisada através da avaliação da resposta tensão-deformação e força-deslocamento. A força produzida pelo músculo pubovisceral nas mulheres com prolapso dos órgãos pélvicos foi de 47% e 82% maior quando comparada à das mulheres sem patologia e com incontinência urinária de esforço, respetivamente.

A análise inversa de elementos finitos parece ser uma ferramenta útil para estimar as propriedades biomecânicas *in vivo* dos músculos do pavimento pélvico para diferentes condições e mostra resultados promissores para análise de um sujeito específico.

Contents

List of Figures

Part A:

Part B: Article 1:

Part B: Article 2:

Part B: Article 3:

Part B: Article 4:

Appendix

Part B: Article 5:

List of Tables

Part B - Article 1:

Part B - Article 2:

Part B - Article 3:

Part B - Article 4:

Part B - Article 5:

List of Abbreviations

AI - anal incontinence.

BMI - body-mass index.

FEA - finite element analysis.

FEM - finite element method.

FI - fecal incontinence.

GA - genetic algorithm.

IAP - intra-abdominal pressure.

LA - *levator ani*.

MRI - magnetic resonance imaging

PFM- pelvic floor muscles.

PFD - pelvic floor dysfunction.

POP - pelvic organ prolapse.

PVM - *puboviscerali*s muscle.

SP - *symphysis pubis.*

SUI - stress urinary incontinence.

UI - Urinary incontinence.

US - ultrasonograp

Part A

Thesis Report

1. Motivation and Introduction

The female pelvic floor is a soft tissue support structure associated with different disorders. These affect the quality of life of many women and can be related with changes in the biomechanical properties of muscles, ligaments and fascia (Abramowitch et al., 2009). The impairment of the pelvic floor muscles (PFM) is a major ingredient to develop urinary incontinence (IU) and/or pelvic organ prolapse (POP) (Schwertner-Tiepelmann et al., 2012). Some of the female pelvic floor dysfunctions (PFD) have been previously studied by different authors, who related them to the weakness or direct injury to the PFM and the pudendal nerve, often occurring during vaginal delivery (Brandão et al., 2013; Dietz et al., 2005). In this sense, the biomechanical analysis of pelvic floor tissues is important to understand different PFD and to be able to improve clinical outcome by better understanding the effect of the decreased elasticity of the tissues, which often causes inability to maintain the normal position of the pelvic organs and *levator hiatus* closure. These disorders may result from changes in the biomechanical properties of the supportive structures that occur from weakness or impairment of muscles or ligaments, or alterations in the stiffness of the pelvic fascia associated with the risk factors - age, hormonal changes, among others (Abramowitch et al., 2009).

Previous experimental *in vitro* studies have been addressed to evaluate biomechanical properties of the pelvic ligaments, vaginal tissue and *levator ani* (LA) muscle (Cosson et al., 2004, 2003a; Lei et al., 2007; Martins, 2010; Rubod et al., 2008).

To obtain these biomechanical properties, acquired tissue during surgery or from female cadaver has been tested using different techniques: uniaxial (Martins, 2010) and biaxial (equibiaxial) tensile tests (Janda, 2006). However, these collected tissues are frequently afflicted in clinical environment, and consequently, the comparison to *in vivo* healthy tissues is difficult (Baah-Dwomoh et al., 2016). Hence, these tensile tests show the nonlinear mechanical behaviour, but they do not reflect the natural conditions for *in vivo* muscle behaviour in the pelvis. In this context, the computational analysis coupled with *in vivo* biomechanical properties may help to correctly reproduce the mechanical behaviour of the PFM.

The female pelvic floor is a soft tissue support structure that includes fascia, ligaments and muscles of the *urogenital* and *anal* regions that extends from the *symphysis pubis* (SP) to the coccyx, and comprises the *levator hiatus* (Sindhwani et al., 2016) for the passage of three orifices - the urethra, vagina and rectum (see Fig.1) (Schwertner-Tiepelmann et al., 2012).

The pelvic cavity is divided in different compartments - the anterior, middle and posterior - to accommodate the pelvic structures (urethra, vagina and rectum, respectively) (see Fig. 2) (Widmaier et al., 2008).

The contraction and relaxation ensure the functional integrity of the pelvic floor, which is responsible for the support the pelvic organs (Elneil, 2009). The passive support of the pelvic floor is unleashed by the endopelvic fascia and pelvic ligaments and the active support is ensured by the muscular contraction of the PFM (Ashton-Miller and DeLancey, 2007; Herschorn, 2004).

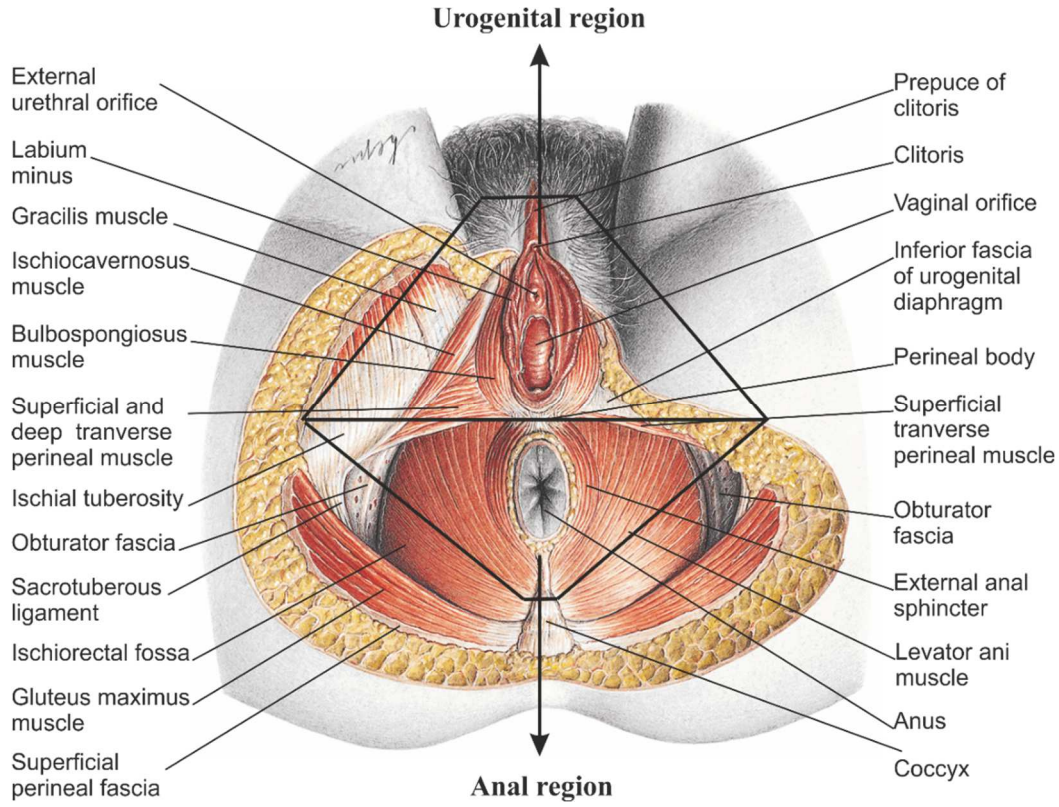

Figure 1. The *urogenital* and *anal* regions, and external female genital organs, viewed from below (adapted from (Sobotta et al., 2001)).

The pelvic floor muscles include the LAM - *iliococcygeus, pubococcygeus,* and *puborectalis* muscles - and the *coccygeus* muscle. The *pubococcygeus,* and *puborectalis* muscles are often called collectively the *pubovisceralis* muscles (PVM), forming a U-shape and they originate from the inner surface of the pubic bone on either side of the midline (Herschorn, 2004).

The *puborectalis* muscle is considered the main constrictor of the PFM and it is central contributor to the active contractile forces (Verelst and Leivseth, 2007). PFM relaxation induces the return of the pelvic organs to its anatomical position, therefore, favouring normal micturition and rectal evacuating (Raizada and Mittal, 2008; Sapsford

and Hodges, 2001). During pelvic floor contraction the anterior movement of the anorectal junction occurs to close the *levator hiatus* (F. S. Brandão et al., 2015; Sapsford and Hodges, 2001). The contraction is important in preventing the involuntary loss of urine and/or rectal contents. The difficulty in maintaining organ support and *levator hiatus* closure may result from muscle disorders along with laxity of the endopelvic fascia and/or impairment in the ligaments or nerves (Hoyte et al., 2001). Furthermore, the ability of the muscle to sustain contractile activity depends on the type of muscle fiber: slow-twitch (type I) or fast-twitch (type II). Type I fibers contract slowly and type II, normally perform powerful contractions, exerting 20% more force than type I (Marques et al., 2010).

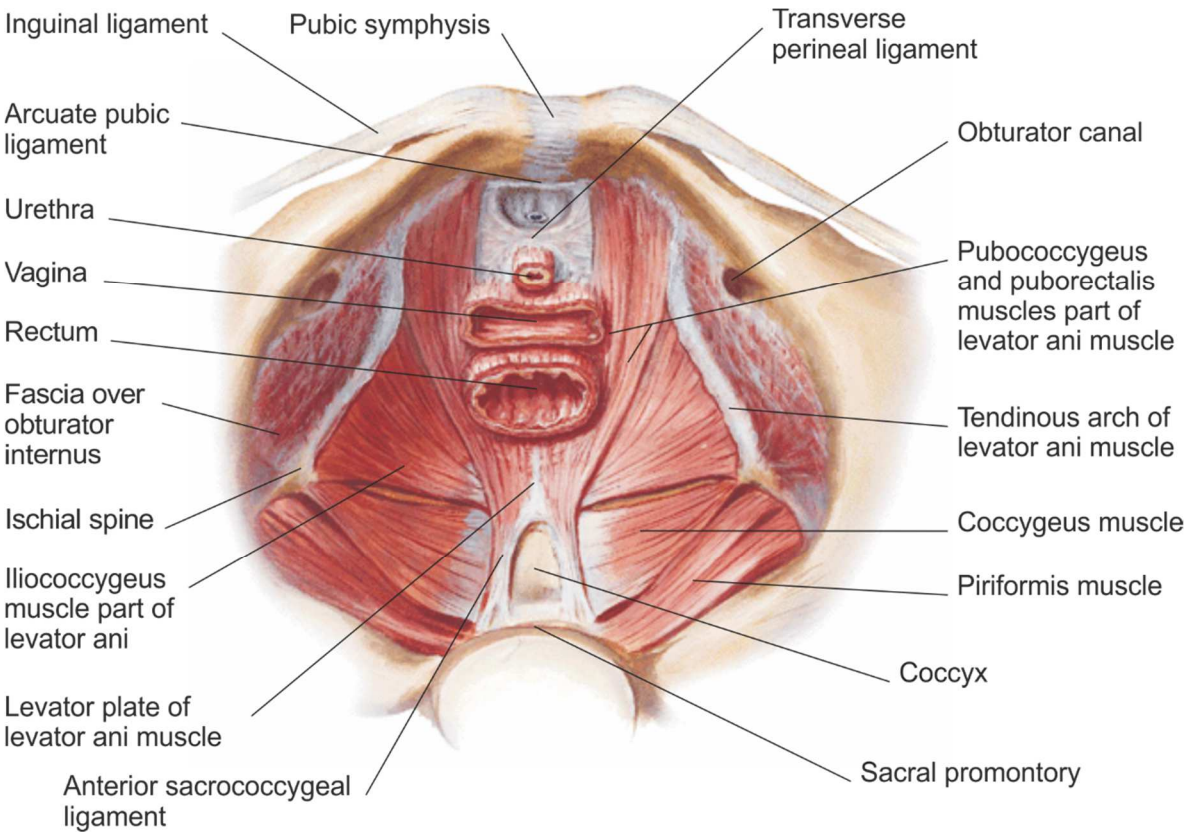

Figure 2. Superior view of the female pelvic floor diaphragm (adapted from (Netter, 2014)).

PFD result in functional disorders (1) in the bladder, causing UI, and voiding dysfunction; (2) in the rectum which can cause fecal (FI) and anal incontinence (AI); (3) of the vagina and/or uterus leading to sexual dysfunctions, POP - the descent of one or more pelvic structures from the normal anatomical location toward or through the *levator hiatus* opening (Elneil, 2009). The origin of these disorders may be the impairment of the muscles or connective tissue of the ligaments and fascia, or changes in their biomechanical properties (Abramowitch et al., 2009).

In the case of the stress urinary incontinence (SUI), the involuntary urine leakage associated with the increase in intra-abdominal pressure (IAP) is often associated with insufficient ligamentous support of the urethra, or weakness of the PFM, that can be associated with decreased total collagen and elastin (Chen and Yeh, 2011). Previous studies showed that women with SUI present a significant reduction of type III collagen, which is not due to a decreased production of collagen but rather due to increased degradation of nascent collagen (Patel et al., 2007). Also, (Rechberger et al., 1998), showed that the weakening of the collagen framework of the *pubovisceralis* fascia affects women of all ages.

POP has been previously associated with muscle defects, but there is also evidence that women with thinner muscles may be more prone to organ descent (DeLancey et al., 2007). Histological studies showed that the thinner muscles in women with prolapse can cause a histological response: decreasing the total collagen content and increasing the concentration of collagen type III (Kerkhof et al., 2009). An increase in collagen type III in combination with an increase in active matrix metalloproteinases (MMP-9) is typical of prolapsed muscles that are actively remodelling to accommodate a progressively increasing mechanical load (Kerkhof et al., 2009; Martins et al., 2013a). Moreover, PFD

affect muscle fiber length and contractile forces, and distensile and stiff muscle fibers have decreased ability to generate power (Marques et al., 2010). In women with POP, the PFM showed an increase in 21% and 61% in the diameters of type I and type II fibers (Beersiek et al., 1979), in women with SUI an increased number of fibers was verified, but significantly narrower than that of the women without pathology (Zhu et al., 2005).

Normally, the PFD are related to the weakness or direct injuries of the PFM associated with different risk factors (Nagle et al., 2014). The most common risk factors responsible for these changes are predisposing factors (genetic predisposition), promoting factors (age and menopause) and other aggravating factors (obesity - increased body-mass index (BMI)) (Abramowitch et al., 2009; Rahn et al., 2008; Schwertner-Tiepelmann et al., 2012). In this sense, the number of the adult women with PFD will increase because the average life expectancy continues to increase. In the United States 24% of women are affected by one of these PFD, with 16% present UI, 3% present POP and 9% of women present FI (Memon and Handa, 2013). The number of women with PFD is estimated to increase from 28.1 million in 2010 to 43.8 million in 2050 (Memon and Handa, 2013; Nygaard et al., 2008). Moreover, 11% of the women will need correction surgery for dysfunction at least once in their lifetime (Luo et al., 2014; Memon and Handa, 2013; Moalli et al., 2003) with a re-operation rate of 30%, reducing the time interval between repeated procedures (Olsen et al., 1997; Segal et al., 2012). Consequently, it is estimated that from 2010 to 2050, the total number of women undergoing surgery for SUI and POP will increase by 47.2% and 48.2%, respectively (Kiyosaki et al., 2012; Wu et al., 2011). The PFD considerably impair the quality of life for many women and imply high costs, and they represent a major public health problem due to their high prevalence (Kiyosaki

et al., 2012; Wu et al., 2011).

Although different medical specialties (for example, gynaecology, obstetrics, physical therapy, radiology and urology) are involved in the study of complex functional connections of all the pelvic structures on the basis of the disorders pathophysiology, it was still not enough to optimize the best management of PFD. To provide correct treatment of the different dysfunctions, it will be essential to understand the function and anatomy of the PFM and supporting structures - pelvic ligaments and fascia (Herschorn, 2004). Thus, the imaging techniques, such as ultrasonography (US), the static and dynamic magnetic resonance imaging (MRI) allow to visualize the pelvic floor anatomy and function due to good soft tissue contrast and spatial resolution (Herschorn, 2004; Peng et al., 2007, 2015a; Singh et al., 2001), nonetheless, the complete muscle structure, connective tissue and muscle fibers are not fully visible through resonance conventional MRI resolution (Brandao et al., 2013; Law and Fielding, 2008).

Using these techniques, it is possible to follow changes in the PFM during contraction, Valsalva manoeuvre or defecation (Herschorn, 2004). The *levator hiatus* becomes smaller during muscle contraction and larger during Valsalva manoeuvre (the changes are predominantly related to the *puborectalis* muscle) (Herschorn, 2004; Tumbarello et al., 2010; Van Delft et al., 2015). In addition, US and MR images help to exhibit the (lack of) support to the pelvic organs and the widening of the *levator hiatus* due to muscle defects or impairment in the connective tissues (Dietz, 2004; Tunn et al., 2006), and still allow to explore the stiffness of the PFM to compare continent and stress urinary incontinence women (Dietz, 2004; Dietz et al., 2008; Siegel et al., 2015; Tunn et

al., 1998) and to determine the degree of POP (Boyadzhyan et al., 2008). The sagittal dynamic MR images performed during Valsalva manoeuvre and coughing can help in the evaluation of the effect of the increase in the IAP over the female pelvic floor, and the counteracting (in)voluntary action of the muscles to suspend the organs (Moerman et al., 2012; Peng et al., 2007; Yang et al., 2009).

Furthermore, in these images the HMO grading system can be applied to help standardizing both interpretation and grading of PFD and to elucidate about pelvic floor relaxation by dividing it into two components - hiatal enlargement (by means of the H-line or puborectal *hiatus* line) and pelvic floor descent (by measuring the M-line, which extends perpendicularly from the pubococcygeal line (PCL) to the posterior end of the H-line). Hence, the POP can be measured through the H-line, using the "O" component of the HMO system, that corresponds to the distance between the H-line and most caudal aspect of a given organ during Valsalva manoeuvre (Boyadzhyan et al., 2008).

The LA muscle provides support to organ systems. Its weakness results in impaired function of the structures that these muscles support. In this sense, the study of the mechanical behaviour of these muscles is important to understand their structure and function. (Janda et al., 2003) began by studying, due to problem of poor visualization of muscle fibers and connective tissue in MR images, the morphological parameters of the PFM of a female cadaver, measuring the length and direction of muscle fibers and cross-sectional area of the sarcomere. Previous experimental tensile tests conducted with the vaginal tissues from women with and without POP, using tissues collected at the time of transvaginal hysterectomy and of fresh female cadavers without prolapse (Jean-Charles

et al., 2010; Lei et al., 2007; Rubod et al., 2008), evidenced that the tissues from women with POP presented increased stiffness. Accordingly, mechanical testing provides important information about physical behaviour of a specific soft tissue (Barber et al., 2002), and these *ex vivo* analyses are important to determining the biomechanical properties (Martins, 2010).

In recent years, with the development of computer technologies, computer modelling tools have emerged, which deal with the application of mathematical models to analyse, understand and study the phenomenology of complex problems, and it has become an essential instrument in the scientific environment due to its wide range of application fields - including medicine. Nonetheless, the modelling of soft biological tissues has been facilitated due to substantial progresses in the fields of constitutive modelling and the finite element method (FEM). The combination - FEM coupled with constitutive modelling - has been used by different authors to study the biomechanics of the PFM, during vaginal delivery (Hoyte et al., 2008; Li et al., 2008; Parente et al., 2010, 2008), Valsalva manoeuvre (Noakes et al., 2008) and voluntary muscle contraction (Saleme et al., 2011).

More recently, several computational models based on the FEM have been developed in studies of female PFD, such as POP (Chen et al., 2015; Luo et al., 2015), vaginal delivery with the modelling of tissue damage process (Oliveira et al., 2016) and ligament impairment (S. Brandão et al., 2015). Furthermore, (Yip et al., 2014) and (S. Brandão et al., 2015) also showed that the effect of structural degradation of the support structures such as the ligaments and fascia is a major ingredient to develop SUI, the involuntary urinary leakage associated with the increase in IAP and the development of cystocele. In addition, (Delancey et al., 2007) stated that SUI is also associated with

weakness of the *levator ani* complex and decreased strength of the urethral sphincter, not always in the presence of direct injury to the PFM. These computational models allowed simulating the biomechanical behaviour, however, they use *in vitro* biomechanical properties obtained from experimental studies with both normal and pathological specimens (Martins et al., 2013b; Rivaux et al., 2013).

Nowadays, computer modelling has proven to be a useful tool due to its ability to correctly simulate various impairment conditions while keeping these comparisons based on a given specific-subject (Peng et al., 2015b; Zhang et al., 2009). Hence, this thesis intends to add some developments and implementation of an inverse finite element analysis (FEA) method, to estimate the most suited *in vivo* biomechanical properties for different conditions - without pathology, with SUI and with POP - in a non-invasive way, using MR images.

2. Objectives

This thesis aims to contribute for a better knowledge related with the biomechanics of the PFM and their associated dysfunctions, developing computational models in order to estimate the *in vivo* biomechanical properties, by using non-invasive input information. To achieve a deeper characterisation of the PFM in terms of biomechanical properties, the objectives defined in this thesis were:

(1) To implement an inverse FEA using the Powell's algorithm, to establish the passive biomechanical properties of the PFM of a woman without pathology, using MRI,

by evaluating the magnitude displacement and the principal logarithmic strain. Additionally, to validate this methodology, the computer simulation of muscle displacement *vs.* dynamic MRI was compared.

(2) To use an inverse FEA to obtain the biomechanical properties of the PVM of continent *vs.* incontinent women, comparing the displacement of the PVM in the numerical simulation *vs.* MRI, as represented by the posterior and inferior movement.

(3) To verify the influence of the POP on the passive biomechanical properties of the PVM, and to compare the stress-stretch mechanical response, the material constants obtained were compared with experimental data from non-prolapsed cadaveric LA muscle.

(4) To estimate the passive and active material parameters of the PVM of three groups of women (without pathology, with SUI and with POP), during Valsalva manoeuvre and muscle active contraction, respectively, using a quasi-incompressible transversely isotropic hyperelastic constitutive model and the inverse FEA.

(5) To develop an optimization scheme, involving a Genetic algorithm (GA) and FEM, in order to estimate the material properties of the PVM of a group of asymptomatic women, in order to reduce the number of simulations when compared to the Powell's algorithm.

3. Thesis Organization

This thesis consists of two main parts. Part A serves as a report and contains five main sub-sections. In these sub-sections, the issues related to the PFD associated with risk factors are introduced. Sub-section 1 deals with the importance of computational models in the study of the biomechanical behaviour of PFM without pathology, with SUI and with POP. The objectives of this thesis are catalogued in sub-section 2 and the developed works are concisely presented (sub-section 4). Lastly, the main contributions achieved during the thesis are summarized in sub-section 5 and the final conclusions and future works are presented in the sub-section 6. Part B is composed of the articles written during the study of the biomechanical properties of the pelvic floor muscles, depicting in greater detail the achievements accomplished. The sequence of articles is organized as follows:

Article 1:

Title: Establishing the Biomechanical Properties of the Pelvic Soft Tissues through an inverse Finite Element Analysis using Magnetic Resonance Imaging

Authors: Elisabete Silva, Sofia Brandão, Marco Parente, Teresa Mascarenhas, Renato Natal Jorge

Published in: Proceedings of the Institution of Mechanical Engineers, Part H: Journal of Engineering in Medicine, 230(4):298-309, 2016.

Article 2:

Title: Biomechanical properties of the pelvic floor muscles of continent and incontinent women using an inverse finite element analysis

Authors: Elisabete Silva, Sofia Brandão, Marco Parente, Teresa Mascarenhas, Renato Natal Jorge

Published in: Computer Methods in Biomechanics and biomedical Engineering Journal, 20(8):842-852, 2017.

Article 3:

Title: The influence of pelvic organ prolapse on the passive biomechanical properties of pelvic floor muscles

Authors: Elisabete Silva, Sofia Brandão, Marco Parente, Teresa Mascarenhas, Renato Natal Jorge

Published in: Journal of Mechanics in Medicine and Biology, 17(5):1750090-1750109, 2017.

Article 4:

Title: Characterisation of the Passive and Active Material Parameters of the *Puboviscerali*s Muscle using an Inverse Numerical Method

Authors: Elisabete Silva, Marco Parente, Sofia Brandão, Teresa Mascarenhas, Renato Natal Jorge

Submitted to Journal of Biomechanics (under review), December 2016.

Article 5:

Title: Characterising the Biomechanical Properties of the *Pubovisceralis* muscle using a Genetic Algorithm and Finite Element Method

Authors: Elisabete Silva, Marco Parente, Sofia Brandão, Teresa Mascarenhas, Renato Natal Jorge

Submitted to Journal of Inverse Problems in Science and Engineering (under review), December 2016.

In the appendix are statements from all the authors authorizing its inclusion in this thesis.

4. Brief description of the developed work

This thesis was dedicated to study the biomechanical properties of the PFM, using the FEM coupled with optimization algorithms in order to understand the PFD and contribute, in the future, in the optimization of the implants meshes so as to reduce failure rates of surgical procedures. Hence, the developed work can be divided into three parts.

The first part is related to the implementation of an inverse FEA, involving the FEM and the Powell's algorithm, to establish the biomechanical properties of the PVM in order to simulate the biomechanical of the PFM behaviour during the Valsalva manoeuvre. By applying this methodology, it was possible to reproduce the passive behaviour of the PFM of different groups - women without pathology, with SUI and POP

- and subsequently, the displacements obtained for the *levator hiatus* were compared with the ones from MRI. A second part is associated with the transversely isotropic hyperelastic material model applied to the PVM, which is essential to understand the passive and active biomechanical behaviour of these muscles. Using an inverse FEA it was possible to determine the extra-cellular material parameters - matrix and fibers. And a third part with an implementation of an optimization scheme, using the FEM and a genetic algorithm (GA) to estimate de biomechanical properties of the PFM, with the aim of reducing the computational time when compared to the optimization scheme involving the Powell's algorithm.

In general, the acquisition of human tissue from the female pelvic floor is troublesome, mainly due to their location. Therefore, computational models are a powerful tool to understand the behaviour of the PFM, being used by several authors (F. S. Brandão et al., 2015; Noakes et al., 2008; Roza et al., 2015; Saleme et al., 2011). Numerical simulations of the mechanical behaviour of the PFM based on the FEM use *in vitro* biomechanical properties obtained from experimental studies with both normal and pathological specimens (Martins et al., 2013b; Rivaux et al., 2013). Nonetheless, to achieve realistic simulation of the PFM, the biomechanical properties constitute key ingredients (Peña et al., 2010). Despite reports regarding the determination of biomechanical properties of tissues from the pelvic cavity, *in vivo* results able to produce a steady and complete knowledge of the biomechanical behaviour of these studies, still do not exist. Hence, in this work, the concern was centered on the study of *in vivo* biomechanical properties of the PFM. For this purpose, an inverse FEA that couples the

FEM and the Powell's optimization algorithm in order to achieve simulated biomechanical behaviour during the Valsalva manoeuvre was implemented. To simulate the passive behaviour of the PFM of women with pathology, with SUI and with POP different isotropic hyperelastic constitutive models were used - Neo-Hookean, Mooney-Rivlin and Yeoh.

Firstly, to obtain accurate biomechanical properties, a subject-specific finite element biomechanical model of a nulliparous 30-year old female with no complains or clinical findings indicating pelvic floor dysfunction was built. It includes the PFM and bony pelvis. Initially, the triangulated 3D surface model was created based on MRI data by applying a semi-automatic procedure using the Mimics Innovation Suite v. 17 (Materialise, Leuven, Belgium) software. Subsequently, the triangulated 3D surface model of the PFM was then imported to Abaqus software v. 6.12 (Dassault Systmes Simulia Corp., Providence, RI, USA) to create the finite element model. The 3D geometric model of the bony pelvis was added to the model of the PFM for visualization purposes only and to help with the correct definition of the boundary conditions. The surrounding structures - as the bony pelvis - of the PFM are important to define the boundary conditions. These were defined in the insertion points of the muscles in the pubic bone, internal obturator fascia and coccyx visualized in the MR images, which were considered fixed (Parente et al., 2008; M. P. L. Parente et al., 2009; Rubod et al., 2012). However, to simulate the passive behaviour during Valsalva manoeuvre, a pressure of 4 kPa was applied to the inner surface of the PFM, following the methodology described by (Noakes et al., 2008).

Secondly, a Powell's optimization algorithm was implemented in the MATLAB MathWorks v. R2016a (Mathematical Computing Software, Natick, Massachusetts, USA) software. This algorithm searches for a suited set of biomechanical properties, in order to minimize the objective function (Gao et al., 2013; Powell, 1977) given by the distance between the two reference curves. One curve represents the position of the deformed *puborectalis* muscle in the numerical model for each iteration, and the other curve represents the position of the *puborectalis* muscle in the dynamic mid-sagittal image acquired at Valsalva manoeuvre. The Python scripting language was used to update the displacements of the nodes defining the curve on a position of the *puborectalis* muscle on the numerical model for each simulation. The Python scripting language coupled with MATLAB and the Abaqus software allow estimating the suited material constants for the Mooney-Rivlin constitutive model and the set is designated as inverse FEA.

After the determination of the material constants, the displacement of the PFM between the deformed numerical model and the mid-sagittal dynamic MR image acquired at Valsalva manoeuvre was compared.

The previous procedure was performed to estimate the material constants of the PVM of different groups of women (without pathology, with SUI and with POP), using three hyperelastic constitutive models - Neo-Hookean, Mooney-Rivlin and Yeoh.

The correct determination of the *in vivo* biomechanical properties allows to understand the passive behaviour based on the non-invasive imaging, for a specific subject, therefore, the inverse FEA can aid in the planning of surgical procedures for incontinence or prolapse. In order to correct these conditions, mesh implants can be used, and to improve their efficiency it is important to characterise the mechanical properties of the pelvic tissues.

To understand the passive biomechanical behaviour of the PFM, after the determination of the material constants the displacement of the PFM was compared between the deformed numerical model and the mid-sagittal dynamic MR image acquired at Valsalva manoeuvre and the stress-strain response was analysed. This approach is described in the articles 1, 2 and 3 included in Part B.

The obtained results (the displacements of the *levator hiatus*) were consistent with the ones obtained with MRI. However, another focus of this thesis was to establish the passive and active parameters of the *puboviscerali*s muscle during Valsalva manoeuvre and voluntary muscle contraction, respectively. Therefore, to correctly simulate the PVM behaviour is essential an accurate material model, i.e., a model that allows to reproduce more accurately the nonlinear stress-strain relationship and anisotropic behaviour of the PVM.

The passive and active behaviour of the PVM were simulated and analysed during Valsalva manoeuvre and contraction, respectively. For this purpose, three groups of the women were recruited - without pathology, with SUI and with POP. Additionally, to characterise more realistically the PVM behaviour - composed by a solid extra-cellular matrix, collagen and muscle fibers with a preferred orientation, a quasi-incompressible transversely isotropic hyperelastic model (proposed by (Martins et al., 1998)) was used. This mathematical-mechanical model describes the stress-strain behaviour of the PFM under large deformations and was already used by (Martins et al., 2007; M. Parente et al., 2009). Regarding the simulations, there are two types of simulations, one for the Valsalva

manoeuvre and another one for the muscle contraction, being the former the first simulation. This work is described in Article 4 include in Part B.

The results achieved through the inverse FEA with Powell's optimization algorithm were promising and comparable with the literature. This algorithm is considered useful for calculating the local minimum of a function and it is most efficient, reliable and also one of the most widely known of the zero-order methods (Powell, 1977), however, it is a local search method. Thereby, at this stage of the work, we implemented a genetic algorithm a global search method (Khalil et al., 2006; Meier et al., 2007) - in order to reduce the computational time.

Therefore, to determine *in vivo* biomechanical properties of the PVM of an asymptomatic group of women, an optimization scheme, based on the FEM and a genetic algorithm was developed. This algorithm was implemented in MATLAB and is inspired by the natural population genetics, used to evolve the solution to problems and it based on the global convergence (McCall, 2005). Operating on a population of several individual solutions, designed chromosomes, it's improves this population towards a better solution. Therefore, such as the Powell's algorithm, the objective of the genetic algorithm implementation was to minimize the objective function mentioned above, but additionally reducing computational time. To simulate the passive behaviour of the PVM during Valsalva manoeuvre, the FEM was used, and the Mooney-Rivlin constitutive model was applied to describe its nonlinear behaviour. Thereby to understand the passive

behaviour, the magnitude of the displacements and the principal logarithmic strain were analysed. This procedure is described in the Article 5 of the Part B.

5. Main Findings Achieved

In this study, a methodology based in inverse FEA using non-invasive input information was developed and applied, in order to estimate the biomechanical properties of the PFM. It can be used in the future as a useful tool to optimize the mechanical properties of the mesh implants (e.g., its stiffness) in order to reduce failure rates of surgical procedures, for correcting of PFD, such as SUI and POP.

The inverse FEA implemented in this work is essential to obtain *in vivo* biomechanical properties of the PFM for a specific subject. However, to better understand the mechanical properties and to simulate the PFM behaviour during Valsalva manoeuvre, muscle contraction and vaginal delivery, it is essential to accurately reproduce the female pelvic anatomy. The boundary conditions to the PFM must be imposed to incorporate the existence of the surrounding structures (coccyx, obturator muscles and *symphysis pubis*), by visualizing muscle insertions in the MR images. The nodes corresponding to the insertion of the PFM in the different structures may be considered as fixed or with some degree of movement. Previous authors consider zero-displacement nodes in the points of insertion between the PFM and the *symphysis pubis* and also the most superior portion of the PFM corresponding to the attachment to the internal obturator fascia in the medial surface of the internal obturator muscle which

constrains lateral movement (Roza et al., 2015). Also, in the models built, the supero-posterior portion the PFM, the nodes were kept unconstrained in the supero-inferior and antero-posterior directions to allow reproducing the coccygeal movements (Bø et al., 2001).

To simulate the passive behaviour of the PFM during Valsalva manoeuvre, the IAP was measured at rest and the average value described by (Noakes et al., 2008) was approximately 0.5 kPa. The IAP was also used under different conditions, such as Valsalva manoeuvre, with average values of 4.5 kPa for subjects lying in the supine position (Noakes et al., 2008). Accordingly, to simulate the Valsalva manoeuvre, we applied a pressure of 4 kPa in the inner surface of the muscle, since the computational model is based on images taken with the subject in a supine position and in a resting position, the muscles already incorporate resting tone.

The constitutive laws are of critical importance for the analysis of mechanical behaviour of soft tissues, i.e., to understand the PFM mechanics. Hence, due to nonlinear behaviour of the PFM it is important the use hyperelastic constitutive models that depend on variables obtained experimentally. (Martins et al., 2006) suggest three hyperelastic models for the study of soft tissues of the pelvis (Humphrey, Martins and Veronda-Westmann), but other hyperelastic models can also be used, such as the Mooney-Rivlin, Neo-Hookean, Ogden and Yeoh models.

The finite element models based in MR imaging have been used to understand the passive behaviour of the LA muscle and to determine the stress and displacements of the *levator hiatus* during strain and Valsalva manoeuvre (Lee et al., 2005; Noakes et al.,

2008) for a healthy specific subject. Due to difficulties in acquiring *in vivo* properties, (Lee et al., 2005) adopted the material constants of the Mooney-Rivlin hyperelastic model of the work of (Gerard et al., 2003) (c_1=2.5 kPa and c_2=6.25E-01 kPa). (Lee et al., 2005) concluded that stress occurs mostly in the *pubococcygeus* and *puborectalis* muscles. (Noakes et al., 2008) assumed the following material constants ($c_1 = 4.5$ kPa and $c_2 = 2$ kPa) and compared the displacements of the *levator hiatus* between the simulation and MR images, being the difference of approximately 74.5% for the antero-posterior displacement.

In the present work, and through inverse FEA (using an optimization algorithm coupled with the FEM in a completely non-invasive way), the material constants obtained for the Mooney-Rivlin model applied to the PFM of a healthy woman were $c_1 = 11.8$ kPa and $c_2 = 5.53\text{E-}02$ kPa, which are different from the ones published in the literature. In this sense, the difference in the range of magnitude can be associated with the subject-specific thickness and morphology of the PFM. For validation of this methodology, the results were compared with the dynamic MRI. Thus, the antero-posterior and supero-inferior displacements of the *levator hiatus* measured in the numerical model *vs.* dynamic MRI were concordant (1.98 mm *vs.* 2.13 mm, and 18.15 mm *vs.* 21.84 mm, respectively). When comparing the two (numerical model *vs.* dynamic MRI), the vertical axis (supero-inferior) showed a higher percentage in variation of the displacements (16.9%) than the horizontal axis - antero-posterior - (7.0%). The higher percentage error in the vertical axis can be caused by thinner *iliococcygeus* muscle, which may not be able to avoid the caudal dislocation. Therefore, the use of data obtained non-invasively and the optimization of algorithms may enable estimating accurate and subject-specific material constants.

Despite the efforts regarding the determination of the biomechanical properties of the PFM, there are not enough studies to produce a steady and complete knowledge of its mechanical behaviour. This lack of knowledge is even higher for the case of the biomechanical properties of muscles with pathology, such as in women with SUI and POP. Hence, the inverse FEA was also used to determine the material constants of different constitutive models applied to PVM, initially to two distinct groups (continent and incontinent women).

The pelvic soft tissues, such as the nerves, muscles and connective tissues, are responsible for maintaining continence, providing resistance to downward displacements during increase in IAP (Denise et al., 2000) and their biomechanical properties are proven to be relevant to explain pelvic disorders (Derpapas, 2015). Hence, the UI can be considered as the consequence of the alteration of a biomechanical process (McGuire, 2004).

For the study of incontinence, eight women were recruited and afterwards divided into two groups - SUI and controls. When comparing these two groups, no significant difference in age, BMI, parity and muscle thickness were found. In addition, to simulate the passive behaviour of the PVM during Valsalva manoeuvre three hyperelastic constitutive models were used - Neo-Hookean, Mooney-Rivlin, Yeoh - and the material constants were significantly higher for women without pathology than for those with SUI. The variation of the c_1 for women without pathology *vs.* incontinent group was approximately 38.46% for the Neo-Hookean, 38.46% for *the* Mooney-Rivlin, and 48.39% for the Yeoh. These results seem to point to the fact that the PVM of incontinent women have lower elasticity than women without pathology. This difference is not associated with the demographic and morphological characteristics, but may be associated with

histological changes, due to the fact that women with incontinence normally present a significant reduction of type III collagen (Patel et al., 2007). Additionally, the variation of the antero-posterior displacement - 42.17% for the Neo-Hookean, 39.8% for the Mooney-Rivlin and 41.6% for the Yeoh are in accordance with the variation of the c_1 - which has greater influence in the mechanical behaviour (Noor & Mahmud 2015) - for the three constitutive models.

During Valsalva manoeuvre, the muscles of the pelvic floor have an outward movement, opening the *levator hiatus* (Herschorn, 2004). The biomechanical simulations reproduced the same mechanical behaviour, and the values of the displacements of the *levator hiatus* were in accordance with the dynamic MR images.

Finally, the results of the uniaxial tension tests obtained analytically were compared to those obtained numerically through the simulations and these were concordant, and can also be compared with the values of the literature (Janda, 2006; Li et al., 2008; Noakes et al., 2008).

Experimental studies have been addressed to evaluate the biomechanical properties of vaginal tissue and pelvic ligaments in women with POP (Cosson et al., 2004; Martins et al., 2013a; Rubod et al., 2008). Previous studies showed that prolapsed vaginal tissue is significantly stiffer than the non-prolapsed (Jean-Charles et al., 2010) and (Lei et al., 2007) found no significant differences in the biomechanical properties between moderate and severe POP. These studies were performed in both cadaver and *ex-vivo* specimens. Due to clinical, technical and ethical reasons, it is not feasible to obtain samples from the vagina of women without POP. More recently, important efforts to perform *in vivo* measurements of biological material parameters have been performed,

using aspiration instruments. However, since this technique is considered invasive (Kauer et al., 2002), the biomechanical behaviour of the PFM remains unclear. Therefore, one of the stages of this work was also the determination of the biomechanical properties of the PVM and to analyse the influence of POP on these properties. For this purpose, was used the inverse FEA - already used to determine the mechanical properties of incontinent women. In our cases, muscles did not present visible defects on MRI.

The material constants of the different constitutive models - Neo-Hookean, Mooney-Rivlin and Yeoh - were determined in this work for two groups. Women with POP presented material constants higher than women without pathology, meaning that women with prolapse presented a higher stiffness. The ratio between the values of the material constants for women without and with prolapse was approximately 43% for the c_1 parameter of the Neo-Hookean constitutive model, 57% and 24% for c_1 and c_2 of the Mooney-Rivlin constitutive model, and 35%, 21% and 14% for c_1, c_2 and c_3 of the Yeoh constitutive model. This difference was not associated with the age, parity and BMI, but it is potentially associated with muscle thickness differences that may be due to histological changes in the pelvic architecture. Previous studies show that the vaginal tissue exposed to an overload alters its biomechanical characteristics becoming more rigid. These studies also show that there is more vaginal tissue in women with prolapse (Martins, 2010), being this evidence also reported in MRI (Hsu et al., 2005). Other studies also suggests that the vagina and the supportive tissues actively remodel in response to different changes (Alperin and Moalli, 2006). Additionally, an increase in collagen type III in combination with an increase in the active matrix metalloproteinases (MMP-9) in prolapsed vaginal tissue suggests that this tissue is actively remodelling to accommodate a progressively increasing mechanical load (Kerkhof et al., 2009; Martins et al., 2013a).

In addition, MRI studies allowed to visualize pelvic floor function during Valsalva manoeuvre, and they showed that the women with POP have a wider antero-posterior diameter - opening of the *levator hiatus* - than women without POP (Brandão et al., 2013; Clark et al., 2010; Ying et al., 2012). This evidence was also reported in this study. Moreover, when comparing the antero-posterior displacement between two groups, there was no significant difference for the numerical models using the different constitutive models and MRI.

In this way, the results obtained - material constants - for the PVM *in vivo*, in a non-invasive manner are promising and can be compared with experimental studies of vaginal tissue (Jean-Charles et al., 2010) and LAM (Martins, 2010). Hence, the presented results suggest that PFM changes caused by POP is followed by modifications in biomechanical properties.

Usually, the PFM have an active nonlinear behaviour, but due to their skeletal muscle structure, namely the existence of oriented muscle fibers, they assume an anisotropic behaviour. Muscles are distinct from other soft tissues because of their capability of active contraction (Martins et al., 1998). Thus, to simulate the active behaviour is also important to obtain an approximation of the muscle fiber direction, which is an important parameter for the constitutive model (Parente et al., 2010).

To simulate the PFM action, the majority of studies have used the material properties of cardiac, fascial muscles (Martins et al., 2007) and human pelvic tissue, characterised using *in vitro* mechanical tests from fresh cadavers. (Brandão et al., 2013) and (Da Silva-Filho et al., 2010) used numerical models to understand the role and the

mechanical behaviour of the pelvic structures in the development of UI and POP, by using the material properties obtained from experimental studies with both normal and pathological specimens. Accordingly, the second part of this work characterises the passive and active behaviour of the PVM, assumed as being composed by a solid extra-cellular matrix, collagen and muscle fibers with a preferred orientation. In this context, we used a quasi-incompressible transversely isotropic hyperelastic model to simulate the PVM of women without pathology, with SUI and with POP.

To estimate the passive and active material parameters during Valsalva manoeuvre and muscle contraction, respectively, the inverse FEA was used. Although the constitutive model applied is different from those used in the above-mentioned studies - reproducing a more realistic behaviour - the passive results were similar, with the PVM of the women with POP being more rigid than those of the women without pathology and with SUI.

The maximum muscular contraction occurs when tension is generated within the sarcomere by maximum overlap of actin and myosin filaments, and this event is due to the capacity of the PFM to sustain contractile activity, which depends, as previously mentioned, on the type of muscle fiber - type I and type II. In this way, the active material parameter (T_0^M) was also different between the groups, being 0.296 MPa for the women with POP, 0.115 MPa for the women without pathology and 0.046 MPa for the women with SUI, which is much lower than in the literature (approximately 0.682 MPa) (M. Parente et al., 2009). This marked difference between groups may be related to the fiber length (Marques et al., 2010). According to the literature, the diameters of type I and type II fibers increase approximately 21% and 61%, respectively, in women with POP

(Beersiek et al., 1979), while in women with SUI the diameters are smaller and there is also an increase in the number of fibers (Zhu et al., 2005).

In this work, to validate these results they were analysed and compared with the MRI. During muscle contraction there is an inward movement, closing the pelvic openings (Herschorn, 2004), and this behaviour was reproduced in this work, being the postero-anterior displacement of the biomechanical simulation in accordance with the dynamic MR images. For Valsalva manoeuvre the same was verified, with a variation of the displacement (numerical model *vs.* MRI) of approximately 8.39% for the women without pathology, 15.89% for women with SUI and 5.49% for women with POP. Furthermore, the antero-posterior diameter measured at rest position in the MRI was higher for the group of the women with POP (60.1 mm ± 7.83) mm. This evidence was previously described by different authors (Brandão et al., 2013; Clark et al., 2010; Ying et al., 2012), the values reported for asymptomatic women and women with POP at rest by (Brandão et al., 2013) were 47.0 mm ± 5.60 mm and 56.0 mm ± 7.10 mm, respectively.

According to (Henderson et al., 2013), women with POP have more difficulty to perform correct contractions of the PFM. From (Ying et al., 2012), the antero-posterior and postero-anterior displacements during Valsalva manoeuvre and muscle active contraction for these women were approximately 6,0 mm and 4,6 mm, respectively, our values (4.1 mm and 4.7 mm) are in accordance with the literature. In spite of the relatively small sample size and having only statistical differences in parity, the results were similar with literature, but the ideal would be to increase the sample size.

A genetic optimization algorithm was also implemented in order to estimate the *in vivo* biomechanical properties of the PVM of a group of the asymptomatic women.

This study aimed at developing a new scheme for the inverse FEA, involving a genetic algorithm and FEM, in order to reduce the computational time (number of numerical simulations), when determining the material constants. The passive behaviour of the PVM during Valsalva manoeuvre was analysed and the Mooney-Rivlin hyperelastic constitutive model was applied to PVM to describe its nonlinear behaviour. Additionally, it was intended to compare the material constants with the ones established through the inverse FEA, using the Powell's algorithm. The dynamic images acquired at Valsalva manoeuvre were used to validate the numerical results. The results showed that the genetic algorithm requires a lower number of simulations when compared to the Powell's algorithm. Nevertheless, the Powell's algorithm presents lower value of the material constants (c_1 and c_2) and consequently, lower values for the objective function. However, the difference of the material constants may not have had much influence in the numerical results. These results are not reflected in the numerical models, i.e., for a difference of 34% for the objective function and 0% and 14% for the c_1 and c_2, respectively, only a difference of 5% and 4% is reflected in the magnitude of the displacement and principal logarithmic strain, respectively.

According to the results obtained, the passive behaviour during Valsalva manoeuvre was reproduced in the biomechanical simulations and the values of the antero-posterior displacement is in accordance with dynamic MR images. Hence, the genetic algorithm was capable of estimating the muscle properties, requiring fewer simulations, reproducing a biomechanical behaviour similar to that of the Powell's algorithm. The difference of the results obtained between algorithms may be associated with their particular characteristics. The Powell's algorithm searches in conjugate direction and it is considered a local method (Gao et al., 2013) while the genetic algorithm insists on

finding a global minimum (McCall, 2005; Meier et al., 2007).

Finally, the GA coupled with FEM appears to be a potential approach to quantify the material properties without explicitly approximating a gradient search direction, while requiring considerable lower number of numerical simulations.

6. Conclusions and Future Work

The biomechanical assessment of the pelvic floor tissues is important to understand pelvic dysfunctions and also to improve clinical outcomes. In this sense, numerical simulations, based on the FEM, provide powerful tools to understand the PFD.

However, material properties required in the simulation are conventionally characterised through *ex vivo* mechanical tests or approximated using other soft tissues, which differ from those in physiological state. *Ex vivo* studies of ligaments and endopelvic fascia have been conducted (Abramowitch et al., 2009; Jelen et al., 2010; Rivaux et al., 2013), through mechanical tests that allow studying their biomechanical behaviour, such as the uniaxial and biaxial tensile tests. There are few studies focused on the PFM in humans due to the ethical challenges, and hence animal models are frequently used (Rahn et al., 2008). Providing an "ideal" mechanical behaviour is essential to estimate the *in vivo* biomechanical properties of the PFM. Furthermore, a correctly characterisation of the biomechanical properties of these muscles can, in the future, help with the planning of surgical procedures, as for example, to improve the efficiency of the mesh implants. Mesh implants are used to repair POP and in the surgical treatment of SUI. However, the stiffness of the mesh implants may not conform to the surrounding

tissue, further interfering with its integration (Cosson et al., 2003b). A previous study showed that the stress transmission at the tissue/implant interface is influenced by the mechanical properties of native tissue and implant, respectively. Hence, the mesh mechanical properties are important in choosing appropriate materials for surgical procedures (Dietz et al., 2003).

The current work presents an inverse FEA able to estimate the material constant that characterise the mechanical behaviour of the PFM in women with different conditions.

The computational results envisage that the PVM of women with POP present higher material constants and, consequently, show a higher stiffness when compared with the PVM of healthy and incontinent women. In addition, to validate the results, the displacements of the *levator hiatus* in the numerical models were similar with ones measured in the dynamic MR images of the same subjects. Thereby, this methodology allowed establishing *in vivo* material constants of the female PFM for woman without pathology, with UI and with POP, which are comparable with *ex vivo* experimental results. This methodology is completely non-invasive, using only MR images to build the computational models and to compare results. This avoids the use of *ex vivo* tissues collected postmortem, hysterectomy or aspiration experiments during surgical proceedings (Jean-Charles et al., 2010; Kauer et al., 2002; Lei et al., 2007), or *in vitro* material properties from experimental studies with both normal and pathological specimens (Rivaux et al., 2013). Due to limitations of the *ex vivo* studies on the PFM, the inverse FEA is an alternative to obtain the biomechanical properties and shows promising results for subject-specific analysis.

The study of the biomechanical properties of PFM presents some complexity. To properly interpret our findings, it is necessary to consider the limitations and simplifications involved, namely the sample size. Furthermore, the connectivity with other tissues (the fascia and ligaments), the pelvic organs and the sliding interactions, which may affect the results, were not considered. Additionally, the pressure applied in the PFM to mimic Valsalva manoeuvre was retrieved from the literature (Noakes et al., 2008), but one cannot guarantee that the same pressure was performed by the subjects during the scanning. In spite of these limitations, the inverse FEA may estimate the stiffness of the native tissues that may eventually applied in the future to optimize those of the mesh implants, in order to reduce failure rates of surgical procedures.

To better understand the biomechanical behaviour of PFM, the pelvic structures (such as pelvic ligaments, fascia and other pelvic structures) should be included, and thus obtain more accurate results regarding the biomechanical properties. Therefore, further refinements should focus on the improvement of the biomechanical models used to simulate passive and active behaviour. Additionally, increasing the sample is essential. However, for a better understanding of the passive behaviour, the pressure during Valsalva manoeuvre would have to be measured by means of an intracavitary measurement instrument. These improvements would allow to better estimate the biomechanical properties and understand the function/dysfunction of the PFM.

In the future, it would be also interesting to characterise the mechanical properties of the PFM of other women's groups, for example athletic women with and without pathology, women after vaginal delivery and women after physiotherapy for correction of dysfunctions.

The inverse FEA coupled with the FEM can accurately estimate the biomechanical properties and it seems to be a promising possibility to evaluate the biomechanical behaviour during Valsalva manoeuvre and muscle contraction.

References

Abramowitch, S.D., Feola, A., Jallah, Z., Moalli, P.A., 2009. Tissue mechanics, animal models, and pelvic organ prolapse: a review. Eur. J. Obstet. Gynecol. Reprod. Biol. 144, S146–S158.

Alperin, M., Moalli, P., 2006. Remodeling of vaginal connective tissue in patients with prolapse. Curr Opin Obs. Gynecol 18, 544–550.

Ashton-Miller, J.A., DeLancey, J.O.L., 2007. Functional anatomy of the female pelvic floor. Ann. N. Y. Acad. Sci. 1101, 266–296.

Baah-Dwomoh, A., McGuire, J., Tan, T., De Vita, R., 2016. Mechanical Properties of Female Reproductive Organs and Supporting Connective Tissues: A Review of the Current State of Knowledge. Appl. Mech. Rev. 68, 60801.

Barber, M.D., Bremer, R.E., Thor, K.B., Dolber, P.C., Kuehl, T.J., Coates, K.W., 2002. Innervation of the female levator ani muscles. Am. J. Obstet. Gynecol. 187, 64–71.

Beersiek, F., Parks, A.G., Swash, M., 1979. Pathogenesis of ano-rectal incontinence: a histometric study of the anal sphincter musculature. J Neurol Sci 42, 111–127.

Bø, K., Lilleås, F., Talseth, T., Hedland, H., 2001. NoDynamic MRI of the pelvic floor muscles in an upright sitting position. Neurourol Urodyn. 20, 167–174.

Boyadzhyan, L., Raman, S.S., Raz, S., 2008. Role of static and dynamic MR imaging in surgical pelvic floor dysfunction. Radiographics 28, 949–967.

Brandão, F.S., Parente, M.P., Rocha, P.A., Saraiva, M.T., Ramos, I.M., Natal Jorge, R.M., 2015. Modeling the contraction of the pelvic floor muscles. Comput Methods Biomech Biomed Engin. 8, 1–10.

Brandão, S., Da Roza, T., Mascarenhas, T., Duarte, S., Ramos, I., Parente, M., Jorge, R.N., 2013. Moment of inertia as a means to evaluate the biomechanical impact of pelvic organ prolapse.

Int. J. Urol. 20, 86–92.

Brandão, S., Parente, M., Mascarenhas, T., da Silva, A.R.G., Ramos, I., Jorge, R.N., 2015. Biomechanical study on the bladder neck and urethral positions: Simulation of impairment of the pelvic ligaments. J. Biomech. 48, 217–223.

Brandao, S., Roza, T.D., Parente, M., Ramos, I., Mascarenhas, T., Natal Jorge, R.M., 2013. Magnetic resonance imaging of the pelvic floor: From clinical to biomechanical imaging. Proc. Inst. Mech. Eng. Part H J. Eng. Med. 227, 1324–1332.

Chen, B., Yeh, J., 2011. Alterations in connective tissue metabolism in stress incontinence and prolapse. J. Urol. 186, 1768–1772.

Chen, Z.W., Joli, P., Feng, Z.Q., Rahim, M., Pirró, N., Bellemare, M.E., 2015. Female patient-specific finite element modeling of pelvic organ prolapse (POP). J. Biomech. 48, 238–245.

Clark, N.A., Brincat, C.A., Yousef, A., DeLancey, J.O.L., 2010. Levator defects affect perineal position independently of prolapse status. Am J Obs. Gynecol. 203, 595.e17-595.e22.

Cosson, M., Boukerrou, M., Lacaze, S., Lambaudie, E., Fasel, J., Mesdagh, H., Lobry, P., Ego, A., 2003a. A study of pelvic ligament strength. Eur. J. Obstet. Gynecol. Reprod. Biol. 109, 80–87.

Cosson, M., Debodinance, P., Boukerrou, M., Chauvet, M.P., Lobry, P., Crépin, I., Ego, A., 2003b. Mechanical properties of synthetic implants used in the repair of prolapse and urinary incontinence in women: which is the ideal material? Int. Urogynecol. J. 14, 169–178.

Cosson, M., Lambaudie, E., Boukerrou, M., Lobry, P., Crépin, G., Ego, A., 2004. A biomechanical study of the strength of vaginal tissues: Results on 16 post-menopausal patients presenting with genital prolapse. Eur. J. Obstet. Gynecol. Reprod. Biol. 112, 201–205.

Da Silva-Filho, A.L., Martins, P.A.L.S., Parente, M.P., Saleme, C.S., Roza, T., Pinotti, M., Mascarenhas, T., Jorge, R.M.N., 2010. Translation of biomechanics research to urogynecology. Arch. Gynecol. Obstet. 282, 149–155.

Delancey, J., Hurd, W., 1998. Size of the urogenital hiatus in the levator ani muscles in normal women and women with pelvic organ prolapse. Obs. Gynecol. 91, 364–368.

DeLancey, J., Morgan, D., Fenner, D., Kearney, R., Guire, K., Miller, J., Hussain, H., Umek, W., Hsu, Y., Ashton-Miller, J., 2007. Comparison of levator ani muscle defects and function in women with and without pelvic organ prolapse. Obs. Gynecol. 109, 295–302.

Delancey, J.O.L., Miller, J.M., Kearney, R., Reddy, P., Umek, W., Guire, K.E., Margulies, R.U., Ashton-miller, J.A., 2007. Vaginal birth and de novo stress incontinence: Relative contributions of urethral dysfunction and mobility. Obs. Gynecol. 110, 354–362.

Denise, H., Janis, M.M., DeLancey, J.O.L., James, A.A.-M., 2000. Differential Effects of Cough, Valsalva, and Continence Status on Vesical Neck Movement. Obs. Gynecol. 95, 535–540.

Derpapas, A., 2015. The use of imaging in the diagnosis of lower urinary tract disorders and pelvic organ prolapse in women. Thesis. Imperial College London Department of Surgery & Cancer.

Dietz, H.P., 2004. Ultrasound imaging of the pelvic floor. Part II: three-dimensional or volume imaging . Ultrasound Obs. Gynecol. 23, 615–25.

Dietz, H.P., Shek, C., Clarke, B., 2005. Biometry of the pubovisceral muscle and levator hiatus by three-dimensional pelvic floor ultrasound. Ultrasound Obstet. Gynecol. 25, 580–585.

Dietz, H.P., Shek, C., De Leon, J., Steensma, A.B., 2008. Ballooning of the levator hiatus. Ultrasound Obstet. Gynecol. 31, 676–680.

Dietz, H.P., Vancaillie, P., Svehla, M., Walsh, W., Steensma, A.B., Vancaillie, T.G., 2003. Mechanical properties of urogynecologic implant materials. Int. Urogynecol. J. Pelvic Floor Dysfunct. 14, 239–243.

Elneil, S., 2009. Complex pelvic floor failure and associated problems. Best Pract. Res. Clin. Gastroenterol. 23, 555–573.

Gao, W., Liu, S., Huang, L., 2013. A novel artificial bee colony algorithm with Powell's method. Appl. Soft Comput. 13, 3763–3775.

Gerard, J., Wilhelms-Tricarico, R., Perrier, P., Payan, Y., 2003. A 3D dynamical biomechanical tongue model to study speech motor control. Recent Res. Dev. Biomech. 49–64.

Henderson, J.W., Wang, S., Egger, M.J., Masters, M., Nygaard, I., 2013. Can women correctly contract their pelvic floor muscles without formal instruction? Computer (Long. Beach. Calif). 19, 8–12.

Herschorn, S., 2004. Female pelvic floor anatomy: the pelvic floor, supporting structures, and pelvic organs. Rev. Urol. 6 Suppl 5, S2–S10.

Hoyte, L., Damaser, M.S., Warfield, S.K., Chukkapalli, G., Majumdar, A., Choi, D.J., Trivedi, A., Krysl, P., 2008. Quantity and distribution of levator ani stretch during simulated vaginal childbirth. Am. J. Obstet. Gynecol. 199.

Hoyte, L., Schierlitz, L., Zou, K., Flesh, G., Fielding, J.R., 2001. Two- and 3-dimensional MRI comparison of levator ani structure, volume, and integrity in women with stress incontinence and prolapse. Am. J. Obstet. Gynecol. 185, 11–19.

Hsu, Y., Chen, L., Delancey, J.O.L., Ashton-Miller, J.A., 2005. Vaginal Thickness, Cross-Sectional Area, and Perimeter in Women With and Those Without Prolapse. Obs. Gynecol 105, 1012–1017.

Janda, S., 2006. Biomechanics of the pelvic floor musculature. PhD. Thesis. Technische Universiteit Delft.

Janda, S., Van Der Helm, F.C.T., De Blok, S., 2003. Measuring morphological parameters of the pelvic floor for finite element modelling purposes. J. Biomech. 36, 749–757.

Jean-Charles, C., Rubod, C., Brieu, M., Boukerrou, M., Fasel, J., Cosson, M., Clay, J.-C., Rubod, C., Brieu, M., Boukerrou, M., Fasel, J., Cosson, M., 2010. Biomechanical properties of prolapsed or non-prolapsed vaginal tissue: impact on genital prolapse surgery. Int. Urogynecol. J. 21, 1535–1538.

Jelen, K., Herman, H., Lopot, F., Kubovy, P., Otcenasek, M., Sedlacek, R., 2010. Women with incorrect pelvic floor statics: a biomechanical answer to the mechanical loading of the vagina-endopelvic fascia complex. Neuroendocrinol. Lett. 31, 413–417.

Kauer, M., Vuskovic, V., Dual, J., Szekely, G., Bajka, M., 2002. Inverse finite element characterization of soft tissues. Med. Image Anal. 6, 275–87.

Kerkhof, M.H., Hendriks, L., Brölmann, H. a M., 2009. Changes in connective tissue in patients with pelvic organ prolapse--a review of the current literature. Int. Urogynecol. J. Pelvic Floor Dysfunct. 20, 461–474.

Khalil, A.S., Bouma, B.E., Kaazempur Mofrad, M.R., 2006. A combined FEM/genetic algorithm for vascular soft tissue elasticity estimation. Cardiovasc. Eng. 6, 93–102.

Kiyosaki, K., Ackerman, L., Histed, S., Sevilla, C., Eilber, K., Maliski, S., Anger, J., 2012. Patient understanding of Pelvic floor disoders: What women Want to Know. Female Pelvic Med Reconstr Surg 18, 137–142.

Law, Y.M., Fielding, J.R., 2008. MRI of pelvic floor dysfunction: Review. Am. J. Roentgenol. 191, 45–53.

Lee, S., Darzi, A., Yang, G., 2005. Subject Specific Finite Element Modelling of the Levator Ani. Med. Image Comput. Comput. Interv. 3749, 360–367.

Lei, L., Song, Y., Chen, R., 2007. Biomechanical properties of prolapsed vaginal tissue in pre- and postmenopausal women. Int. Urogynecol. J. Pelvic Floor Dysfunct. 18, 603–607.

Li, X., Kruger, J.A., Chung, J.H., Nash, M.P., Nielsen, P.M.F., 2008. Modelling childbirth: Comparing athlete and non-athlete pelvic floor mechanics. Med Image Comput Comput - Assist Interv. 11, 750–757.

Luo, J., Chen, L., Fenner, D.E., Ashton-Miller, J.A., Delancey, J.O.L., 2015. A multi-compartment 3-D finite element model of rectocele and its interaction with cystocele. J. Biomech. 48, 1580–1586.

Luo, J., Smith, T.M., Ashton-Miller, J. a, Delancey, J.O.L., 2014. In Vivo Properties of Uterine Suspensory Tissue in Pelvic Organ Prolapse. J. Biomech. Eng. 136, 1–6.

Marques, A., Stothers, L., Macnab, A., 2010. The status of pelvic floor muscle training for women. Can Urol Assoc J 4, 419–24.

Martins, J.A.C., Pires, E.B., Salvado, R., Dinis, P.B., 1998. A numerical model of passive and active behavior of skeletal muscles. Comput. Methods Appl. Mech. Eng. 151, 419–433.

Martins, J. a C., Pato, M.P.M., Pires, E.B., Natal Jorge, R.M., Parente, M., Mascarenhas, T., 2007. Finite element studies of the deformation of the pelvic floor. Ann. N. Y. Acad. Sci. 1101, 316–334.

Martins, P.A.L., 2010. Experimental and numerical studies of soft biological tissues. PhD. Thesis. Faculty of Engineering, University of Porto, Portugal.

Martins, P., Jorge, R.N., Ferreira, A., 2006. A Comparative Study of Several Material Models for Prediction of Hyperelastic Properties: Application to Silicone-Rubber and Soft Tissues. Strain 42, 135–147.

Martins, P., Lopes Silva-Filho, A., Rodrigues Maciel Da Fonseca, A.M., Santos, A., Santos, L., Mascarenhas, T., Natal Jorge, R.M., Ferreira, A.J.M., 2013a. Biomechanical properties of vaginal tissue in women with pelvic organ prolapse. Gynecol. Obstet. Invest. 75, 85–92.

Martins, P., Silva-Filho, A.L., Fonseca, A.M.R.M., Santos, A., Santos, L., Mascarenhas, T., Jorge, R.M.N., Ferreira, A.M., 2013b. Strength of round and uterosacral ligaments: a biomechanical study. Arch. Gynecol. Obstet. 287, 313–8.

McCall, J., 2005. Genetic algorithms for modelling and optimisation. J. Comput. Appl. Math. 184, 205–222.

McGuire, E.J., 2004. Pathophysiology of Stress Urinary Incontinence. Rev. Urol. 6, S11–S17.

Meier, C., Yassine, A. a., Browning, T.R., 2007. Design Process Sequencing With Competent Genetic Algorithms. J. Mech. Des. 129, 566.

Memon, H.U., Handa, V.L., 2013. Vaginal childbirth and pelvic floor disorders. Womens Heal. 9.

Moalli, P.A., Jones Ivy, S., Meyn, L.A., Zyczynski, H.M., 2003. Risk factors associated with pelvic floor disorders in women undergoing surgical repair. Obstet. Gynecol. 101, 869–874.

Moerman KM, Sprengers AM, Simms CK, Lamerichs RM, Stoker J, N.A., 2012. Validation of continuously tagged MRI for the measurement of dynamic 3D skeletal muscle tissue deformation. Med Phys. 39, 1973–810.

Nagle, A.S., Barker, M.A., Kleeman, S.D., Haridas, B., Mast, T.D., 2014. Passive biomechanical properties of human cadaveric levator ani muscle at low strains. J. Biomech. 47, 583–6.

Netter, F., 2014. Atlas of Human Anatomy, 6 th. ed. Saunders.

Noakes, K.F., Pullan, A.J., Bissett, I.P., Cheng, L.K., 2008. Subject specific finite elasticity simulations of the pelvic floor. J. Biomech. 41, 3060–3065.

Nygaard, I., Barber, M., Burgio, K., Kenton, K., Meikle, S., Schaffer, J., Spino, C., Whitehead, W., Wu, J., Brody, D., 2008. Prevalence of Symptomatic Pelvic Floor Disorders in US Women. Jama 300, 1311–1316.

Oliveira, D.A., Parente, M.P.L., Calvo, B., Mascarenhas, T., Natal Jorge, R.M., 2016. Numerical simulation of the damage evolution in the pelvic floor muscles during childbirth. J. Biomech. 49, 594–601.

Olsen, A., Smith, V., Bergstrom, J., Colling, J., Clark, A., 1997. Epidemiology of surgically managed pelvic organ prolapse and urinary incontinence. Obs. Gynecol 89, 501–506.

Parente, M., Natal Jorge, R., Mascarenhas, T., Fernandes, A., Martins, J., 2009. The influence of the material properties on the biomechanical behavior of the pelvic floor muscles during vaginal delivery. J. Biomech. 42, 1301–1306.

Parente, M., Natal Jorge, R., Mascarenhas, T., Fernandes, A., Martins, J., 2008. Deformation of the pelvic floor muscles during a vaginal delivery. Int. Urogynecol. J. Pelvic Floor Dysfunct. 19, 65–71.

Parente, M., Natal Jorge, R., Mascarenhas, T., Silva-Filho, A., 2010. The Influence of Pelvic Muscle Activation During Vaginal Delivery. Obs. Gynecol. 115, 804–808.

Parente, M.P.L., Jorge, R.M.N., Mascarenhas, T., Fernandes, A.A., Martins, J.A.C., 2009. The

influence of an occipito-posterior malposition on the biomechanical behavior of the pelvic floor. Eur. J. Obstet. Gynecol. Reprod. Biol. 144, S166–S169.

Patel, P.D., Amrute, K. V., Badlani, G.H., 2007. Pelvic organ prolapse and stress urinary incontinence: A review of etiological factors. Indian J Urol. 23, 135–141.

Peña, E., Calvo, B., Martínez, M.A., Martins, P., Mascarenhas, T., Jorge, R.M.N., Ferreira, A., Doblaré, M., 2010. Experimental study and constitutive modeling of the viscoelastic mechanical properties of the human prolapsed vaginal tissue. Biomech. Model. Mechanobiol. 9, 35–44.

Peng, Q., Jones, R., Shishido, K., Constantinou, C.E., 2007. Ultrasound evaluation of dynamic responses of female pelvic floor muscles. Ultrasound Med. Biol. 33, 342–352.

Peng, Y., Khavari, R., Nakib, N.A., Boone, T.B., Zhang, Y., 2015a. Assessment of urethral support using MRI-derived computational modeling of the female pelvis. Int. Urogynecol.

Peng, Y., Khavari, R., Nakib, N.A., Stewart, J.N., Boone, T.B., Zhang, Y., 2015b. The Single-Incision Sling to Treat Female Stress Urinary Incontinence: A Dynamic Computational Study of Outcomes and Risk Factors. J. Biomech. Eng. 137, 91007.

Powell, M.J.D., 1977. Restart procedures for the conjugate gradient method. Math. Program. 12, 241–254.

Rahn, D.D., Ruff, M.D., Brown, S.A., Tibbals, H.F., Word, R.A., 2008. Biomechanical properties of the vaginal wall: effect of pregnancy, elastic fiber deficiency, and pelvic organ prolapse. Am. J. Obstet. Gynecol. 198, 590.e1-590.e6.

Raizada, V., Mittal, R.K., 2008. Pelvic Floor Anatomy and Applied Physiology. Gastroenterol Clin North Am 37, 493–497.

Rechberger, T., Postawski, K., Jakowicki, J.A., Gunja-Smith, Z., Woessner J.F., J., 1998. Role of fascial collagen in stress urinary incontinence. Am. J. Obstet. Gynecol. 179, 1511–1514.

Rivaux, G., Rubod, C., Dedet, B., Brieu, M., Gabriel, B., Cosson, M., 2013. Comparative analysis of pelvic ligaments: a biomechanics study. Int. Urogynecol. J. 24, 135–9.

Roza, T. Da, Brandão, S., Oliveira, D., Mascarenhas, T., Parente, M., Duarte, J.A., Jorge, R.N., 2015. Football practice and urinary incontinence: Relation between morphology, function and biomechanics. J. Biomech. 48, 1587–1592.

Rubod, C., Boukerrou, M., Brieu, M., Jean-Charles, C., Dubois, P., Cosson, M., 2008. Biomechanical properties of vaginal tissue: Preliminary results. Int. Urogynecol. J. Pelvic

Floor Dysfunct. 19, 811–816.

Rubod, C., Brieu, M., Cosson, M., Rivaux, G., Clay, J.C., De Landsheere, L., Gabriel, B., 2012. Biomechanical properties of human pelvic organs. Urology 79, 968.e17-968.e22.

Saleme, C.S., Parente, M.P.L., Natal Jorge, R.M., Pinotti, M., Silva-Filho, A.L., Roza, T., Mascarenhas, T., Tavares, J.M.R.S., 2011. An approach on determining the displacements of the pelvic floor during voluntary contraction using numerical simulation and MRI. Comput. Methods Biomech. Biomed. Engin. 14, 365–370.

Sapsford, R.R., Hodges, P.W., 2001. Contraction of the pelvic floor muscles during abdominal maneuvers. Arch. Phys. Med. Rehabil. 82, 1081–1088.

Schwertner-Tiepelmann, N., Thakar, R., Sultan, A.H., Tunn, R., 2012. Obstetric levator ani muscle injuries: Current status. Ultrasound Obstet. Gynecol. 39, 372–383.

Segal, S., Arya, L.A., Smith, A.L., 2012. Functional Outcomes for Incontinence and Prolapse Surgery. Curr. Bladder Dysfunct. Rep. 7, 179–186.

Siegel, S., Noblett, K., Mangel, J., Giebling, T., Sutherland, S.E., Bird, E.T., 2015. Results of a prospective, randomized , multicenter study evaluating sacral neuromodulation with Interstim therapy compared to standard medical therapy at 6 monts in subjects with mild symptoms of overactive bladder. Neurourol. Urodyn. 34, 224–230.

Sindhwani, N., Barbosa, D., Alessandrini, M., Heyde, B., Dietz, H.P., D'Hooge, J., Deprest, J., 2016. Semi-automatic outlining of levator hiatus. Ultrasound Obstet. Gynecol. 48, 98–105.

Singh, K., Reid, W.M., Berger, L. a, 2001. Assessment and grading of pelvic organ prolapse by use of dynamic magnetic resonance imaging. Am. J. Obstet. Gynecol. 185, 71–77.

Sobotta, J., Putz, R., Pabst, R., Bedoui, S., 2001. Sobotta Atlas of Human Anatomy, 13 th. ed. Lippincott Williams & Wilkins.

Tumbarello, J.A., Hsu, Y., Lewicky-Gaupp, C., Rohrer, S., DeLancey, J.O.L., 2010. Do repetitive Valsalva maneuvers change maximum prolapse on dynamic MRI? Int. Urogynecol. J. Pelvic Floor Dysfunct. 21, 1247–1251.

Tunn, R., Goldammer, K., Neymeyer, J., Gauruder-Burmester, A., Hamm, B., Beyersdorff, D., 2006. MRI morphology of the levator ani muscle, endopelvic fascia, and urethra in women with stress urinary incontinence. Eur. J. Obstet. Gynecol. Reprod. Biol. 126, 239–245.

Tunn, R., Paris, S., Fischer, W., Hamm, B., Kuchinke, J., 1998. Static magnetic resonance imaging of the pelvic floor muscle morphology in women with stress urinary incontinence

and pelvic prolapse. Neurourol. Urodyn. 17, 579–589.

Van Delft, K., Thakar, R., Sultan, A.H., 2015. Pelvic floor muscle contractility: Digital assessment vs transperineal ultrasound. Ultrasound Obstet. Gynecol. 45, 217–222.

Verelst, M., Leivseth, G., 2007. Force and Stiffness of the Pelvic Floor as Function of Muscle Length : A Comparison Between Women With and Without Stress Urinary Incontinence. Neurourol. Urodyn. 857, 852–857.

Widmaier, E.P., Raff, H., Strang, K.T., 2008. Vander's human physiology: the mechanisms of human body function, 11 th. ed. McGraw-Hill, New York, NY.

Wu, J.M., Kawasaki, A., Hundley, A.F., Dieter, A.A., Myers, E.R., Sung, V.W., 2011. Predicting the number of women who will undergo incontinence and prolapse surgery, 2010 to 2050. Am. J. Obstet. Gynecol. 205, 1–5.

Yang, J., Yang, S., Yang, S., Yang, E., Huang, W., 2009. Reliability of real-time ultrasound to detect pelvic floor muscle contraction in urinary incontinent women. J Urol. 182, 2392–2396.

Ying, T., Li, Q., Xu, L., Liu, F., Hu, B., 2012. Three-dimensional ultrasound appearance of pelvic floor in nulliparous women and pelvic organ prolapse women. Int. J. Med. Sci. 9, 894–900.

Yip, C., Kwok, E., Sassani, F., Jackson, R., Cundiff, G., 2014. A biomechanical model to assess the contribution of pelvic musculature weakness to the development of stress urinary incontinence. Comput. Methods Biomech. Biomed. Engin. 17, 163–176.

Zhang, Y., Kim, S., Erdman, A.G., Roberts, K.P., Timm, G.W., 2009. Feasibility of using a computer modeling approach to study sui induced by landing a jump. Ann. Biomed. Eng. 37, 1425–1433.

Zhu, L., Lang, J.H., Chen, J., Chen, J., 2005. Morphologic study on levator ani muscle in patients with pelvic organ prolapse and stress urinary incontinence. Int. Urogynecol. J. Pelvic Floor Dysfunct. 16, 401–404.

Part B - Article 1

Establishing the Biomechanical Properties of the Pelvic Soft Tissues through an inverse Finite Element Analysis using Magnetic Resonance Imaging

M.E.T. Silva[a], S. Brandão[a,b], M.P.L. Parente[a], T. Mascarenhas[c],

R.M. Natal Jorge[a]

[a]LAETA, INEGI, Faculty of Engineering, University of Porto, Porto, Portugal
[b]Department of Radiology, Centro Hospitalar de São João-EPE, Faculty of Medicine, University of Porto, Porto, Portugal
[c]Department of Gynecology and Obstetrics, Centro Hospitalar de São João-EPE, Faculty of Medicine, University of Porto, Porto, Portugal

Published in: Proceedings of the Institution of Mechanical Engineers, Part H: Journal of Engineering in Medicine, 230(4):298-309, 2016.
doi: 10.1177/0954411916630571

Abstract

The mechanical characteristics of the female pelvic floor are relevant when explaining pelvic dysfunction. The decreased elasticity of the tissue often causes inability to maintain urethral position, also leading to vaginal and rectal descend when coughing or defecating as a response to an increase of the internal abdominal pressure. These conditions can be associated with changes in the mechanical properties of the supportive structures - namely the pelvic floor muscles - including impairment.

In this work, we used an inverse Finite Element Analysis to calculate the material constants for the passive mechanical behaviour of the pelvic floor muscles. The numerical model of the pelvic floor muscles and bones was built from magnetic resonance (MR) axial images acquired at rest. Muscle deformation, simulating the Valsalva manoeuvre with a pressure of 4 kPa, was compared with the muscle displacement obtained through additional dynamic MRI. The difference in displacement was of 0.15 mm in the antero-posterior direction and 3.69 mm in the supero-inferior direction, equating to a percentage error of 7.0% and 16.9%, respectively. We obtained the shortest difference in the displacements by using an iterative process that reached the material constants for the Mooney-Rivlin constitutive model *and* (C_{10}=11.8 kPa and C_{20}= 5.53E-02 kPa. For each iteration, the orthogonal distance between each node from the group of nodes, which defined the puborectal muscle in the numerical model *vs.* dynamic MRI, was computed.

With the methodology used in this work it was possible to obtain *in vivo* biomechanical properties of the pelvic floor muscles for a specific subject using input information acquired non-invasively.

Keywords: Soft Tissues, Pelvic Floor Muscles, Material Constants, Inverse Finite Element Analysis.

1. Introduction

The biological soft tissues connect, support, and surround organs and not only bone. These include tendons, ligaments, fascia, synovial membranes, muscles, nerves and blood vessels (Rivaux et al., 2013) that, due to high water content, can be seen as incompressible materials (Kauer et al., 2002). The elastic properties of these soft tissues depend on micro- and macroscopic structural organization (Murphy, 2013; Ophir et al., 2002), and generally they are able to support large deformations while returning to the initial configuration once the load is removed.

The female pelvic floor is an example of a soft tissue support structure that includes fascia, ligaments and muscles of the urogenital region. It extends from the *symphysis pubis* to the coccyx, and comprises the *urogenital hiatus* for the passage of the urethra, vagina and rectum (see Figure 1).

The mechanical characteristics of the female pelvic floor are relevant to explain pelvic dysfunction. The decreased elasticity of the tissues often causes inability to maintain the normal positions of the urethra, vagina and rectum. In this context, urinary incontinence and pelvic organ prolapse commonly occur when coughing or defecating due to an increase in intra-abdominal pressure (Thyer et al., 2008). Pelvic floor pathologies may result from impairment of the muscles or ligaments, or changes in their stiffness, as well as those in the pelvic fascia, associated to the changes in hormonal levels during pregnancy or menopause (Abramowitch et al., 2009; Rahn et al., 2008).

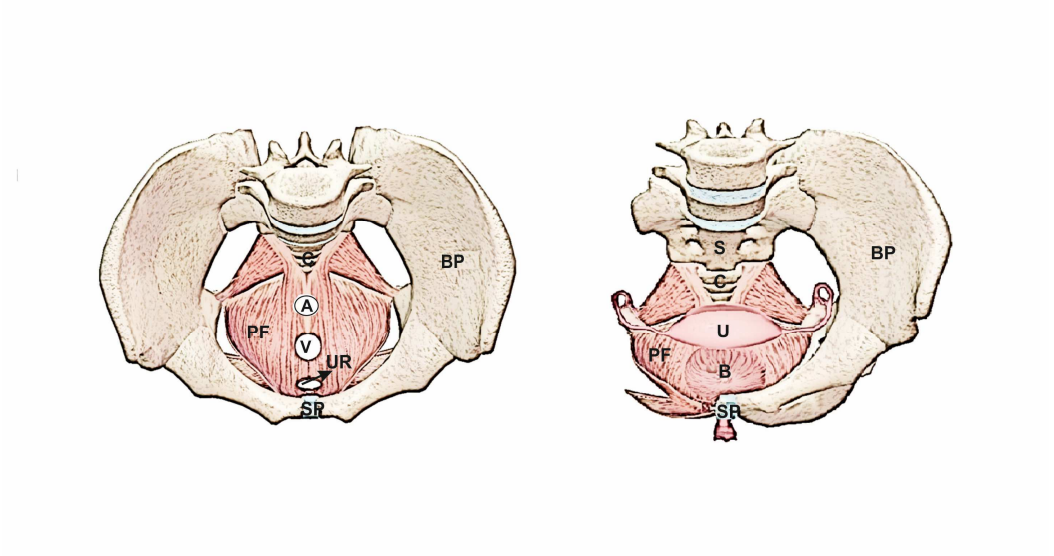

Figure 1. Female pelvic (floor) anatomy. (A - anus; B - bladder; BP - bony pelvis; C - coccyx; PF - pelvic floor muscles; SP - *symphysis pubis*; S - sacrum; U - uterus; Ur - urethra; V - vagina).

Radiographic evidence of lack of support to the pelvic organs and the widening of the *urogenital hiatus* comes mainly from evaluating muscle defects or ligament rupture on ultrasound or Magnetic Resonance (MR) images (Dietz, 2004; Tunn et al., 2006). By performing additional sagittal dynamic images during the Valsalva manoeuvre and coughing, one can evaluate the effect of the increase in intra-abdominal pressure over the pelvic viscera, and the counteracting (in)voluntary action of the muscles to suspend the organs (Moerman et al., 2012, 2011; Peng et al., 2007; Yang et al., 2009).

Furthermore, it is already possible to apply these two techniques to the *in vivo* analysis of the mechanical properties of soft tissues by performing elastography. Elastographic imaging uses mechanical waves made by hardware probes to quantify tissue response. The strain, the stiffness and Young´s *modulus* can be obtained by analysing the induced motion, images and quantitative measures of the tissue mechanical properties (Gennisson et al., 2010; Mariappan et al., 2010; Wells and Liang, 2011).

Ultrasound-based estimation of soft tissue strain and elasticity has been used by both to evaluate the reduction in uterine cervix stiffness during pregnancy and to predict successful labor induction (Swiatkowska-Freund and Preis, 2011). Similarly, this non-invasive assessment of the viscoelastic properties of skeletal muscle was applied to the study of normal and diseased muscle biomechanics, since changes in these properties can be associated with pathological conditions such as neuromuscular disorders (Mariappan et al., 2010). MR elastography has been shown to be sensitive to both relaxed and contracted states of the upper and lower limb muscles, mostly those fusiform, parallel or with low pennation angle (Dresner et al., 2001; Jenkyn et al., 2003; Ringleb et al., 2007). These are promising non-invasive tools for biomechanical analysis. However, they require additional hardware and software and therefore are still not available in all institutions; moreover, their validation is still an ongoing process (Oudry et al., 2009).

In this sense, most of the literature still focuses on *ex vivo* studies of the mechanical properties of the pelvic ligaments and fascia (Abramowitch et al., 2009; Jelen et al., 2010; Kirilova et al., 2011, 2009; Kondo et al., 1994; Rivaux et al., 2013) through mechanical tests that allow studying their biomechanical behaviour, such as the uniaxial and biaxial tensile tests(Jelen et al., 2010; Rivaux et al., 2013).These may be used to obtain information on force and displacement of the material, and therefore can be called as experimental or direct methods. For example, the endopelvic fascia, which surrounds the pelvic organs and attaches to the pelvic walls has a fibrous consistency due to its content in collagen fibers, elastic and a scattering of smooth muscle fibers (Jelen et al., 2010; Kirilova et al., 2009). Previous work has showed that high inter-individual variability of mechanical properties of the vaginal wall may be caused by the differences

in physical load, by the number of pregnancies and by the presence of other factors, e.g. obesity (Jelen et al., 2010).

On the other hand, the uterosacral ligaments, which are the main uterine supporters that maintain pelvic statics, demonstrated higher maximum stress and stiffness in uniaxial tensile tests when compared to the broad, and round ligaments (Martins et al., 2013; Rivaux et al., 2013). These studies showed that pelvic ligaments have a nonlinear mechanical behaviour, i.e., a nonlinear relationship between force and displacement.

The group of *levator ani* muscles (the puborectal, *pubococcygeus* and *iliococcygeus* muscles) is very important to the support of the pelvic organs and urethral closure as they counter the downward forces imposed to the organs and to the pelvic floor whenever intra-abdominal pressure is increased. Deficient contraction, which may be caused by direct neuromuscular damage, can result in major defecation disorders or vesico-uterine prolapse (Abramowitch et al., 2009). However, to our best knowledge, few studies have focused on the pelvic floor muscles in humans, due to the ethical challenges in obtaining samples (Abramowitch et al., 2009; Rahn et al., 2008). *Ex vivo* studies or animal models were used to investigate how risk factors (i.e. menopause and delivery) affect pelvic soft tissues biomechanical properties (Abramowitch et al., 2009; Rahn et al., 2008), and computer models using those mechanical properties were set to study their behaviour while simulating vaginal labor or defecation, and also when considering their damage (S. Brandão et al., 2015; Noakes et al., 2008; M. Parente et al., 2009; Parente et al., 2008; Saleme et al., 2011; Yip et al., 2014).

The finite element method is one of the most widely used approaches to discretize and solve complex modelling problems (Kaufmann et al., 2013). Numerical simulations of the pelvis use *in vitro* material properties from experimental studies with both normal

and pathological specimens (Martins et al., 2013; Rivaux et al., 2013; Rubod et al., 2012). To solve this issue, an inverse Finite Element Analysis (FEA) may be used to estimate the most accurate as well as the most-specific biomechanical properties. This process is known as the inverse FEA (Kauer et al., 2002).

Accordingly, the aim of this work was to use the inverse FEA to establish the biomechanical properties of the female pelvic floor muscles in order to achieve simulated biomechanical behaviour during the Valsalva manoeuvre. The model was built from static MR images, and has included the pelvic floor muscles and the bony pelvis. The numerical simulation was based on the finite element method, likewise the material constants of the Mooney-Rivlin constitutive model for the passive behaviour of the pelvic floor muscles were obtained through the inverse FEA. After the determination of the material constants, we compared the displacement of the pelvic floor muscle between the deformed numerical model and the 2D dynamic mid-sagittal image acquired at Valsalva manoeuvre.

2. Materials and Methods

Subject and Imaging

The Institutional Review Board approved this work (protocol: CES195/12). A nulliparous 30-year old female, with no complains or clinical findings indicating pelvic floor dysfunction, was scanned for a pelvic MRI exam. Sagittal, coronal and axial T2w

images were acquired in the supine position at rest using a 3T scanner (Magnetom® Tim Trio, Siemens Medical Solutions, Erlangen, Germany).

The MRI protocol included T2w fast spin-echo (FSE) 3-mm images acquired at rest in the three orthogonal planes. The main scanning parameters of these three sequences are: 24 slices in the axial plane along the puborectal line (Figure 2.a); 3 mm slices; 0.6 mm inter slice gap; TE/TR = 63/4270 ms; field-of-view 230x230 mm; matrix 224x320; voxel size 1.0×0.7×3.0 mm; 4 NSA (number of signals averaged); parallel imaging acceleration factor of two (iPAT 2) was applied; 2:39 min scanning time. Thirty six 3-mm slices were acquired in the sagittal plane; 0.6 mm gap; TE/TR = 69/4300 ms; field-of-view 260x260 mm; matrix 269x384; voxel size 1.0×0.7×3.0 mm; 3 NSA; iPAT 2; 2:54 min scanning time. Coronal images were also added (29 slices, 3 mm slices; 0.6 mm inter slice gap; TE/TR = 64/3800 ms; field-of-view 240x240 mm; matrix 288x320; voxel size 0.8×0.8×3.0 mm; 2 NSA; iPAT 2; 3:12 min scanning time.

Additional dynamic images at maximal Valsalva were obtained in the mid-sagittal plane, approximately every 2.0 s for a 10 s-period (5 images) using a half-Fourier acquisition single-shot turbo spin-echo (HASTE) pulse sequence (4 mm slice; TE/TR 95/2000 ms; field-of-view 260x260 mm; matrix 256x320; voxel size 1.0×0.8×4.0 mm; 1 NSA; iPAT 2). The mid-sagittal image was planned using the previous multiplanar scans. Three successive sets of these dynamic images were acquired with a 3 min interval. Prior to entering the MR room, and just before the dynamic acquisitions, the volunteer was instructed on how to perform the Valsalva manoeuvre properly by a physiotherapist with 4 years' experience in pelvic floor rehabilitation.

The radiologist observed all the datasets, and the best maximal Valsalva image was selected for analysis by measuring the most evident vertical descent of the organs

along a horizontal axis drawn at the outer side of the *periosteum* in the inferior edge of the pubic bone, and simultaneously having the wider hiatal sagittal diameter (Figure 2.c), as in (S. Brandão et al., 2015; Tumbarello et al., 2010). No pathological findings were described.

Figure 2 shows axial (a) and sagittal (b) images acquired at rest. (c) is the dynamic image in the mid-sagittal plane that was considered to better represent maximal Valsalva manoeuvre. Figure 2.a) shows that the puborectal muscle (PR) forms a sling around the *urogenital hiatus* to promote its closure, especially when performing voluntary contraction of the pelvic floor muscles. During the Valsalva manoeuvre, the relaxation of the puborectal muscle allows some degree of hiatal widening, as well as the opening of the anorectal angle, which is accompanied by some degree of verticalization of the *levator plate* (formed by the iliococcygeous muscle, in the upper portion of the pelvic floor). These features were previously described by both clinical dynamic MR imaging (Raizada and Mittal, 2008), and numerical simulation (Noakes et al., 2008), and are illustrated by the red line in Figure 2.c comparing its position at rest (Figure 2.b).

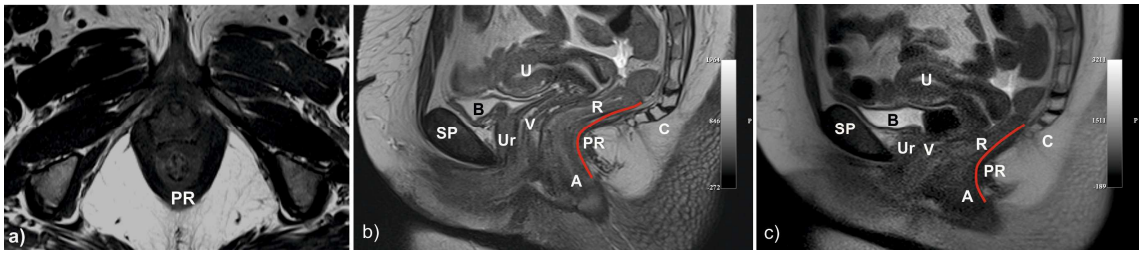

Figure 2. Magnetic Resonance images in the axial (a), sagittal (b) plane acquired at rest position, and during maximal Valsalva manoeuvre (c). The main pelvic organs are identified (A - anus; B - bladder; C - coccyx; PR - puborectal muscle; R - rectum; SP - *symphysis pubis*; U - uterus; Ur - urethra V - vagina).

Comparison between MR images acquired at rest vs. maximal Valsalva manoeuvre

To evaluate the displacement of the pelvic floor muscles obtained during maximal Valsalva, the dynamic image acquired in the mid-plane was compared with the one acquired at rest (Figure 3). For that purpose, a reference axis was set on the lower and posterior border of the *symphysis pubis* (F. S. Brandão et al., 2015; Peng et al., 2007) (straight white orthogonal lines). The antero-posterior diameter of the *urogenital hiatus* - measured from the postero-inferior border of the *symphysis pubis* to the puborectal muscle (dashed green line) - and the vertical position of the puborectal muscle (straight green line) were assessed. Since the puborectal muscle is considered the main constrictor of the pelvic floor, its displacement in the antero-posterior axis was considered as the difference between the length of the dashed green line in Figure 3.a) and b). Similarly, the supero-inferior displacement was considered as the vertical downward of the muscle (the sum of the length of the two straight green lines).

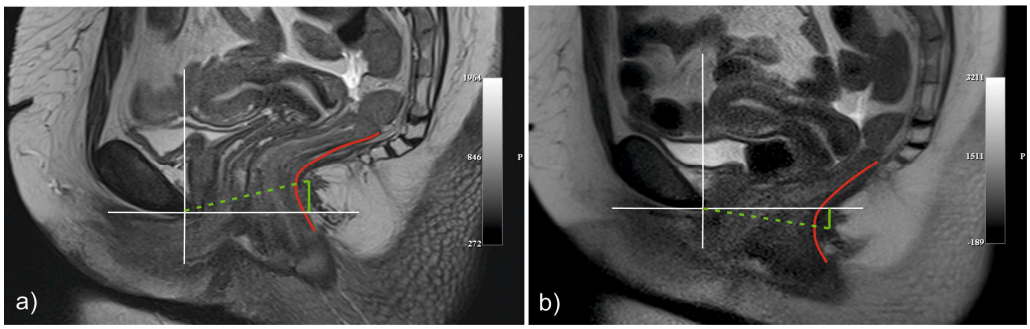

Figure 3. MR images in the mid-sagittal plane acquired at rest (a) and at maximal Valsalva manoeuvre (b). The antero-posterior *urogenital hiatus* diameter (dashed green line) and the supero-inferior displacement of the puborectal muscle (straight green line) were measured in both conditions. The difference and sum, respectively, were considered as reflecting the displacement of the pelvic floor muscles in both axes.

Finite Element Model

The T2w axial images were used to identify and segment the pelvic floor muscles and the surrounding bone structures by applying a semi-automatic procedure using the Mimics® software v. 16 (Software and Services for Biomedical Engineering, Materialise HQ, Belgium). To construct the primary 3D voxel volume of the *levator ani* and bones, an initial pixel intensity threshold was set for each one, and then the contours of their shape were obtained for the different slices. Additional refinements were hand-made using the anatomical images as reference. The resulting 3D triangulated surface model was generated from the voxel volume, and then the Mimics 3D default smoothing algorithm - based on the Laplacian 1st order function - was applied.

The triangulated 3D surface model was then imported to Abaqus software v. 6.12 (Dassault Systmes Simulia Corp., Providence, RI, USA). Subsequently, the finite element mesh (FEM) of the *levator ani* (with 16578 nodes, 78142 elements) was created, as shown in Figure 4. The FEM was generated by using hybrid linear tetrahedral elements (Abaqus C3D4H). The element size set was approximately constant throughout the geometry, resulting in a mesh with a characteristic element length of 2.3 mm.

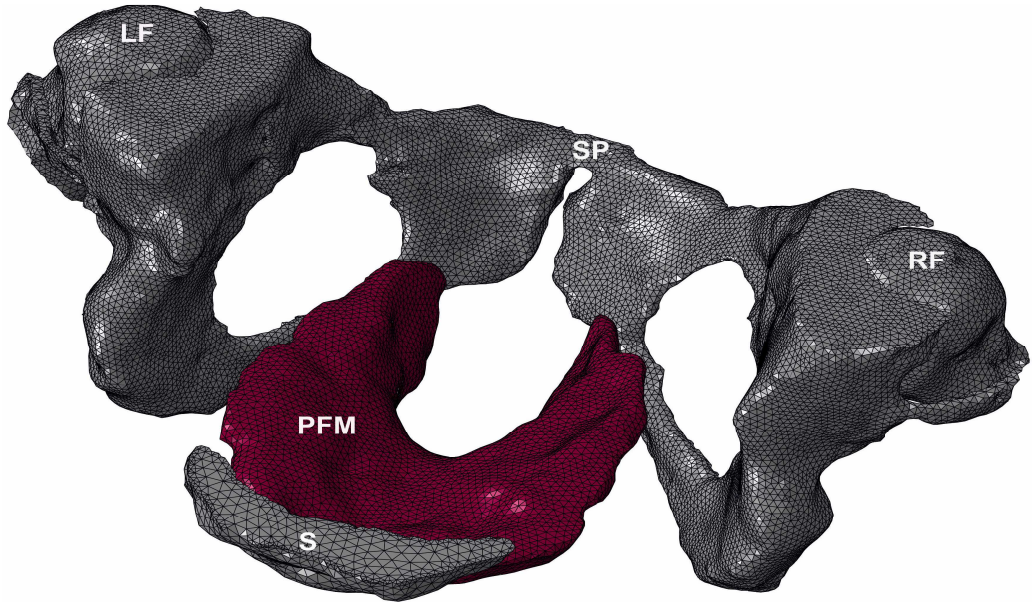

Figure 4. Oblique view of the finite element mesh built from the MR axial images. The pubic bone was included in the model to help defining the boundary conditions. LF - left femur; PFM - pelvic floor muscles; RF - right femur; S - sacrum; SP - *symphysis pubis*.

Definition of the boundary and loading conditions

The boundary conditions were defined in the insertion points of the muscles in the pubic bone, internal obturator fascia and coccyx visualized in the MR images, which were considered fixed (Parente et al., 2008; M. P. L. Parente et al., 2009; Rubod et al., 2012).

Loadings of 5.0E-01 kPa and 4.5 kPa were used, as simulating the mean intra-abdominal pressure value for supine at rest - representative of organ load - and Valsalva manoeuvre, respectively. The final pressure of 4 kPa was applied to the inner surface of the pelvic floor muscles, following the methodology described by (Noakes et al., 2008). This value of mean pressure was referred to as representative for numerical models of young women, with no complaints or clinical findings suggestive of pelvic floor

dysfunction, and taking into account the supine position inside the MR scanner during the exam (S. Brandão et al., 2015; Noakes et al., 2008).

The optimization process

The optimization algorithm searches for the suited set of material constants of the Mooney-Rivlin constitutive model, in order to minimize its objective function (Gao et al., 2013; Powell, 1977). In this study the objective function is the distance between the two reference curves represented in Figure 7. The material constants corresponding to the computed minimum of the objective function are assumed to represent the real tissue constants.

The Mooney-Rivlin constitutive model was used in this work, firstly because it is a simple model - with only two material constants to optimize - and also because it has been previously used by other authors to model the biomechanical behaviour of the pelvic floor muscles during simulation of Valsalva manoeuvre and defecation (Lee et al., 2005; Noakes et al., 2008).

From the many algorithms available for parameter optimization, we used the Powell's method. This is a local direct search algorithm that does not use the objective function derivatives. The advantages are its simplicity and efficiency, despite the fact that it is easily entrapped in a local optimum and its convergence being extremely sensitive to the starting point (Powell, 1977).

An inverse FEA was implemented to obtain the suited material constants for the Mooney-Rivlin constitutive model by using the Python scripting language to couple the MATLAB MathWorks v. R2013b (Mathematical Computing Software, Natick,

Massachusetts, USA) and the Abaqus software. A Python script was used to update the displacements of the nodes along a portion of the curve the puborectal muscle on the numerical model for each simulation (see Figure 5). To evaluate the objective function, we used a MATLAB code.

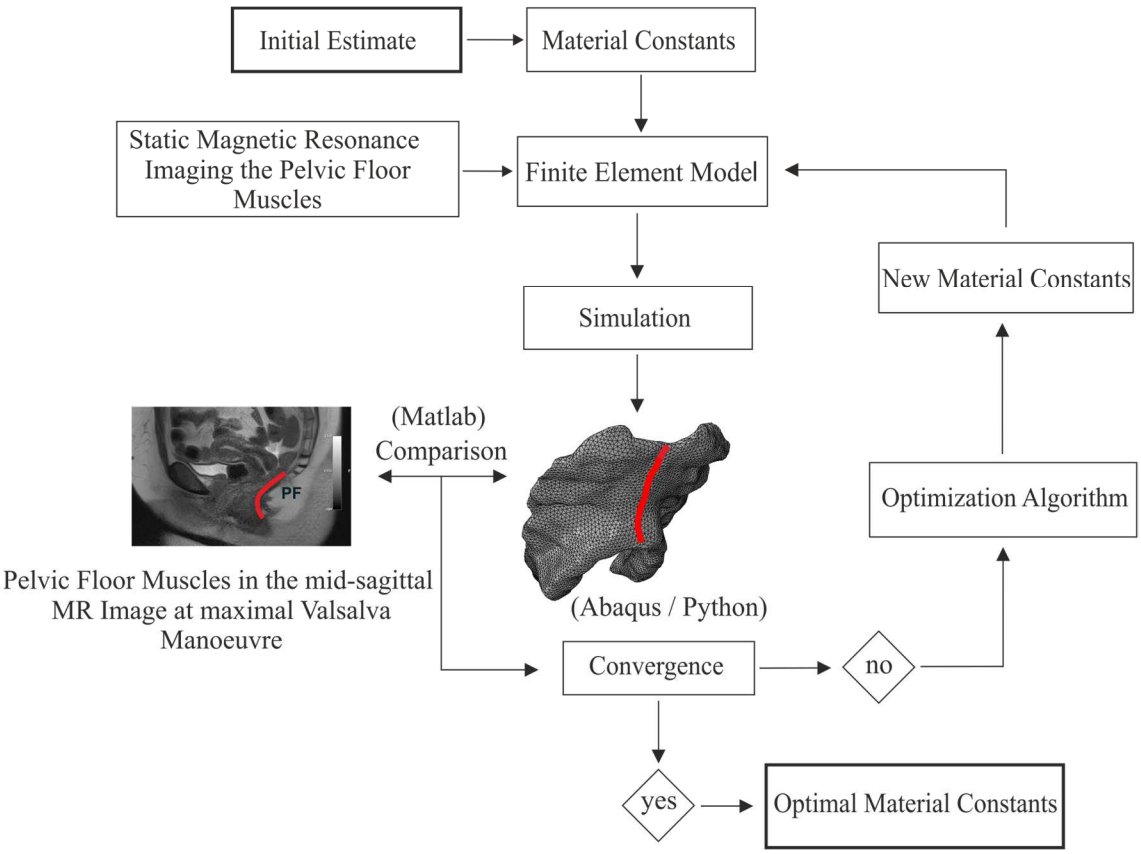

Figure 5. Flow chart of the inverse FEA. Several procedures were set to get the adjusted material constants of the Mooney-Rivlin constitutive model.

In order to simulate the mechanical behaviour of the non-striated pelvic floor muscles we used the Mooney-Rivlin constitutive material model (Martins et al., 2006). This was done because the Mooney-Rivlin constitutive material model is characterised by Eq. (1) when considering a fully incompressible material. It employs a nonlinear relationship between stress and strain to describe incompressible hyperelastic materials,

$$W = c_{10}(I_1 - 3) + c_{20}(I_2 - 3) \quad (1)$$

where W is the strain energy function and c_{10} and c_{20} are material constants that have dimensions of stress and that must be determined from experiments on the particular material being modelled, and I_1 and I_2 are principal strain invariants of the right Cauchy-Green tensor (Noakes et al., 2008).

The material law has to be chosen according to *a priori* knowledge of the mechanical properties of the target tissue. The determination of the material constants of the Mooney-Rivlin constitutive model contained in the chosen material law was then carried out by comparing the two curves representing the position of the puborectal muscle in both the deformed numerical model (see Figure 6) and the dynamic mid-sagittal image acquired at maximal Valsalva manoeuvre (see Figure 2.c).

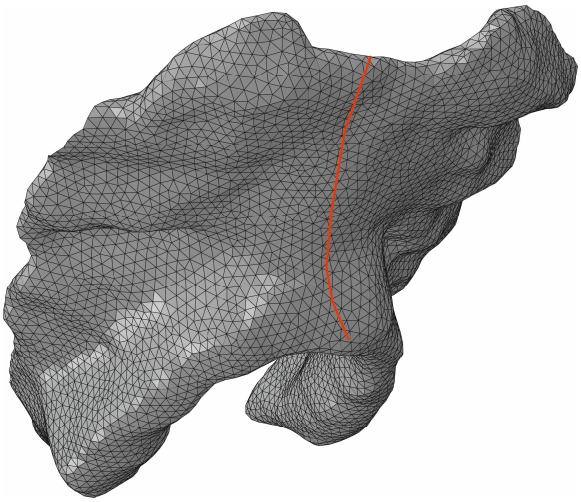

Figure 6. Numerical model of the pelvic floor muscles. The red line represents the curve drawn in the mid-sagittal plane from where nodes were chosen to calculate the error in the inverse FEA.

The inverse FEA using the Powell's method

Powell's method does not calculate the gradient, which is one of the most efficient, reliable and also one of the most widely known of the zero-order methods (Powell, 1977). It is based on the concept of conjugate directions $\mathbf{D}$, where $\mathbf{D}^i$ and $\mathbf{D}^j$ are conjugate if (Eq. 2):

$$(\mathbf{D}^j)^T \mathbf{H} \mathbf{D}^j = 0 \tag{2}$$

In Eq. (2), $\mathbf{H}$ is the Hessian matrix containing the second-order partial derivatives of the objective function $F(\mathbf{X})$, where $\mathbf{X} = \{x_1, x_2, \ldots, x_n\}$ is the vector enclosing the function material constants, as characterised by Eq. (3):

$$\mathbf{H} = \begin{bmatrix} \frac{\partial^2 F(\mathbf{X})}{\partial X_1^2} & \frac{\partial^2 F(\mathbf{X})}{\partial X_1 \partial X_2} & \cdots & \frac{\partial^2 F(\mathbf{X})}{\partial X_1 \partial X_n} \\ \frac{\partial^2 F(\mathbf{X})}{\partial X_2 \partial X_1} & \frac{\partial^2 F(\mathbf{X})}{\partial X_2^2} & \cdots & \frac{\partial^2 F(\mathbf{X})}{\partial X_2 \partial X_n} \\ \vdots & \vdots & \ddots & \vdots \\ \frac{\partial^2 F(\mathbf{X})}{\partial X_n \partial X_1} & \frac{\partial^2 F(\mathbf{X})}{\partial X_n \partial X_2} & \cdots & \frac{\partial^2 F(\mathbf{X})}{\partial X_n^2} \end{bmatrix} \tag{3}$$

While a detailed discussion of mathematical ramifications is not the subject here, it is important to understand that the concept of conjugacy is the basis of some of the more powerful search algorithms. The principal significance is that if we are given a quadratic function, it will be minimized in n or fewer conjugate search directions (Powell, 1977).

Since it is not possible to obtain the Hessian matrix for the present problem, an approximation for the Hessian matrix is used. The info resulting from the search is used

to build this approximation to $\mathbf{H}$. The procedure starts by assuming $\mathbf{H}$ as the identity matrix, as illustrated by Eq. (4),

$$\mathbf{H} = \begin{bmatrix} 1 & 0 & \dots & 0 \\ 0 & 1 & \dots & 0 \\ \vdots & \vdots & \ddots & \vdots \\ 0 & 0 & \dots & 1 \end{bmatrix} \tag{4}$$

where each column of $\mathbf{H}$ represents the unidirectional search vector $\mathbf{D}^i, i = 1, \ n$.

The basic concept of Powell's method is to start by searching the coordinate directions in the n orthogonal directions, with $\mathbf{D}^i, i = 1 \ldots n$. In each search, the vector $\mathbf{X}$ is updated according to Eq. (5):

$$\mathbf{X}^i = \mathbf{X}^{i-1} + \beta_i^* \mathbf{X}^{i-1} \mathbf{D}^i \tag{5}$$

Since the function to be optimized is the result of a finite element simulation, in order to obtain the optimum value for β^* in each direction, the constant β^* was tested with values from the vector: $\{-0.75, -0.50, -0.35, -0.25, 0.0, 0.25, 0.35, 0.50, 0.75\}$. After that, $\mathbf{D}^i$ is replaced in the matrix $\mathbf{H}$ by $\beta_i^* \mathbf{D}^i$ to give.

$$\mathbf{H} = \beta_1^* \mathbf{D}^1, \beta_2^* \mathbf{D}^2, ..., \beta_n^* \mathbf{D}^n \tag{6}$$

These directions do not usually conjugate but provide a starting point from which conjugate directions are built. Having completed the n unidirectional searches, a new

conjugate search direction is created by adding all the columns of $\mathbf{H}$. This becomes the $n+1$ search direction (Powell, 1977).

$$\mathbf{D}^{n+1} = \sum_{i=1}^{n} \beta_i^* \mathbf{D}^i \tag{7}$$

After the conjugate direction $\mathbf{D}^{n+1}$ is obtained, a new search for the optimum set of materials constants is conducted according to Eq. (8).

$$\mathbf{X}^{n+1} = \mathbf{X}^n + \beta_{n+1}^* \mathbf{D}^{n+1} \tag{8}$$

The first column of $\mathbf{H}$ which represents the direction of the first search in the matrix $\mathbf{H}$, is now deleted and all the columns orders are shifted in order for the new direction $\beta_{n+1}^* \mathbf{D}^{n+1}$ to be added. The entire process is repeated until convergence is satisfied.

Application of the inverse FEA to the pelvic floor muscles

In the present case, the material constants for the Mooney-Rivlin constitutive model were obtained from the vector associated to $\mathbf{X}^{n+1}$ in Eq. (8) through the inverse FEA. The aim was to update the material constants along an iteration process. The error measure was based on the comparison of a set of points in two different curves: one representing the position of the puborectal muscle in the numerical model for each iteration and consequent deformation, and the other curve represents of the position of

the puborectal muscle in the dynamic mid-sagittal image acquired at Valsalva manoeuvre. For each of the iterations, we computed the orthogonal distance between each point from the group of nodes that define the puborectal muscle in the numerical model *vs.* dynamic MR image (Figure 7). The sum of all the distances represents the error measure between the two curves, and the stopping criteria was set to <10mm. Eq. (9) characterises the computation of the error measure, as follows:

$$Error = \sum_{i=1}^{np} \left\| d_{MRI_i} - d_{FEA_i} \right\| \tag{9}$$

Where *np* is the number of points d_{MRI_i} is used to define the first curve and d_{FEA_i} is the closest point projection of d_{MRI_i} on the second curve. By applying an iterative process, the suited material constants were found, corresponding to the ones in the iteration with a minimum error (Table 1).

The resulting values of displacements of the pelvic floor muscles in the antero-posterior and supero-inferior directions were compared for the numerical model *vs.* the dynamic MRI by calculating the percentage of error (Table 2), having in the same reference axis (see Figure 3).

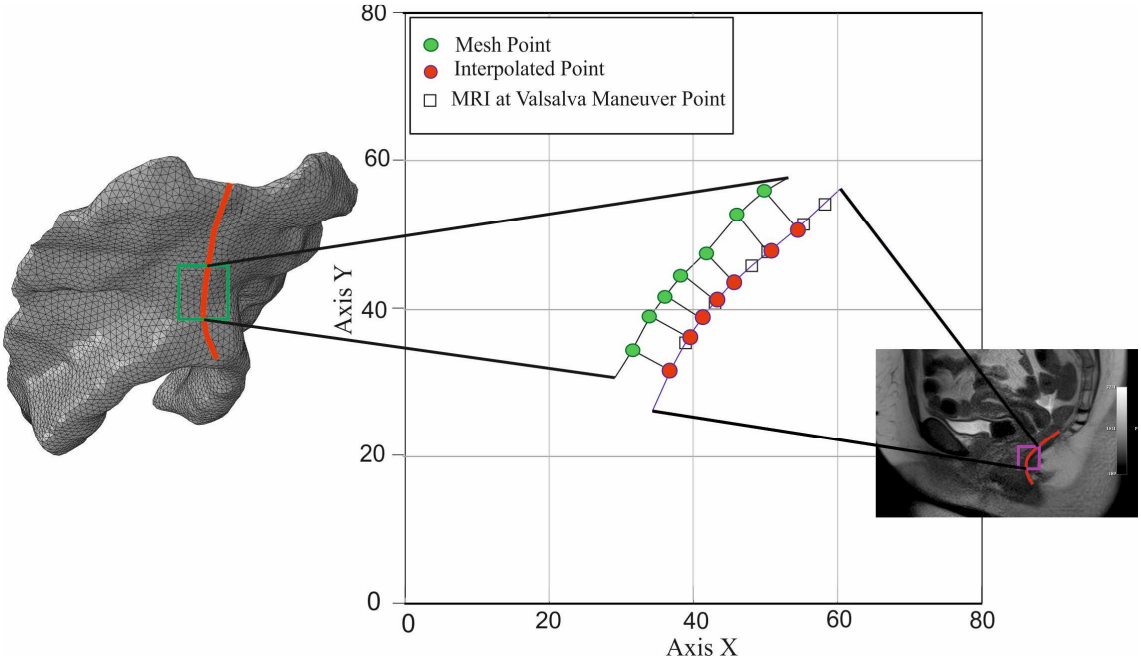

Figure 7. Illustration of the points chosen to represent the puborectal muscle on the numerical model (green points), the curve showing the deformed muscle in the mid-sagittal MR image acquired at Valsalva manoeuvre (blue curve with the black squares) and the interpolated points (red points).

3. Results

The antero-posterior displacement of the puborectal muscle opened the *urogenital hiatus* from 55.22 mm at rest (dashed green line in Figure 3.a)) to 57.35 mm in Valsalva (dashed green line in Figure 3.b)), while the muscle descended 21.84 mm (straight green line in Figure 3).

Table 1 shows the number of iterations of the inverse FEA, the material constants of the Mooney-Rivlin constitutive model, and the error, respectively. After 5 iterations, the material constants for the passive behaviour of the pelvic floor muscles obtained in

Valsalva converged to c_{10} =11.8 kPa and c_{20} =5.53E−2 kPa with a minimum error margin of 8.73 mm.

Table 1. Values of the material constants for the Mooney-Rivlin constitutive model and the error measure during the iterative process.

Iterations	***c_{10} (kPa)***	***c_{20} (kPa)***	***Error (mm)***
0 (Initial)	2000	1000	84.2
1	253	2.51	75.9
2	251	1.18	75.8
3	62.8	2.95E-1	57.3
4	15.7	7.38E-2	13.4
5 (Final)	11.8	5.53E-2	8.73

Table 2 presents the differences in the displacement of the pelvic floor muscles in the numerical simulation *vs.* in MRI, as represented by the posterior and inferior displacement of the puborectal muscle. When comparing the two, the vertical axis showed a higher error percentage (16.9%) than the horizontal axis (7.0%).

Figures 8 shows the numerical model overlaid with the sagittal MR images at rest (Figure 8.a)) and Valsalva manoeuvre (Figure 8.b)), when a pressure of 4 kPa was applied.

Table 2. Displacement of the pelvic floor muscles mesh, obtained from the 5th iteration, compared with the dynamic MRI. Evolution of the percentage of error, calculated for the different iterations. (PFM = pelvic floor muscles).

Displacement axis	***PFM displacement from MRI (rest vs. Valsalva) (mm)***	***PFM displacement from the numerical model (rest vs. Valsalva) (mm)***	***% Error for the iteration***				
			1	***2***	***3***	***4***	***5***
antero-posterior (opening of the urogenital hiatus)	2.13	1.98	85.9	81.6	43.7	36.6	7.0
supero-inferior (puborectal muscle)	21.84	18.15	91.1	91.1	73.5	32.7	16.9

The numerical simulation of the passive behaviour of the pelvic floor muscles at Valsalva manoeuvre showed a downward and posterior movement. Figure 9 illustrates the magnitude of the displacement (a) and the principal logarithmic strain (b). The greatest displacement was observed for the posterior area of the puborectal muscle, ranging from [18.18 - 19.83] mm, using the material constants obtained in the 5th iteration. The principal logarithmic strain shows that the elements that represent the insertion points display the highest values, along with the mid-posterior portion of the puborectal muscle.

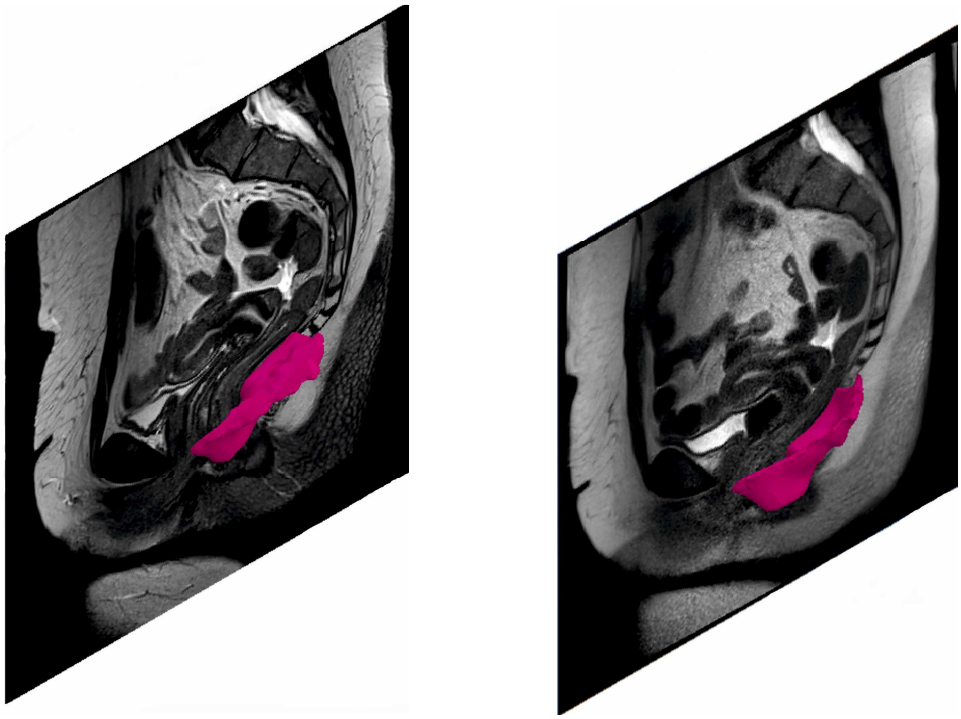

a) b)

Figure 8. The pelvic floor muscles overlaid with the mid-sagittal slices acquired at rest (a) and at maximal Valsalva (b).

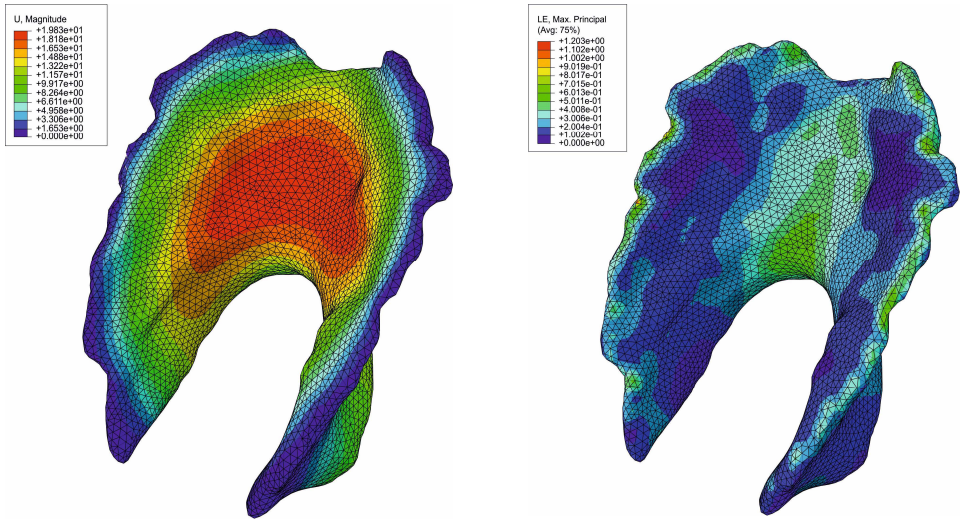

a) b)

Figure 9. Pelvic floor muscles displacement (a) and logarithmic strain (b) for Valsalva manoeuvre.

4. Discussion

The deformation of the pelvic floor muscles depends on the material constants for the Mooney-Rivlin constitutive model. The inverse FEA with an optimization algorithm was used in this work, and the values for the material constants obtained were $c_{10} = 11.8$ kPa and $c_{20} = 5.53E-02$ kPa, which are different from the ones published by (Lee et al., 2005) ($c_{10} = 2.5$ kPa and $c_{20} = 6.25E-01$ kPa). This difference in the range of magnitude can be associated, not only to the subject-specific thickness and morphology of the pelvic floor muscles, but also with the pressure applied. A thinner muscle or higher pressure would most probably determine a higher degree of muscle downward displacement.

The Valsalva manoeuvre is frequently performed in clinical environments to assess muscle (in)ability to prevent urethral hypermobility or organ prolapse, which are the basis pelvic disorders (Hendrix et al., 2002; Swift, 2000). Future work will focus on analysing numerical models from women with thinner or disrupted muscles presenting urinary incontinence or pelvic prolapse.

We used live-subject data to study the passive mechanical behaviour of the pelvic floor muscles by comparing computer simulation of muscle displacement *vs.* dynamic MRI. The values of antero-posterior and supero-inferior directions were concordant in the two methods (1.98 mm *vs.* 2.13 mm, and 18.15 mm *vs.* 21.84 mm, respectively). During the Valsalva manoeuvre, the puborectal muscle is the main constrictor of the *urogenital hiatus*, and counteracts organ descend during intra-abdominal pressure (Noakes et al., 2008) by avoiding posterior dislocation, and this is the reason why the antero-posterior displacement (rest *vs.* Valsalva) is a mere 2.13 mm. The inverse FEA seems to correctly mimic that behaviour, since the displacement obtained was of 1.98

mm. On the contrary, the thinner iliococcygeus muscle may not be able to avoid the caudal dislocation of the organs.

The higher percentage error in the vertical axis (16.9% *vs.* 7.0%) may be related to the differences between the pressure applied in the numerical simulation *vs.* the live subject scanning, and also to assumptions and simplifications in the finite element model, as for example, the fixed boundary conditions in the obturator fascia. This fact may also explain the areas of higher strain values along the insertion points.

To properly interpret our findings, it is important to consider the limitations and simplifications involved. The first one is related to the absence of the connectivity with other tissues (the pelvic organs, fascia and ligaments) and the sliding interactions, which would render a more realistic model of the pelvic cavity. Secondly, information about muscle tone will also be important to better understand the contractile behaviour of the pelvic floor muscles. This is important since, if the muscle contracts and relaxes in a non-uniform manner when subjected to intra-abdominal pressure, then incorporating this irregularity into the simulation will require the use of an active contractile mechanical model, as previously published (M. Parente et al., 2009). Thirdly, the pressure applied in the model to mimic Valsalva manoeuvre was retrieved from the literature (Noakes et al., 2008), but one cannot guarantee that the same pressure was performed by the young female during the scanning. A better approximation would be achieved by means of an intracavitary measurement instrument. Finally, the Mooney-Rivlin constitutive model was used to characterise the mechanical behaviour of the pelvic floor muscles. Future work may include applying spatially varying mechanical properties to obtain more realistic results. In that sense, the numerical simulation of this study was based on passive mechanical behaviour of the pelvic floor muscles; in this passive state, the viscoelastic properties were neglected to simplify the model. A quasi-incompressible transversely

isotropic hyperelastic model (Martins et al., 1998) could perhaps more accurately reproduce the nonlinear stress-strain relationship and anisotropic behaviour of the muscles, although at the expense of an increased number of material constants.

Despite the limitations mentioned above, this numerical simulation yielded promising results that were consistent with published experimental data. Therefore, the use of data obtained non-invasively and the optimization of algorithms may enable estimating accurate and subject-specific material constants. This can help understand the influence of the tissue mechanical properties on the development of pelvic floor disorders.

Another possible improvement is the incorporation of tissue anisotropy in the finite element model. Diffusion Tensor (DT) MRI (Damon et al., 2011; Oudeman et al., 2016) can be used to non-invasively assess muscle fiber directions throughout the field-of-view. These directions (given by the first eigenvectors of the diffusion tensor) can then be directly incorporated to set the local fiber directions in the finite element model for each element.

DTI was recently applied to the study of the female pelvic floor muscles (Zijta et al., 2012, 2011), and fiber tractography - the three-dimensional representation - was satisfactory for the global morphology and fiber direction of the pubovisceral muscle, perineal body and internal obturator muscle, among other structures. Although DTI is feasible for the pelvic floor, it has to be carefully considered in the clinical setting. This technique is very prone to several sources of artifacts, such as the ones resulting from breathing or peristalsis, requiring the patient´s careful preparation and cooperation. Additionally, ghosting artifacts due to eddy currents may hamper the images and have to be removed. Furthermore, echo planar imaging - which is the basis for DTI studies - often suffers from positional shift and distortion due to the low bandwidth applied, and also from susceptibility artifacts resulting from field heterogeneities that arise from the

presence of air in the bowel. Also, in addition to the complex multidirectional anatomy, the small thickness of the pelvic floor requires a trade-off between spatial resolution and signal-to-noise ratio that may impair the accuracy of the DTI and fiber tractography. Due to these drawbacks, the post-processing of the DTI datasets requires filtering for noise suppression and distortion correction to minimize these sources of image quality loss. Furthermore, as a non-automatic method, the post processing is time-consuming, iterative and user-dependent.

Another approach in the biomechanical modelling could be the 3D computation of motion from 2D MR tagged images in order to improve the quantification of the soft tissue motion (Xiaofeng et al., 2012). MR tagging is a well-known method to track local deformations during contraction of the heart. It enables parameters such as twist, strain and strain rate to be derived (Axel et al., 2005). Although accurate, it is time consuming and presents lower spatial resolution of tags than other experimental measurements such as optical or digital image correlation techniques. The main limitation of this technique is the large amount of repetitions that are often required. Some studies applied 60 repetitions (Axel et al., 2005; Ozturk and McVeigh, 2000) while (Moerman et al., 2012) performed 3 repetitions in a study of skeletal muscle, i.e. once for each motion direction. 3D tagging of a grid of points with a spacing of 3mm could be considered as a potential improvement to manual contour.

More recently, the development of harmonic phase (HARP) (Osman et al., 1999) and displacement encoding stimulated echo (DENSE) (Aletras and Wen, 2001) methods have made it possible to quantify the displacement at each voxel of the myocardium. HARP and DENSE have been used in 3D, however like for all of these methods, to obtain 3D displacements, a combination of 3 measurements is required, i.e. 1 for each direction.

Although these approaches still present some limitations, future developments will facilitate obtaining the biomechanical properties of the pelvic floor muscles *in vivo* based on the combination of non-invasive imaging and inverse FEA.

The inverse FEA allowed obtaining a displacement field from different MRI datasets, and the iterative process reached subject-specific tissue properties that enabled representing the (ab)normal kinematics of daily life activities of many women. We believe that this method can be clinically used in the planning of surgical procedures for incontinence or prolapse. In order to correct these conditions, mesh implants can be used, and to improve their efficiency it is important to characterise the mechanical properties of the pelvic tissues. In this sense, the inverse FEA implemented in this work may provide the mechanical properties of the pelvic floor muscles that can be used to optimize those of the mesh implants - such as its stiffness - in order to reduce failure rates of surgical procedures.

In conclusion, the inverse FEA used in this study allowed establishing the material constants of the female pelvic floor muscles in order to simulate a more realistic behaviour. Muscle deformation in the numerical simulation was compared to muscle displacement in the dynamic MRI and the results were consistent.

Conflict of interest statement

The authors declare that there is no financial, professional or other personal interest of any nature or kind in any product, service and/or company that could be constructed as influencing the position.

Acknowledgment

The authors gratefully acknowledge the funding by Ministério da Ciência Tecnologia, e Ensino Superior, FCT, Portugal, under grants SFRH/BD/89519/2012 and IF/00159/2014, and the project UID/EMS/50022/2013.

References

Abramowitch, S.D., Feola, A., Jallah, Z., Moalli, P.A., 2009. Tissue mechanics, animal models, and pelvic organ prolapse: a review. Eur. J. Obstet. Gynecol. Reprod. Biol. 144, S146–S158.

Aletras, A.H., Wen, H., 2001. Mixed echo train acquisition displacement encoding with stimulated echoes: an optimized DENSE method for in vivo functional imaging of the human heart. Magn. Reson. Med. 46, 523–34.

Axel, L., Montillo, A., Kim, D., 2005. Tagged magnetic resonance imaging of the heart: a survey. Med. Image Anal. 9, 376–393.

Brandão, F.S., Parente, M.P., Rocha, P.A., Saraiva, M.T., Ramos, I.M., Natal Jorge, R.M., 2015. Modeling the contraction of the pelvic floor muscles. Comput Methods Biomech Biomed Engin. 8, 1–10.

Brandão, S., Parente, M., Mascarenhas, T., da Silva, A.R.G., Ramos, I., Jorge, R.N., 2015. Biomechanical study on the bladder neck and urethral positions: Simulation of impairment of the pelvic ligaments. J. Biomech. 48, 217–223.

Damon, B.M., Buck, A.K.W., Ding, Z., 2011. Diffusion-tensor MRI-based skeletal muscle fiber tracking. Imaging Med. 3, 675–687.

Dietz, H.P., 2004. Ultrasound imaging of the pelvic floor. Part II: three-dimensional or volume imaging . Ultrasound Obs. Gynecol. 23, 615–25.

Dresner, M.A., Rose, G.H., Rossman, P.J., Muthupillai, R., Manduca, A., Ehman, R.L., 2001. Magnetic resonance elastography of skeletal muscle. J. Magn. Reson. Imaging 13, 269–276.

Gao, W., Liu, S., Huang, L., 2013. A novel artificial bee colony algorithm with Powell's method.

Appl. Soft Comput. 13, 3763–3775.

Gennisson, J., Deffieux, T., Macé, E., Montaldo, G., Fink, M., Tanter, M., 2010. Viscoelastic and anisotropic mechanical properties of in vivo muscle tissue assessed by supersonic shear imaging. Ultrasound Med Biol 35, 789–801.

Hendrix, S.L., Clark, A., Nygaard, I., Aragaki, A., Barnabei, V., McTiernan, A., 2002. Pelvic organ prolapse in the women's health initiative: Gravity and gravidity. Am. J. Obstet. Gynecol. 186, 1160–1166.

Jelen, K., Herman, H., Lopot, F., Kubovy, P., Otcenasek, M., Sedlacek, R., 2010. Women with incorrect pelvic floor statics: a biomechanical answer to the mechanical loading of the vagina-endopelvic fascia complex. Neuroendocrinol. Lett. 31, 413–417.

Jenkyn, T., Ehman, R., An, K., 2003. Noninvasive muscle tension measurement using the novel technique of magnetic resonance elastography (MRE). J Biomech 36, 1917–21.

Kauer, M., Vuskovic, V., Dual, J., Szekely, G., Bajka, M., 2002. Inverse finite element characterization of soft tissues. Med. Image Anal. 6, 275–87.

Kaufmann, P., Wang, O., Sorkine-Hornung, A., Sorkine-Hornung, O., Smolic, A., Gross, M., 2013. Finite Element Image Warping. Comput. Graph. Forum 32, 31–39.

Kirilova, M., Stoytchev, S., Pashkouleva, D., Kavardzhikov, V., 2011. Experimental study of the mechanical properties of human abdominal fascia. Med. Eng. Phys. 33, 1–6.

Kirilova, M., Stoytchev, S., Pashkouleva, D., Tsenova, V., Hristoskova, R., 2009. Visco-elastic mechanical properties of human abdominal fascia. J. Bodyw. Mov. Ther. 13, 336–337.

Kondo, A., Narushima, M., Yoshikawa, Y., Hayashi, H., 1994. Pelvic fascia strength in women with stress urinary incontinence in comparison with those who are continent. Neurourol. Urodyn. 13, 507–13.

Lee, S., Darzi, A., Yang, G., 2005. Subject Specific Finite Element Modelling of the Levator Ani. Med. Image Comput. Comput. Interv. 3749, 360–367.

Mariappan, Y.K., Glaser, K.J., Ehman, R.L., 2010. Magnetic resonance elastography: A review. Clin. Anat. 23, 497–511.

Martins, J.A.C., Pires, E.B., Salvado, R., Dinis, P.B., 1998. A numerical model of passive and active behavior of skeletal muscles. Comput. Methods Appl. Mech. Eng. 151, 419–433.

Martins, P., Jorge, R.N., Ferreira, A., 2006. A Comparative Study of Several Material Models for Prediction of Hyperelastic Properties: Application to Silicone-Rubber and Soft Tissues.

Strain 42, 135–147.

Martins, P., Silva-Filho, A.L., Fonseca, A.M.R.M., Santos, A., Santos, L., Mascarenhas, T., Jorge, R.M.N., Ferreira, A.M., 2013. Strength of round and uterosacral ligaments: a biomechanical study. Arch. Gynecol. Obstet. 287, 313–8.

Moerman, K., Sprengers, A., Simms, C., Lamerichs, R., Stoker, J., Nederveen, A., 2012. Validation of continuously tagged MRI for the measurement of dynamic 3D skeletal muscle tissue deformation. Med Phys. 39, 1973–810.

Moerman, K., Sprengers, A., Simms, C., Lamerichs, R., Stoker, J., Nederveen, A., 2011. Validation of SPAMM tagged MRI based measurement of 3D soft tissue deformation. Med Phys. 38, 1248–1260.

Murphy, J.G., 2013. Transversely isotropic biological, soft tissue must be modelled using both anisotropic invariants. Eur. J. Mech. - A/Solids 42, 90–96.

Noakes, K.F., Pullan, A.J., Bissett, I.P., Cheng, L.K., 2008. Subject specific finite elasticity simulations of the pelvic floor. J. Biomech. 41, 3060–3065.

Ophir, J., Alam, S.K., Garra, B.S., Kallel, F., Konofagou, E.E., Krouskop, T., Merritt, C.R.B., Righetti, R., Souchon, R., Srinivasan, S., Varghese, T., 2002. Elastography: Imaging the elastic properties of soft tissues with ultrasound. J. Med. Ultrason. 29, 155–171.

Osman, N.F., Kerwin, W.S., McVeigh, E.R., Prince, J.L., 1999. Cardiac motion tracking using CINE harmonic phase (HARP) magnetic resonance imaging. Magn. Reson. Med. 42, 1048–60.

Oudeman, J., Nederveen, A.J., Strijkers, G.J., Maas, M., Luijten, P.R., Froeling, M., 2016. Techniques and applications of skeletal muscle diffusion tensor imaging: A review. J. Magn. Reson. Imaging 43, 773–788.

Oudry, J., Chen, J., Glaser, K., Miette, V., Sandrin, L., Ehman, R., 2009. Cross-validation of magnetic resonance elastography and ultrasound-based transient elastography: a preliminary phantom study. J Magn Reson Imaging 30, 1145–50.

Ozturk, C., McVeigh, E.R., 2000. Four-dimensional B-spline based motion analysis of tagged MR images: introduction and in vivo validation. Phys Med Biol. 45, 1683–1702.

Parente, M., Natal Jorge, R., Mascarenhas, T., Fernandes, A., Martins, J., 2009. The influence of the material properties on the biomechanical behavior of the pelvic floor muscles during vaginal delivery. J. Biomech. 42, 1301–1306.

Parente, M., Natal Jorge, R., Mascarenhas, T., Fernandes, A., Martins, J., 2008. Deformation of the pelvic floor muscles during a vaginal delivery. Int. Urogynecol. J. Pelvic Floor Dysfunct. 19, 65–71.

Parente, M.P.L., Jorge, R.M.N., Mascarenhas, T., Fernandes, A.A., Martins, J.A.C., 2009. The influence of an occipito-posterior malposition on the biomechanical behavior of the pelvic floor. Eur. J. Obstet. Gynecol. Reprod. Biol. 144, S166–S169.

Peng, Q., Jones, R., Shishido, K., Constantinou, C.E., 2007. Ultrasound evaluation of dynamic responses of female pelvic floor muscles. Ultrasound Med. Biol. 33, 342–352.

Powell, M.J.D., 1977. Restart procedures for the conjugate gradient method. Math. Program. 12, 241–254.

Rahn, D.D., Ruff, M.D., Brown, S.A., Tibbals, H.F., Word, R.A., 2008. Biomechanical properties of the vaginal wall: effect of pregnancy, elastic fiber deficiency, and pelvic organ prolapse. Am. J. Obstet. Gynecol. 198, 590.e1-590.e6.

Raizada, V., Mittal, R.K., 2008. Pelvic Floor Anatomy and Applied Physiology. Gastroenterol Clin North Am 37, 493–497.

Ringleb, S.I., Bensamoun, S.F., Chen, Q., Manduca, A., An, K.N., Ehman, R.L., 2007. Applications of magnetic resonance elastography to healthy and pathologic skeletal muscle. J. Magn. Reson. Imaging 25, 301–309.

Rivaux, G., Rubod, C., Dedet, B., Brieu, M., Gabriel, B., Cosson, M., 2013. Comparative analysis of pelvic ligaments: a biomechanics study. Int. Urogynecol. J. 24, 135–9.

Rubod, C., Brieu, M., Cosson, M., Rivaux, G., Clay, J.C., De Landsheere, L., Gabriel, B., 2012. Biomechanical properties of human pelvic organs. Urology 79, 968.e17-968.e22.

Saleme, C.S., Parente, M.P.L., Natal Jorge, R.M., Pinotti, M., Silva-Filho, A.L., Roza, T., Mascarenhas, T., Tavares, J.M.R.S., 2011. An approach on determining the displacements of the pelvic floor during voluntary contraction using numerical simulation and MRI. Comput. Methods Biomech. Biomed. Engin. 14, 365–370.

Swiatkowska-Freund, M., Preis, K., 2011. Elastography of the uterine cervix: implications for success of induction of labor. Ultrasound Obs. Gynecol. 38, 52–6.

Swift, S.E., 2000. The distribution of pelvic organ support in a population of female subjects seen for routine gynecologic health care. Am. J. Obstet. Gynecol. 183, 277–85.

Thyer, I., Shek, C., Dietz, H.P., 2008. New imaging method for assessing pelvic floor

biomechanics. Ultrasound Obstet. Gynecol. 31, 201–205.

Tumbarello, J.A., Hsu, Y., Lewicky-Gaupp, C., Rohrer, S., DeLancey, J.O.L., 2010. Do repetitive Valsalva maneuvers change maximum prolapse on dynamic MRI? Int. Urogynecol. J. Pelvic Floor Dysfunct. 21, 1247–1251.

Tunn, R., Goldammer, K., Neymeyer, J., Gauruder-Burmester, A., Hamm, B., Beyersdorff, D., 2006. MRI morphology of the levator ani muscle, endopelvic fascia, and urethra in women with stress urinary incontinence. Eur. J. Obstet. Gynecol. Reprod. Biol. 126, 239–245.

Wells, P.N., Liang, H.D., 2011. Medical ultrasound: imaging of soft tissue strain and elasticity. J R Soc Interface 7;8, 1521–49.

Xiaofeng, L., Z. Abd-Elmoniem, K., Stone, M., Murano, E.Z., Zhuo, J., Gullapalli, R.P., Prince, J.L., 2012. Incompressible Deformation Estimation Algorithm (IDEA) from Tagged MR Images. IEEE Trans Med Imaging 31, 326–340.

Yang, J., Yang, S., Yang, S., Yang, E., Huang, W., 2009. Reliability of real-time ultrasound to detect pelvic floor muscle contraction in urinary incontinent women. J Urol. 182, 2392–2396.

Yip, C., Kwok, E., Sassani, F., Jackson, R., Cundiff, G., 2014. A biomechanical model to assess the contribution of pelvic musculature weakness to the development of stress urinary incontinence. Comput. Methods Biomech. Biomed. Engin. 17, 163–176.

Zijta, F.M., Froeling, M., Van Der Paardt, M.P., Lakeman, M.M.E., Bipat, S., Montauban Van Swijndregt, A.D., Strijkers, G.J., Nederveen, A.J., Stoker, J., 2011. Feasibility of diffusion tensor imaging (DTI) with fibre tractography of the normal female pelvic floor. Eur. Radiol. 21, 1243–1249.

Zijta, F.M., Lakeman, M.M.E., Froeling, M., Van Der Paardt, M.P., Borstlap, C.S. V, Bipat, S., Montauban Van Swijndregt, A.D., Strijkers, G.J., Roovers, J.P., Nederveen, A.J., Stoker, J., 2012. Evaluation of the female pelvic floor in pelvic organ prolapse using 3.0-Tesla diffusion tensor imaging and fibre tractography. Eur. Radiol. 22, 2806–2813.

Part B - Article 2

Biomechanical properties of the pelvic floor muscles of continent and incontinent women using an inverse finite element analysis

M.E.T. Silva[a], S. Brandão[a,b] , M.P.L. Parente[a], T. Mascarenhas[c],

R.M. Natal Jorge[a]

[a]LAETA, INEGI, Faculty of Engineering, University of Porto, Porto, Portugal
[b]Department of Radiology, Centro Hospitalar de São João-EPE, Faculty of Medicine, University of Porto, Porto, Portugal
[c]Department of Gynecology and Obstetrics, Centro Hospitalar de São João-EPE, Faculty of Medicine, University of Porto, Porto, Portugal
Published in: Computer Methods in Biomechanics and biomedical Engineering, 20(8):842-852, 2017.
doi: 10.1080/10255842.2017.1304542

Abstract

Pelvic disorders can be associated with changes in the biomechanical properties in the muscle, ligaments and/or connective tissue form fascia and ligaments. In this sense, the study of their mechanical behavior is important to understand the structure and function of these biological soft tissues.

The aim of this study was to establish the biomechanical properties of the pelvic floor muscles of continent and incontinent women, using an inverse finite element analysis (FEA). The numerical models, including the pubovisceral muscle and pelvic bones were built from magnetic resonance (MR) images acquired at rest. The numerical simulation of Valsalva manoeuvre was based on the finite element method and the material constants were determined for different constitutive models (Neo-Hookean, Mooney-Rivlin and Yeoh) using an iterative process. The material constants (MPa) for Neo-Hookean (c_1) were 0.039±0.022 and 0.024±0.004 for continent *vs.* incontinent women. For Mooney-Rivlin (c_1) the values obtained were 0.026±0.010 *vs.* 0.016±0.003, and for Yeoh (c_1) the values obtained were 0.031±0.023 *vs.* 0.016±0.002, ($p<0.05$). Muscle displacements obtained in the numerical simulations of Valsalva manoeuvre were compared with the muscle displacements obtained through additional dynamic MRI. Incontinent women presented a higher antero-posterior displacement than the continent women. The results were also similar between MRI and numerical simulations (40.27% *vs*. 42.17% for Neo-Hookean, 39.87% for Mooney-Rivlin and 41.61% for Yeoh).

Using an inverse FEA coupled with MR images allowed to obtain the *in vivo* biomechanical properties of the pelvic floor muscles, leading to a relationship between them for the continent and incontinent women in a non-invasive manner.

Keywords: Pelvic Floor Muscles; Stress Urinary Incontinence; Material Constants; Inverse Finite Element Analysis.

1. Introduction

The female pelvic floor is a support structure that includes fascia, ligaments and muscles (PFM) of the urogenital region. It extends from the symphysis pubis to the coccyx, and comprises the *levator hiatus* for the passage of the urethra, vagina and rectum. The group of *levator ani* muscle (the puborectal, pubococcygeal - that together form the pubovisceral - and iliococcygeal muscles) (Schwertner-Tiepelmann et al., 2012) is one of the most important structures that support the pelvic organs (Barber et al., 2002). These muscles help maintaining the anorectal and urethral closure by resisting the downward forces imposed to the organs and the pelvic floor whenever the intra-abdominal pressure (IAP) is increased (Bø and Sherburn, 2005; Schwertner-Tiepelmann et al., 2012).

The *levator ani* muscle differs from most other skeletal muscles in that it maintains a constant tone, except during voiding, defecation and Valsalva manoeuvre (Schwertner-Tiepelmann et al., 2012). Additionally, it has the ability to perform quick contractions in response to the sudden increase of the IAP, e.g. during cough, sneeze or physical activity, thereby maintaining continence and the pelvic organs in their anatomical positions (Schwertner-Tiepelmann et al., 2012).

The mechanical characteristics of the female pelvic floor are relevant to explain pelvic disorders (Barber et al., 2002). The decreased elasticity of the tissues often causes inability to maintain the normal positions of the pelvic organs. Pelvic floor disorders (PFD) (Schwertner-Tiepelmann et al., 2012) may result from inadequate mechanical

properties of the supportive structures, such as the impairment of the muscles or ligaments, or changes in their stiffness, as well as those in the pelvic fascia, associated with changes in hormonal levels during pregnancy, vaginal delivery or menopause (Abramowitch et al., 2009; Barber et al., 2002; Rahn et al., 2008).

Urinary incontinence (UI) is the most common pelvic disorder among aging females, greatly affecting their quality of life. The most common type of UI in women is stress UI (SUI), defined as the complaint of involuntary leakage of urine (Bø, 2004; Bø and Sherburn, 2005) on effort or exertion, or on sneezing or coughing (Abrams et al., 2002; Thyer et al., 2008).

Previous works have shown that the decreased total collagen and elastin can be associated with the abnormalities in the pelvic ligaments (Chen and Yeh, 2011) and fascia (Klutke et al., 2008) , leading to loss of support and SUI and pelvic organ prolapse (POP) symptoms (Chen and Yeh, 2011; Tinelli et al., 2010). This has also been studied through biomechanical modelling; the effect of structural degradation of the support structures such as the ligaments and fascia can be another ingredient to develop SUI and cystocele (F. S. Brandão et al., 2015; Yip et al., 2014). Furthermore, despite the proved association between SUI and direct damage to the pelvic floor muscles (often during vaginal delivery (Delancey et al., 2007)), SUI is also associated with weakness of the *levator ani* complex, and poor function or decreased strength of the urethral sphincter, not always in the presence of PFM injury (McGuire, 2004).

Magnetic resonance imaging (MRI) shows anatomic information on the status of the pelvic floor due to the high soft-tissue contrast, and the availability of acquiring functional (dynamic) images (Majida et al., 2010; Tunn et al., 1998). By performing these additional sagittal dynamic images during Valsalva manoeuvre or straining one can

evaluate the action of the PFM counteracting the increase in IAP (Peng et al. 2007; Yang et al. 2009). Additionally, to explore the stiffness of the PFM, imaging techniques based on ultrasound and MRI were used to compare continent and stress urinary incontinent women (Dietz, 2004; Dietz et al., 2008; Siegel et al., 2015; Tunn et al., 1998).

The pelvic soft tissues are the major focus of several research groups (Janda, 2006; Noakes et al., 2008; M. Parente et al., 2009) have been studied, but since *in vivo* experimental studies are very difficult to undertake in this field, *ex vivo* studies or animal models allowed to determine the biomechanical properties (Rahn et al. 2008; Abramowitch et al. 2009). Furthermore, biomechanical models have been applied to better understand the role and the mechanical behaviour of the pelvic structures in the development of UI and prolapse (Da Silva-Filho et al. 2010; S. Brandão et al. 2015), by using the material properties retrieved from experimental studies with both normal and pathological specimens (Rubod et al. 2012; Martins et al. 2013; Rivaux et al. 2013). More recently, computational model based on MR images of a young and asymptomatic and an inverse Finite Element Analysis (FEA) were used to determine *in vivo* biomechanical properties of the PFM for a non-pathologic case (Silva et al. 2016). In the same line, the aim of this work was to use identical methodology for two distinct groups (continent and incontinent women), by which the material constants for different constitutive models (Neo-Hookean, Mooney-Rivlin and Yeoh) for the passive behaviour of the PFM were obtained. After the determination of the material constants, the displacement of the PFM at Valsalva manoeuvre was compared between the deformed numerical model and the dynamic MR images.

2. Methods

A set of women was asked to complete the International Consultation of Incontinence Questionnaire-Short Form (ICIQ-SF) - which is validated for the Portuguese language (Nunes Tamanini et al., 2004) - to evaluate the presence and symptoms of UI. In addition, demographic characteristics such as age, body mass index (BMI) and parity were obtained. For this work, the exclusion criteria included pregnancy and previous pelvic surgery. A convenient sample of 8 women who gave informed consent was recruited. Four incontinent women (with SUI) and other four continent women (control group) were recruited at a regular urogynecology consultation.

MR Images Acquisition and Analysis

All women undertook a pelvic MR exam with multiplanar T2w images acquired in the supine position at rest using a 3T scanner (Magnetom® Tim Trio, Siemens Medical Solutions, Erlangen, Germany), along with cine images acquired at Valsalva manoeuvre.

Before the dynamic acquisitions acquired in the mid-sagittal plane, women were instructed on how to perform the Valsalva manoeuvre properly by a physiotherapist with 4 years knowledge in pelvic floor rehabilitation, as described elsewhere. The MR datasets used in this work were the same as previous works.

Figure 1 shows sagittal images at rest and at maximal Valsalva manoeuvre from two women, a continent 28-year-old ((a) and (b)), and an incontinent 30-year old ((c) and (d)).

To evaluate muscle displacement, horizontal and vertical axes (orange lines) were placed in the inferior and posterior border of the *symphysis pubis* (F. S. Brandão et al., 2015; Peng et al., 2007). The antero-posterior diameter of the *levator hiatus* - measured from the postero-inferior border of the *symphysis pubis* to the puborectal muscle (the main constrictor of the pelvic floor muscles) (straight blue line) - and its vertical position (dashed blue line) were assessed. The displacement in the antero-posterior axis was considered as the difference between the length of the straight blue line between the images acquired at rest and Valsalva.

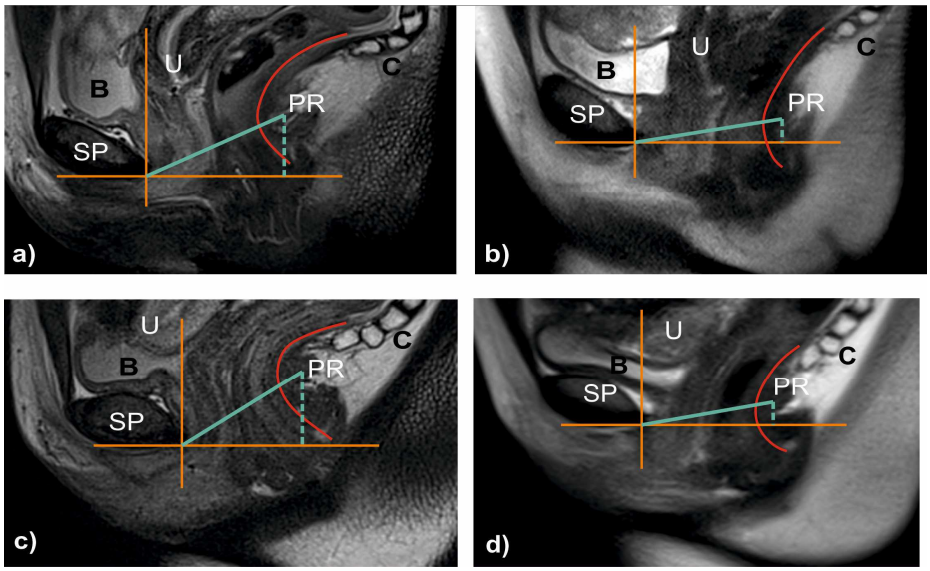

Figure 1. MR images in the mid-sagittal plane of a continent (a and b) and incontinent woman (c and d). Images acquired at rest position (a and c), and during maximal Valsalva manoeuvre (b and d). The antero-posterior *levator hiatus* displacement (straight blue line) and the supero-inferior displacement of the puborectal muscle (dashed blue line). B - bladder; C - coccyx; PR - puborectal muscle; SP - *symphysis pubis*; U - uterine cervix.

During Valsalva manoeuvre, the descent of the organs along the horizontal axis is verified, along with the widening of the *levator hiatus* in some degree, and opening of the anorectal angle, which is accompanied by some degree of verticalization of the *levator plate* (S. Brandão et al., 2015; Tumbarello et al., 2010). Previous works on clinical dynamic MR imaging (Raizada and Mittal, 2008) and numerical simulation (Noakes et al., 2008) described these features. The red lines illustrated in Figure 1 were used to compare the position of the anorectal angle and *levator plate* at rest *vs.* Valsalva manoeuvre.

The T2w axial images were used to measure the pubovisceral muscle thickness at the level of the midvagina and anal canal for the continent and incontinent women (Figure 2 (a) and (b)). The plane of minimal hiatal dimensions was used to measure the thickness, such as described by (Majida et al., 2010) and (Roza et al., 2015).

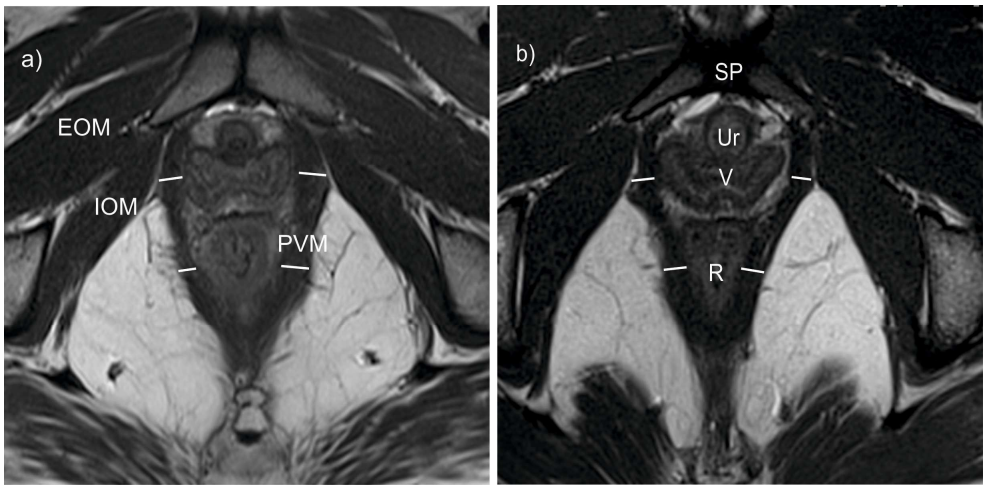

Figure 2. Magnetic Resonance images in the axial plane of a continent (a) and incontinent woman (b). The measurements of muscle thickness were made at the level of the midvagina and the anal

canal. EOM - external obturator muscle; IOM - internal obturator muscle; PVM - pubovisceral muscle; R - rectum; SP - *symphysis pubis*; Ur - urethra V - vagina.

Numerical Simulation

The biomechanical models of the pubovisceral muscle and the surrounding bone structures were built from the axial images. The 3D solid models of these structures were obtained by applying a semi-automatic procedure using the Mimics® software v. 16 (Software and Services for Biomedical Engineering, Materialise HQ, Belgium), as in previous work (Silva et al., 2016). After this procedure, the geometrical model of the muscle and the finite element mesh (with hybrid tetrahedral elements - C3D4H) were created using the Abaqus software v. 6.12 (Dassault Systmes Simulia Corp., Providence, RI, USA) (see Figure 3). The number of elements and volume in the meshes varied among the subjects due to the individual differences in the muscle geometry.

To simulate Valsalva manoeuvre, the boundary conditions to the pubovisceral muscle were imposed to incorporate the existence of the surrounding structures - *symphysis pubis*, internal obturator fascia and coccyx, visualized in the MR images. The nodes corresponding to the insertion of the pubovisceral muscle in the different structures were considered fixed (Parente et al., 2008; M. P. L. Parente et al., 2009; Rubod et al., 2012). A pressure of the 4 kPa was applied to the inner surface of the muscle, following the methodology described by (Noakes et al., 2008).

The inverse finite element analysis

In this work, an inverse FEA implemented by (Silva et al., 2016) was used to obtain the material constants for different constitutive models (Neo-Hookean, Mooney-Rivlin and Yeoh). The inverse FEA uses the optimization algorithm to search for the most suited set of material constants of the different constitutive models, in order to minimize its objective function (Gao et al., 2013; Powell, 1977), by allowing the minimum distance between the two reference curves drawn on Figure 1 for each subject (Figure 4). One curve represents the position of the puborectal muscle in the numerical model for each iteration and related deformation, and the other curve represents its position in the dynamic mid-sagittal image acquired at Valsalva manoeuvre. The Powell optimization algorithm was used because it does not calculate the gradient and it is one of the most efficient, reliable and also one of the most widely known of the zero-order methods (Powell, 1977).

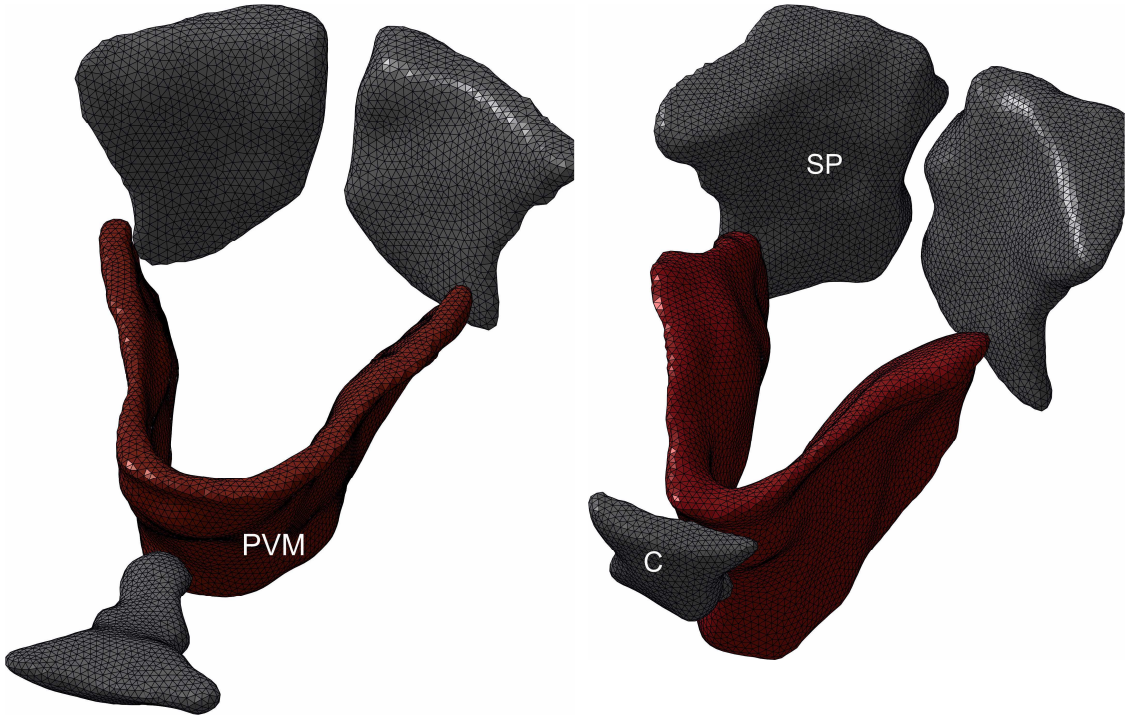

a) b)

Figure 3. Finite element mesh built from the MR axial images of a continent (a) and an incontinent woman (b). C - coccyx; PVM - pubovisceral muscle; SP - *symphysis pubis*.

The inverse FEA was used to obtain the suited material constants for the different constitutive models by using the Python scripting language to couple with the MATLAB MathWorks v. R2013b (Mathematical Computing Software, Natick, Massachusetts, USA) and the Abaqus software. A Python script was used to update the displacements of the nodes along a portion of the curve representing the position of the puborectal muscle on the numerical model for each simulation (see Figure 4).

The error measure represents the sum of all the distances between the two curves and the stopping criteria was set to <10mm. Eq. (1) (Silva et al., 2016).

$$Error = \sum_{i=1}^{np} \left\| d_{MRI_i} - d_{FEA_i} \right\| \quad (1)$$

By applying an iterative process, the most suited material constants were found, corresponding to the ones in the iteration with a minimum error.

In order to simulate the mechanical behaviour of the skeletal pubovisceral muscle - which was considered fully incompressible - the following distinct constitutive models were used (Neo-Hookean, Mooney-Rivlin and Yeoh) for two main reasons: firstly because they are simple models (with few constants to optimize) that employ a nonlinear relationship between stress and strain to describe incompressible hyperelastic materials, and also because they have proved to correctly describe the biomechanical behaviour of the PFM during simulation of Valsalva manoeuvre and defecation (Janda, 2006; Lee et al., 2005; Noakes et al., 2008), and vaginal delivery (Li et al., 2008).

The Neo-Hookean (Equation 2), Mooney-Rivlin (Equation 3) and Yeoh (Equation 4), constitutive models are characterised by:

$$W = c_1(I_1 - 3) \quad (2)$$

$$W = c_1(I_1 - 3) + c_2(I_2 - 3) \quad (3)$$

$$W = c_1(I_1 - 3) + c_2(I_1 - 3)^2 + c_3(I_1 - 3)^3 \quad (4)$$

where W is the strain energy function and c_1, c_2 and c_3 are the material constants to be determined and have dimensions of stress, I_1, I_2 and I_3 are the principal strain invariants (Equation 5) of the right Cauchy-Green tensor (Noakes et al., 2008). For the case uniaxial stretching, the principal strain invariants are represented as follows:

$$\begin{aligned} I_1 &= \lambda^2 + \frac{2}{\lambda} \\ I_2 &= 2\lambda + \frac{1}{\lambda^2} \\ I_3 &= 1 \end{aligned} \tag{5}$$

where λ is the maximum principal stretch.

In the case of uniaxial stretching, the Cauchy stress σ, a function of the invariants (Equation 6), can be described by the following equation (Martins et al., 2006):

$$\sigma = 2\left(\lambda^2 - \frac{1}{\lambda}\right)\left(\frac{\partial W}{\partial I_1} + \frac{1}{\lambda}\frac{\partial W}{\partial I_2}\right) \tag{6}$$

The particular expression of the Cauchy stresses is obtained for each material constitutive model depending on the invariants. The Neo-Hookean material model depends on the invariant I_1 (Equation 2), so the Cauchy stress obtained using Equation 6 is,

$$\sigma_{Hookean} = 2\left(\lambda^2 - \frac{1}{\lambda}\right)c_1 \tag{7}$$

The Mooney-Rivlin material model also depends on the invariants I_1 and I_2 (Equation 3), and also enables the use of the Equation 6 to obtain the Cauchy stress represented in Equation 8,

$$\sigma_{Mooney} = 2\left(\lambda^2 - \frac{1}{\lambda}\right)\left(c_1 + c_2\frac{1}{\lambda}\right) \tag{8}$$

The Cauchy stress for Yeoh material model is,

$$\sigma_{Yeoh} = 2\left(\lambda^2 - \frac{1}{\lambda}\right)\left(c_1 + 2c_2\left(I_1 - 3\right) + 3c_3\left(I_1 - 3\right)^2\right) \tag{9}$$

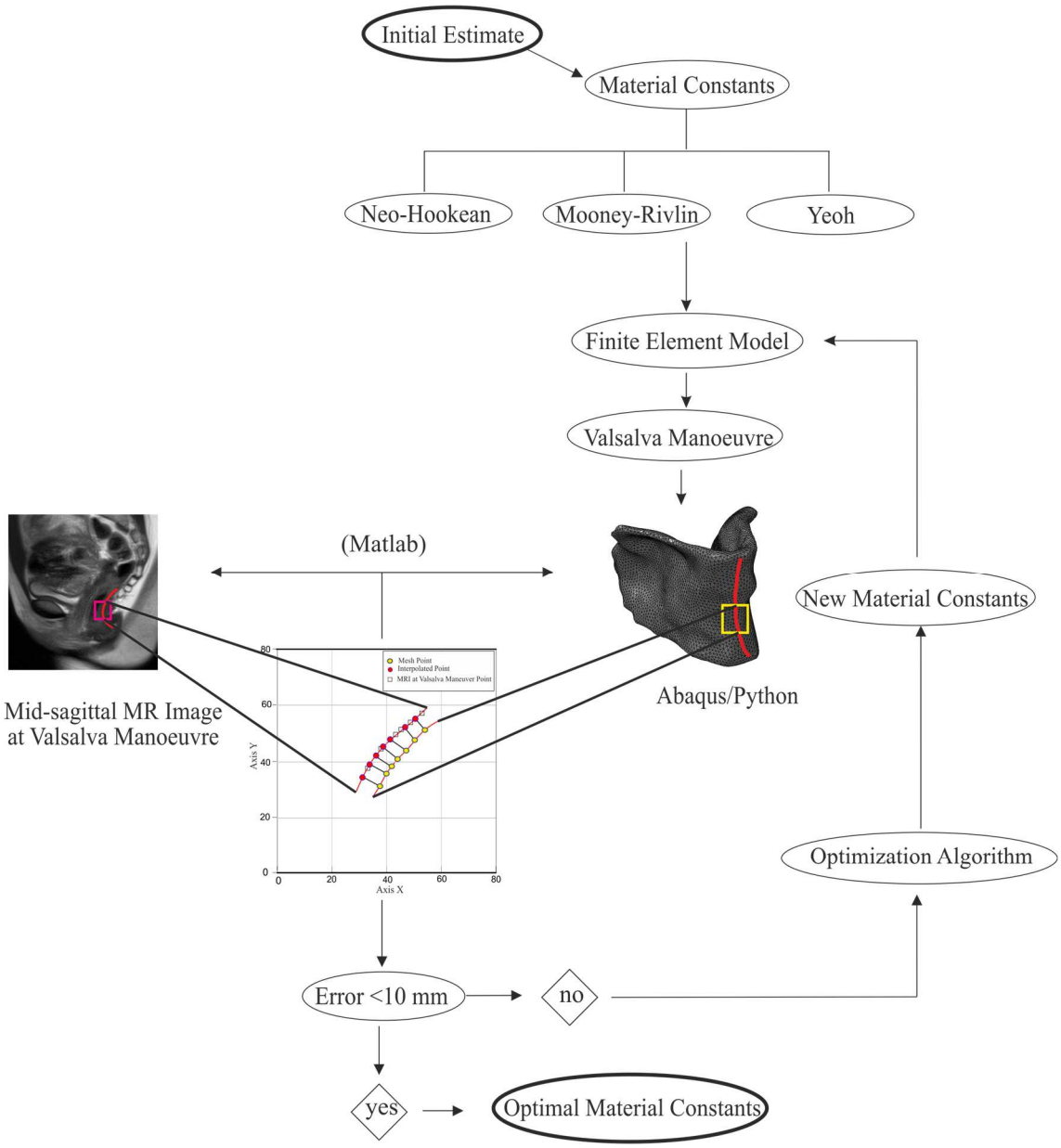

Figure 4. Flow chart of the inverse FEA applied to obtain the material constants of the Neo-Hookean, Mooney-Rivlin and Yeoh constitutive models.

In order to check the usefulness of the established parameters, a numerical simulation representing a uniaxial tensile test was performed. Figure 5 shows the finite element model to obtain the numerical stress-strain response. This numerical model was

created with 3366 nodes and 2500 elements. The FEM was generated by using hybrid linear tetrahedral elements (Abaqus C3D8H). The element size set was approximately constant throughout the geometry, resulting in a mesh with a characteristic element length of 1.0 mm.

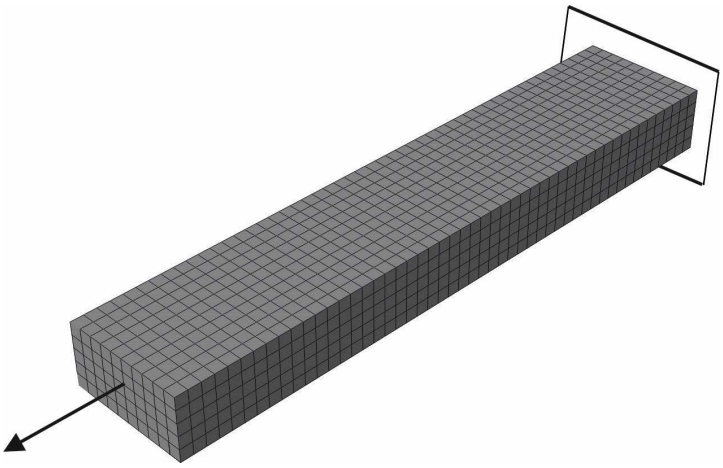

Figure 5. Finite element model used to obtain numerical stress-strain response.

Statistical analysis

The continuous variables were described by means of the mean value and standard deviation (SD). The demographic features, the morphological characteristics of the muscle and its displacement for Valsalva manoeuvre, and also the material constants of the three different constitutive models were compared between two groups by using the Mann-Whitney *U* test. A *P* value of <0.05 was considered statistically significant. All analyses were computed using IBM SPSS Statistics 23.0 software.

3. Results

Demographic and morphological characteristics of the continent and incontinent women are presented in Table 1. When comparing the two groups, no significant difference in age, BMI, parity and muscle thickness were found.

Table 1. Demographic characteristics and muscle morphological features for the two groups.

variable		*CG (n=4)*	*IG (n=4)*	*p value*
age		30.50±10.44	30.75±21.67	0.486
BMI		24.62±4.61	22.23±4.13	0.343
parity		0.50±1.00	0.50±1.00	1.000
thickness (mm)	**MidVa (left)**	8.12±2.00	5.43±1.50	0.200
	MidVa (right)	7.29±2.28	5.95±1.63	0.343
	AC (left)	5.20±1.27	4.14±1.01	0.486
	AC (right)	5.68±1.78	4.28±0.26	0.343

AC: anal canal; BMI: body mass index; CG: continent group; IG: incontinent group; MidVa: midvagina; mm: millimeters.

Table 2 presents the mean values of the material constants for three different constitutive models obtained by inverse FEA, which show significant differences.

Table 2. Material constants of the pubovisceral muscle in women with and without UI, and variation between the groups.

variable		*CG (n=4)*	*IG (n=4)*	*p value*	*variation (%)*
Neo-Hookean	**c_1(MPa)**	0.039±0.022	0.024±0.004	0.029*	38.46%
Mooney-Rivlin	**c_1(MPa)**	0.026±0.010	0.016±0.003	0.029*	38.46%
	c_2(MPa)	0.014±0.014	0.005±0.001	0.029*	64.29%
Yeoh	**c_1(MPa)**	0.031±0.023	0.016±0.002	0.029*	48.39%
	c_2(MPa)	0.025±0.028	0.004±0.001	0.029*	84.00%
	c_3(MPa)	0.023±0.038	0.001±0.001	0.029*	95.65%

CG: continent group; IG: incontinent group.
*statistically significant.

Figure 6 shows the stress-stretch response for the study of the nonlinear mechanical behaviour of the uniaxial tension test with the means values of the material constants obtained for the continent (a) and incontinent (b) women. The results correspond to the comparison between uniaxial tension tests obtained analytically from the Equations (7), (8) and (9) and those obtained numerically through the simulations.

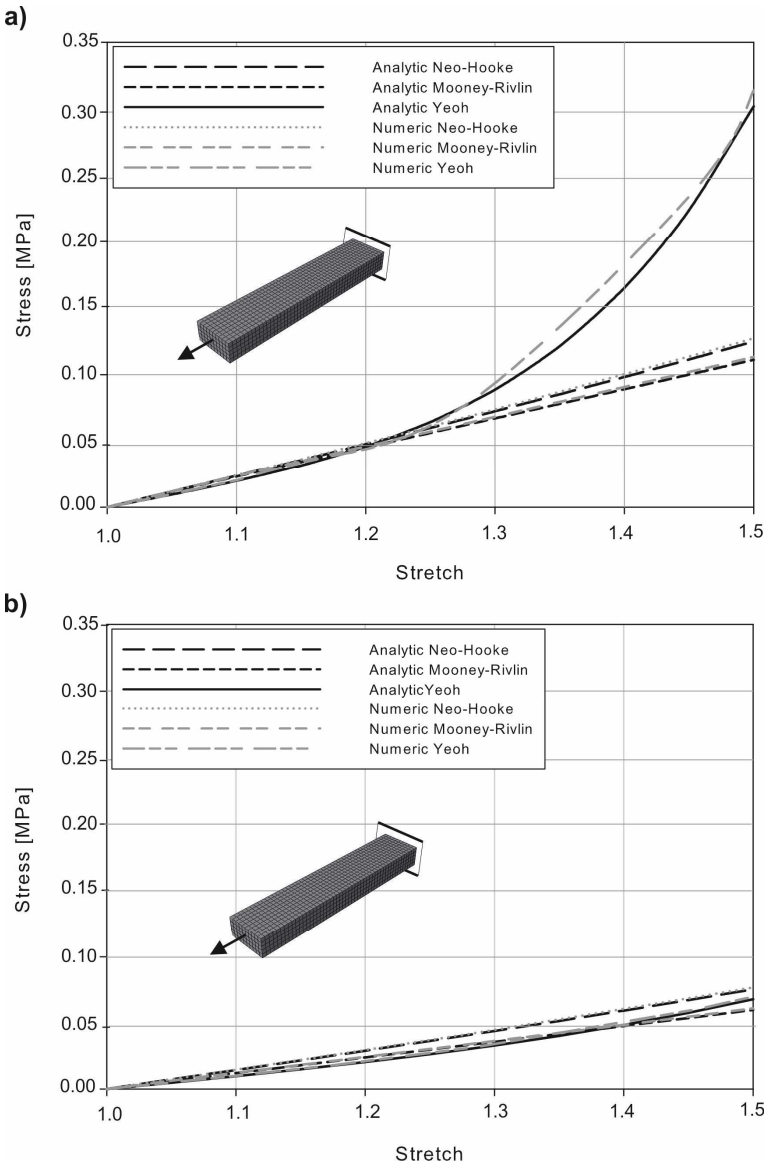

Figure 6. Stress-stretch response for passive behaviour of the pubovisceral muscle for the different constitutive models. (a) for the continent and (b) for the incontinent group. The response obtained analytically and numerically was compared.

Figure 7 presents the mechanical response of the uniaxial stress-stretch response from continent and incontinent women to compare the effect of material constants (Table 2) obtained in this work with other material constants existing in literature. The material constants for the Yeoh constitutive model of the table in Figure 7 were estimated in the

Abaqus software through experimental curves (softer and stiffer) extracted from cadaveric muscle (Janda, 2006). All the experimental/numerical curves were compared with the analytical curves from Equations (7) to (9). The continent group showed higher values for the stress (MPa). The curve of the Yeoh constitutive model for the continent women follows the non-linear behaviour of the stiffer experimental curve, and the curves for the incontinent women follow the behaviour of the softer experimental and Neo-Hookean curve of the literature. The maximum stress values are higher for the continent women and for the three constitutive models.

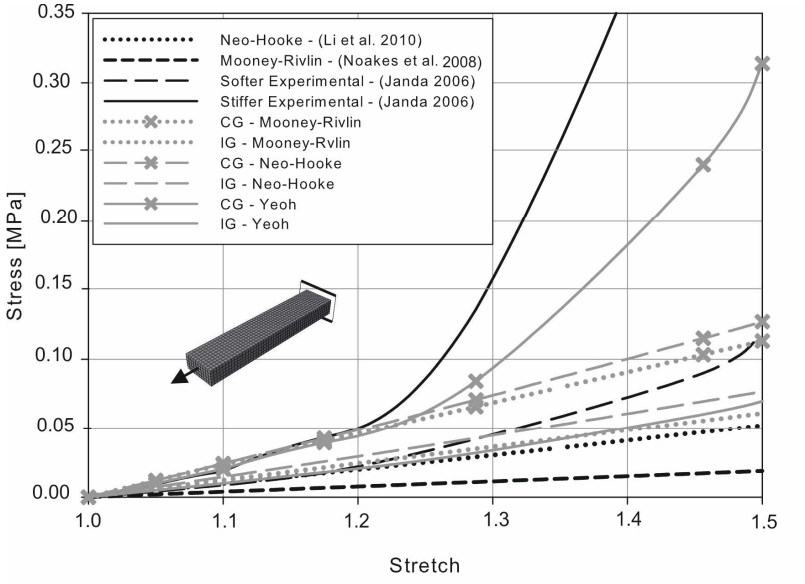

Model	c_1 *(MPa)*	c_2 *(MPa)*	c_3 *(MPa)*	*Experimental/Numerical data*
Neo-Hooke	1.61E-02	……..	……..	(Li et al. 2010)
Mooney-Rivlin	4.50E-03	2.00E-03	……..	(Noakes et al. 2008)
Yeoh (softer curve)	1.31E-02	1.49E-02	2.79E-02	(Janda 2006)
Yeoh (stiffer curve)	2.87E-02	8.21E-02	9.36E-02	

Figure 7. Uniaxial stress-stretch response for passive behaviour of the pubovisceral muscle for the different constitutive models and experimental/numerical data of the literature.

Table 3 presents the displacement of the pubovisceral muscle in the numerical simulation *vs.* MRI, as represented by the posterior and inferior movement. The displacements obtained in the numerical simulation were similar with the one obtained in the dynamic MRI for the three constitutive models (p-values>0.05). When comparing the two groups, the difference for the antero-posterior displacement for continent and incontinent women was approximately 42.17% for the Neo-Hookean, 39.87% for the Mooney-Rivlin and 41.61% for the Yeoh models, respectively, and the supero-inferior displacement was approximately 15.69% for the Neo-Hookean, 17.17% for the Mooney-Rivlin and 11.00% for the Yeoh models, respectively. The horizontal displacement measured in the MR images was 40.27% higher in incontinent women while the one along the vertical axis was 6.34% higher for the continent women.

Table 3. Displacements of the dynamic MRI compared with the displacements of the numerical models for two groups of women.

variable	**MRI (mm)**	**Neo-Hookean (mm)**	**Mooney-Rivlin (mm)**	**Yeoh (mm)**
CG-AP	4.495±1.560	4.475±1.534	4.755±1.529	4.630±1.366
IG-AP	7.525±1.306	7.738±1.984	7.908±1.698	7.930±1.651
p value	0.057	0.114	0.057	0.057
variation (%)	40.27%	42.17%	39.87%	41.61%

CG-AP: continent group – antero-posterior; CG-SP: continent group – supero-inferior.
IG-AP: incontinent group – antero-posterior; IG-SP: incontinent group – supero-inferior.

Table 3. (cont.) Displacements of the dynamic MRI compared with the displacements of the numerical models for two groups of women.

variable	**MRI (mm)**	**Neo-Hookean (mm)**	**Mooney-Rivlin (mm)**	**Yeoh (mm)**
CG-SI	6.235±4.004	4.768±3.503	5.113±3.818	4.983±3.387
IG-SI	5.845±2.238	4.020±2.355	4.235±2.004	4.435±1.742
p value	1.000	0.886	1.000	1.000
variation (%)	6.34%	15.69%	17.17%	11.00%

CG-AP: continent group – antero-posterior; CG-SP: continent group – supero-inferior.
IG-AP: incontinent group – antero-posterior; IG-SP: incontinent group – supero-inferior.

Figure 8 shows the contour of the pubovisceral muscle to better illustrate the displacement for the three constitutive models, (a) Neo-Hookean, (b) Mooney-Rivlin and (c) Yeoh. Since the morphological analysis showed no significant differences between groups, a pubovisceral muscle of a continent woman was used to analyse the influence of using the three constitutive models. The figure shows the contour at rest position and Valsalva manoeuvre achieved through of the material constants obtained for continent group and incontinent group (Table 2). When comparing the three constitutive models, the displacement between Neo-Hookean and Mooney-Rivlin was similar, but it tends to be a little bit greater when using the material constants of the Yeoh constitutive model for incontinent group.

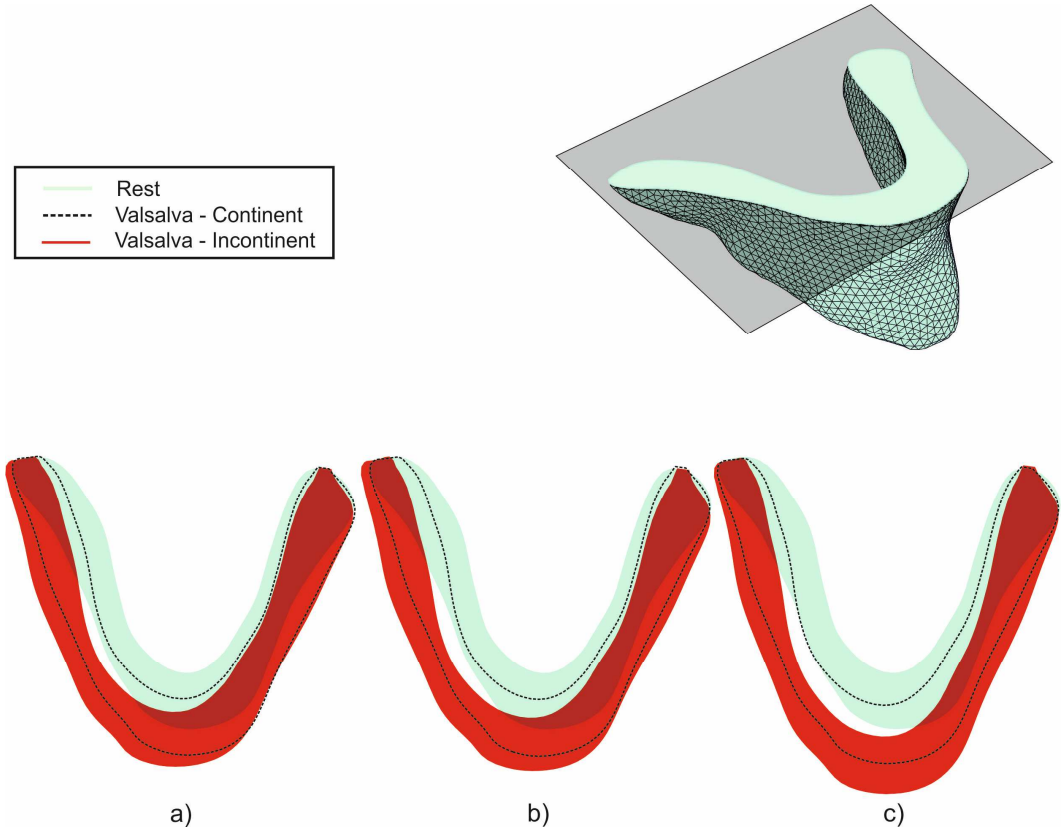

Figure 8. Pubovisceral muscle contour for a continent woman using Neo-Hookean (a), Mooney-Rivlin (b) and Yeoh (c) constitutive models.

4. Discussion

UI may be considered as the consequence of the alteration of a biomechanical process (McGuire, 2004). The nerves, muscles and connective tissues are responsible for maintaining continence, providing resistance to downward displacements during increase in IAP (Denise et al., 2000).Their biomechanical properties are proven to be relevant to explain the pelvic disorders (Derpapas, 2015).

In the present work, an inverse FEA was used to obtain the most suited biomechanical properties of the pubovisceral muscle for continent and incontinent

women, using an optimization algorithm coupled with the FEM in a completely non-invasive way.

There were no significant differences in the demographic characteristics or in the morphological measurements of muscle between continent and incontinent women. Therefore, the higher anterior-to-posterior displacement, corresponding to the opening of the *levator hiatus* in incontinent women can be associated with changes in the biomechanical properties of the pelvic floor muscles. Previous studies show that women with SUI present a significant reduction of type III collagen, which is not due to a decreased production of collagen but due to increased degradation of nascent collagen (Patel et al., 2007). Also, (Rechberger et al., 1998) showed that weakening of the collagen framework of the pubovisceral fascia affects women of all ages.

The values of the material constants are significantly higher for the continent than for the incontinent women. The variation for continent *vs.* incontinent group was approximately 38.46% for the c_1 for the Neo-Hookean, 38.46% and 64.29% for c_1 and c_2 of the Mooney-Rivlin, and 48.39%, 84.00% and 95.65% for c_1, c_2 and c_3 of the Yeoh. Assuming that the c_1 has greater influence in the mechanical behaviour (Noor & Mahmud 2015), the variation of this material constant for the three constitutive models are in accordance with the variation of the antero-posterior displacement - 42.17% for the Neo-Hookean, 39.8% for the Mooney-Rivlin and 41.6% for the Yeoh, respectively. Incontinent women have an antero-posterior displacement higher than continents, as previously described (Peng et al., 2007). Comparing the muscle displacement through numerical simulation *vs.* dynamic MRI during Valsalva manoeuvre, the values of antero-posterior was similar in the two methods for the two groups. The lower variation in the supero-inferior displacement between the methods can be associated with assumptions

and simplifications in the model, as for example, due to the fixed boundary conditions in the obturator fascia.

Despite the limitations mentioned above, the numerical results were concordant with the analytical results, as shown in Figure 6, and the uniaxial stress-stretch response presented in this work shows that the values of the material constants for the different constitutive models can be compared with the experimental/numerical data existent in the literature.

To properly interpret our findings, it is important to consider the limitations and simplifications involved. Firstly, this sample is small, secondly, the numerical models did not include the connective tissues (fascia and ligaments) and pelvic organs, which would be more realistic.

Taking these limitations into account, the inverse FEA could be used as a means to evaluate the changes in PFM after conservative treatment via a longitudinal evaluation, by associating changes in thickness and strength measured through results of muscle contraction and strength from the Oxford Grading Scale in the vaginal palpation, the increase in muscle thickness and improved *levator hiatus* closure from dynamic MRI, and the changes in the material constants throughout the process. On the other hand, when there is not evidence of clinical improvement, surgical treatment with synthetic slings is always an option. In those cases, by knowing the stiffness of the native tissue, subject-specific adequacy of the mesh material properties could be an issue in the future.

In conclusion, the inverse FEA used in this study allowed establishing the material constants of the female PFM for continent and incontinent women, which substantiated more realistic results. With the most suited material properties the results of numerical simulation *vs.* muscle displacement in dynamic MRI were similar. Nevertheless, material

properties for women of the incontinent group were lower, which means softer muscles, and that is clinically reasonable. Furthermore, it is corroborated by the fact that incontinent women showed higher hiatal opening at maximal Valsalva manoeuvre in both dynamic MRI and numerical simulation.

Conflict of interest statement

The authors declare that there is no financial, professional or other personal interest of any nature or kind in any product, service and/or company that could be constructed as influencing the position.

Acknowledgements

The authors gratefully acknowledge the funding by Ministério da Ciência Tecnologia, e Ensino Superior, FCT, Portugal, under grants SFRH/BD/89519/2012 and IF/00159/2014, and the project UID/EMS/50022/2013. The fifth author acknowledge the funding of Project NORTE-01-0145-FEDER-000022 - SciTech - Science and Technology for Competitive and Sustainable Industries, cofinanced by Programa Operacional Regional do Norte (NORTE2020), through Fundo Europeu de Desenvolvimento Regional (FEDER).

References

Abramowitch, S.D., Feola, A., Jallah, Z., Moalli, P.A., 2009. Tissue mechanics, animal models, and pelvic organ prolapse: a review. Eur. J. Obstet. Gynecol. Reprod. Biol. 144, S146–S158. doi:10.1016/j.ejogrb.2009.02.022

Abrams, P., Cardozo, L., Fall, M., Griffiths, D., Rosier, P., Ulmsten, U., Van Kerrebroeck, P., Victor, A., Wein, A., 2002. The standardisation of terminology in lower urinary tract function: Report from the standardisation sub-committee of the International Continence Society. Neurourol. Urodyn. 21, 37–49.

Barber, M.D., Bremer, R.E., Thor, K.B., Dolber, P.C., Kuehl, T.J., Coates, K.W., 2002. Innervation of the female levator ani muscles. Am. J. Obstet. Gynecol. 187, 64–71.

Bø, K., 2004. Pelvic floor muscle training is effective in treatment of female stress urinary incontinence, but how does it work? Int. Urogynecol. J. Pelvic Floor Dysfunct. 15, 76–84.

Bø, K., Sherburn, M., 2005. Evaluation of Female Pelvic-Floor Muscle Function and Strength. Phys. Ther. 85, 269–282. doi:10.1093/ptj/85.3.269

Brandão, F.S., Parente, M.P., Rocha, P.A., Saraiva, M.T., Ramos, I.M., Natal Jorge, R.M., 2015. Modeling the contraction of the pelvic floor muscles. Comput Methods Biomech Biomed Engin. 8, 1–10.

Brandão, S., Parente, M., Mascarenhas, T., da Silva, A.R.G., Ramos, I., Jorge, R.N., 2015. Biomechanical study on the bladder neck and urethral positions: Simulation of impairment of the pelvic ligaments. J. Biomech. 48, 217–223.

Chen, B., Yeh, J., 2011. Alterations in connective tissue metabolism in stress incontinence and prolapse. J. Urol. 186, 1768–1772.

Delancey, J.O.L., Miller, J.M., Kearney, R., Reddy, P., Umek, W., Guire, K.E., Margulies, R.U., Ashton-miller, J.A., 2007. Vaginal birth and de novo stress incontinence: Relative contributions of urethral dysfunction and mobility. Obs. Gynecol. 110, 354–362.

Denise, H., Janis, M.M., DeLancey, J.O.L., James, A.A.-M., 2000. Differential Effects of Cough, Valsalva, and Continence Status on Vesical Neck Movement. Obs. Gynecol. 95, 535–540.

Derpapas, A., 2015. The use of imaging in the diagnosis of lower urinary tract disorders and pelvic organ prolapse in women. Thesis. Imperial College London Department of Surgery & Cancer.

Dietz, H.P., 2004. Ultrasound imaging of the pelvic floor. Part II: three-dimensional or volume imaging . Ultrasound Obs. Gynecol. 23, 615–25.

Dietz, H.P., Shek, C., De Leon, J., Steensma, A.B., 2008. Ballooning of the levator hiatus. Ultrasound Obstet. Gynecol. 31, 676–680.

Gao, W., Liu, S., Huang, L., 2013. A novel artificial bee colony algorithm with Powell's method. Appl. Soft Comput. 13, 3763–3775.

Janda, S., 2006. Biomechanics of the pelvic floor musculature. PhD. Thesis. Technische Universiteit Delft.

Klutke, J., Ji, Q., Campeau, J., Starcher, B., Felix, J., Stanczyk, F., Klutke, C., 2008. Decreased endopelvic fascia elastin content in uterine prolapse. Acta Obstet. Gynecol. Scand. 87, 111–115.

Lee, S., Darzi, A., Yang, G., 2005. Subject Specific Finite Element Modelling of the Levator Ani. Med. Image Comput. Comput. Interv. 3749, 360–367.

Li, X., Kruger, J.A., Chung, J.H., Nash, M.P., Nielsen, P.M.F., 2008. Modelling childbirth: Comparing athlete and non-athlete pelvic floor mechanics. Med Image Comput Comput - Assist Interv. 11, 750–757.

Majida, M., Brækken, I.H., Bø, K., Šaltyte Benth, J., Engh, M.E., 2010. Validation of three-dimensional perineal ultrasound and magnetic resonance imaging measurements of the pubovisceral muscle at rest. Ultrasound Obstet. Gynecol. 35, 715–722.

Martins, P., Jorge, R.N., Ferreira, A., 2006. A Comparative Study of Several Material Models for Prediction of Hyperelastic Properties: Application to Silicone-Rubber and Soft Tissues. Strain 42, 135–147.

McGuire, E.J., 2004. Pathophysiology of Stress Urinary Incontinence. Rev. Urol. 6, S11–S17.

Moerman, K., Sprengers, A., Simms, C., Lamerichs, R., Stoker, J., Nederveen, A., 2012. Validation of continuously tagged MRI for the measurement of dynamic 3D skeletal muscle tissue deformation. Med Phys. 39, 1973–810.

Moerman, K., Sprengers, A., Simms, C., Lamerichs, R., Stoker, J., Nederveen, A., 2011. Validation of SPAMM tagged MRI based measurement of 3D soft tissue deformation. Med Phys. 38, 1248–1260.

Noakes, K.F., Pullan, A.J., Bissett, I.P., Cheng, L.K., 2008. Subject specific finite elasticity simulations of the pelvic floor. J. Biomech. 41, 3060–3065.

Nunes Tamanini, J.T., Dambros, M., D'Ancona, C.A.L., Rodrigues Palma, P.C., Rodrigues Netto, N., 2004. Validation of the "International Consultation on Incontinence Questionnaire - Short Form" (ICIQ-SF) for Portuguese. Rev. Saude Publica 38, 438–444.

Parente, M.P., Jorge, R.M.N., Mascarenhas, T., Fernandes, A.A., Martins, J.A.C., 2009a. The influence of an occipito-posterior malposition on the biomechanical behavior of the pelvic floor. Eur. J. Obstet. Gynecol. Reprod. Biol. 144, S166–S169.

Parente, M.P., Natal Jorge, R., Mascarenhas, T., Fernandes, A., Martins, J., 2009b. The influence of the material properties on the biomechanical behavior of the pelvic floor muscles during vaginal delivery. J. Biomech. 42, 1301–1306.

Parente, M.P., Natal Jorge, R., Mascarenhas, T., Fernandes, A., Martins, J., 2008. Deformation of the pelvic floor muscles during a vaginal delivery. Int. Urogynecol. J. Pelvic Floor Dysfunct. 19, 65–71.

Patel, P.D., Amrute, K. V., Badlani, G.H., 2007. Pelvic organ prolapse and stress urinary incontinence: A review of etiological factors. Indian J Urol. 23, 135–141.

Peng, Q., Jones, R., Shishido, K., Constantinou, C.E., 2007. Ultrasound evaluation of dynamic responses of female pelvic floor muscles. Ultrasound Med. Biol. 33, 342–352.

Powell, M.J.D., 1977. Restart procedures for the conjugate gradient method. Math. Program. 12, 241–254.

Rahn, D.D., Ruff, M.D., Brown, S.A., Tibbals, H.F., Word, R.A., 2008. Biomechanical properties of the vaginal wall: effect of pregnancy, elastic fiber deficiency, and pelvic organ prolapse. Am. J. Obstet. Gynecol. 198, 590.e1-590.e6.

Raizada, V., Mittal, R.K., 2008. Pelvic Floor Anatomy and Applied Physiology. Gastroenterol Clin North Am 37, 493–497.

Rechberger, T., Postawski, K., Jakowicki, J.A., Gunja-Smith, Z., Woessner J.F., J., 1998. Role of fascial collagen in stress urinary incontinence. Am. J. Obstet. Gynecol. 179, 1511–1514.

Roza, T. Da, Brandão, S., Oliveira, D., Mascarenhas, T., Parente, M., Duarte, J.A., Jorge, R.N., 2015. Football practice and urinary incontinence: Relation between morphology, function and biomechanics. J. Biomech. 48, 1587–1592.

Rubod, C., Brieu, M., Cosson, M., Rivaux, G., Clay, J.C., De Landsheere, L., Gabriel, B., 2012. Biomechanical properties of human pelvic organs. Urology 79, 968.e17-968.e22.

Schwertner-Tiepelmann, N., Thakar, R., Sultan, A.H., Tunn, R., 2012. Obstetric levator ani muscle injuries: Current status. Ultrasound Obstet. Gynecol. 39, 372–383.

Siegel, S., Noblett, K., Mangel, J., Giebling, T., Sutherland, S.E., Bird, E.T., 2015. Results of a prospective, randomized , multicenter study evaluating sacral neuromodulation with Interstim therapy compared to standard medical therapy at 6 monts in subjects with mild symptoms of overactive bladder. Neurourol. Urodyn. 34, 224–230.

Silva, M., Brandao, S., Parente, M., Mascarenhas, T., Natal Jorge, R., 2016. Establishing the biomechanical properties of the pelvic soft tissues through an inverse finite element analysis using magnetic resonance imaging. Proc. Inst. Mech. Eng. Part H J. Eng. Med. 230, 298–309.

Thyer, I., Shek, C., Dietz, H.P., 2008. New imaging method for assessing pelvic floor biomechanics. Ultrasound Obstet. Gynecol. 31, 201–205.

Tinelli, A., Malvasi, A., Rahimi, S., Negro, R., Vergara, D., Martignago, R., Pellegrino, M., Cavallotti, C., 2010. Age-related pelvic floor modifications and prolapse risk factors in postmenopausal women. Menopause 17, 204–212.

Tumbarello, J.A., Hsu, Y., Lewicky-Gaupp, C., Rohrer, S., DeLancey, J.O.L., 2010. Do repetitive Valsalva maneuvers change maximum prolapse on dynamic MRI? Int. Urogynecol. J. Pelvic Floor Dysfunct. 21, 1247–1251.

Tunn, R., Paris, S., Fischer, W., Hamm, B., Kuchinke, J., 1998. Static magnetic resonance imaging of the pelvic floor muscle morphology in women with stress urinary incontinence and pelvic prolapse. Neurourol. Urodyn. 17, 579–589.

Yang, J., Yang, S., Yang, S., Yang, E., Huang, W., 2009. Reliability of real-time ultrasound to detect pelvic floor muscle contraction in urinary incontinent women. J Urol. 182, 2392–2396.

Yip, C., Kwok, E., Sassani, F., Jackson, R., Cundiff, G., 2012. A biomechanical model to assess the contribution of pelvic musculature weakness to the development of stress urinary incontinence. Comput. Methods Biomech. Biomed. Engin. 17, 163–176.

Part B - Article 3

The influence of pelvic organ prolapse on the passive biomechanical properties of pelvic floor muscles

M.E.T. Silva[a], S. Brandão[a,b], M.P.L. Parente[a], T. Mascarenhas[c], R.M. Natal Jorge[a]

[a]LAETA, INEGI, Faculty of Engineering, University of Porto, Porto, Portugal
[b]Department of Radiology, Centro Hospitalar de São João-EPE, Faculty of Medicine, University of Porto, Porto, Portugal
[c]Department of Gynecology and Obstetrics, Centro Hospitalar de São João-EPE, Faculty of Medicine, University of Porto, Porto, Portugal

Published in: Journal of Mechanics in Medicine and Biology, 17(5):1750090-1750109, 2017.
doi: 10.1080/10255842.2017.1304542

Abstract

The biomechanical properties of the female pelvic floor tissues, such as muscles, fascia or ligaments are relevant when explaining pelvic disorders, since these may result from changes in the properties of those tissues. The aim of this study is to understand the influence of pelvic organ prolapse on the passive biomechanical properties of the pelvic floor muscles. For this purpose, Magnetic Resonance images at Valsalva manoeuvre were used, and an inverse Finite Element Analysis technique was applied. The numerical models of the *puboviscerali*s muscle and pelvic bones were built from axial Magnetic Resonance images acquired at rest. The numerical simulation was based on the Finite Element Method, by which the material constants were determined for three different constitutive models (Neo-Hookean, Mooney-Rivlin and Yeoh). The ratio between the values of the material constants for women with and without prolapse was approximately 43% for the parameter c_1 in the Neo-Hookean constitutive model, 57% and 24% for c_1 and c_2 in the Mooney-Rivlin constitutive model, and 35%, 21% and 14% for c_1, c_2 and c_3 in the Yeoh constitutive model. For the three constitutive models the mean values of the material properties related with stiffness were higher for the muscles of women with pelvic organ prolapse. These increases in stiffness are in line with other experimental works involving vaginal tissue, which showing that the elasticity module is significantly higher in the prolapsed tissue when compared with normal tissue.

The present work presents a non-invasive methodology based on the application of the Finite Element Method, which allows the establishment of a relationship between the stiffness of the pelvic floor muscles of women with pelvic organ prolapse and without this pathology.

Keywords: Pelvic Floor Muscles; Pelvic Organ Prolapse; Material Constants; Inverse Finite Element Analysis.

1. Introduction

The *levator ani* (LA) muscle is composed by the *puborectalis* and *pubococcygeus,* which together form the *puboviscerali*s muscle (PVM) and the *iliococcygeus* muscles. The LA is one of the most important structures to provide support, contributing to maintaining the pelvic organs in their correct position [1–3]. Weakness or direct injury to the LA muscle and the pudendal nerve that may occur during vaginal delivery are associated with pelvic floor disorders, such as urinary and fecal incontinence and pelvic organ prolapse (POP) (Brandão et al., 2013; Dietz et al., 2005; Hendrix et al., 2002). Previous hysterectomy, repeated increase in intra-abdominal pressure from chronic coughing, from straining due to constipation, or repeated heavy lifting may also contribute to the loss of pelvic organ support (Kuncharapu et al., 2010).

POP is the descent of one or more pelvic structures from the normal anatomical location toward or through the *levator hiatus* opening (Boyadzhyan et al., 2008). Although many women with pelvic organ prolapse are asymptomatic, the sense of bulging or protrusion in the vagina is the most common symptom. Management options for women with symptomatic prolapse include pelvic floor muscle rehabilitation, mechanical support and surgery. Dynamic magnetic resonance imaging (MRI) may offer useful information to the clinical evaluation regarding morphological changes of the pelvic floor anatomy and pelvic floor dynamics during Valsalva manoeuvre, so as to stage the degree of POP (Boyadzhyan et al., 2008).

Previous works evaluated vaginal tissues with and without prolapse by performing

experimental uniaxial tension tests to tissues collected at the time of transvaginal hysterectomy and from fresh female cadavers (Jean-Charles et al., 2010; Lei et al., 2007; Rubod et al., 2008), and higher stiffness seems to be found in the context of prolapse. *Ex vivo* analyses of female pelvic floor muscles were also used by previous authors to determine their mechanical properties (Martins, 2010) and to provide input of tissue properties for pelvic modelling using the Finite Element Method (FEM) (Janda, 2006; Janda et al., 2003). Those mechanical properties were also applied to characterize the biomechanical behavior of the pelvic floor muscles during vaginal delivery or defecation (Noakes et al., 2008; Parente et al., 2009b, 2008; Saleme et al., 2011).

POP has been previously associated with muscle defects (DeLancey et al., 2007), but there is also evidence that women with thinner muscles can present prolapse (Brandão et al., 2013). Therefore, the inner structure of the muscle, its structural and material properties may give additional information for the overall model of developing POP. However, obtaining data from uniaxial tension tests does not reflect the natural conditions for muscle behavior in the pelvis, and hence computational analysis may help in simulating those *in vivo* relations and behavior.

The aim of the present work is to determine, in non-invasively based procedure, the influence of POP on the biomechanical properties of the pelvic floor muscles. An inverse Finite Element Analysis (FEA) was applied to estimate the material constants for the passive muscle behavior during the Valsalva manoeuvre of a set of non-pathological women and also from a group of women with POP. In this process, three different isotropic constitutive models - Neo-Hookean, Mooney-Rivlin, and the Yeoh - were used.

2. Methods

Subjects and Image analysis

Nine women participated in this study, and were observed by the same gynaecologist. Clinical evaluation and POP-Q were carried out to assess the degree of POP. Demographic data was also obtained (age, BMI and parity). Based on the POP-Q classification system, women were divided in two groups: 4 without pelvic organ prolapse (w/o POP) and 5 women with pelvic organ prolapse (w/ POP).

Women (w/ POP and w/o POP) were scanned for a pelvic MR exam. The multiplanar T2w images acquired at rest were obtained from a previous study of Brandão et al. (Brandão et al., 2013) where the value of the second moment of inertia of the PVM was compared between women with POP and controls.

The Valsalva manoeuvre is defined as forced expiration, causing a markedly increased intra-abdominal pressure (IAP) (Ornö and Dietz, 2007). It is often used to verify the continence *status*, and is also commonly applied during clinical evaluation and dynamic MR acquisition in order to furthermore determine the associated degree of organ descent (Ornö and Dietz, 2007).

The degree of POP is based in a correct Valsalva manoeuvre. However, in many cases, it is performed incorrectly. Therefore, the images should always be evaluated for the effectiveness of the Valsalva manoeuvre. The opening of the anorectal angle, which is accompanied by some degree of verticalization of the *levator plate* (formed by the *iliococcygeous* muscle, in the upper portion of the pelvic floor) (Brandão et al., 2015;

Tumbarello et al., 2010) and the increase in sagittal antero-posterior diameter of the *levator hiatus* should be visualized.

For this work, the subjects were instructed on how to properly perform a Valsalva manoeuvre by a physiotherapist in pelvic floor rehabilitation just before the dynamic acquisitions. Three successive sets of dynamic images in the mid-sagittal plane were acquired with a 3 min interval. Posteriorly, an experienced observer selected the best maximal Valsalva image, presenting the most evident vertical descent of the organs and wider hiatal sagittal diameter, and also revised the morphology and signal intensity of the PVM. There was no evidence of injury.

Figure 1 shows dynamic mid-sagittal images of a woman w/o prolapse (a and b) and one w/ prolapse (d and e)). Images b and d, acquired at maximal Valsalva manoeuvre, were compared with the ones acquired at rest to determine the antero-posterior diameter of the *levator hiatus* - measured from the postero-inferior border of the *symphysis pubis* to the *puborectalis* muscle (straight red line), which is considered the main constrictor of the pelvic floor.

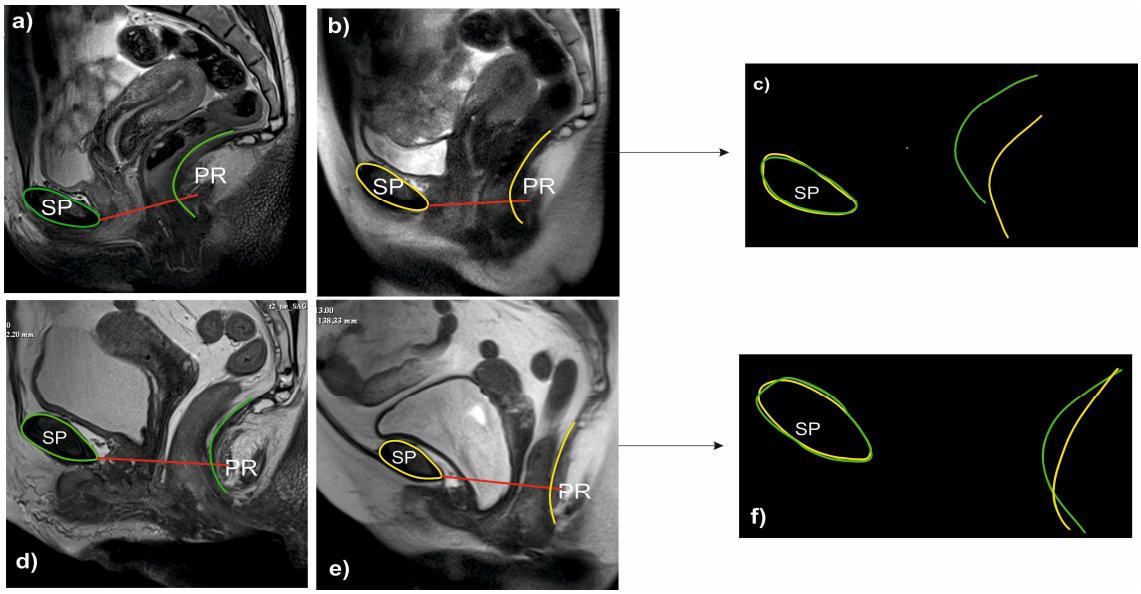

Figure 1. MR images in the mid-sagittal plane of a woman w/o (upper row) and woman w/ (lower row) prolapse. Images were acquired at rest position (a and d), and during maximal Valsalva manoeuvre (b and e). (c and f) show the overlapping of the curves of the rest vs. Valsalva. PR - *puborectalis* muscle; SP - *symphysis pubis*.

In this study, we applied the H-line, M-line, and Organ prolapse (HMO) classification system to the dynamic images acquired at maximal Valsalva. The HMO grading system(Boyadzhyan et al., 2008) elucidates about pelvic floor relaxation by dividing it into two components - hiatal enlargement (by means of the H-line or puborectal *hiatus* line, i.e., the distance between A and B as shown in Figure 2.b) and pelvic floor descent (by measuring the M-line, which extends perpendicularly from the pubococcygeal line (PCL) to the posterior end of the H-line (point B)).

The table on Figure 2 illustrates how pelvic floor relaxation and POP stratified. In women without prolapse, the length of the H-line (straight green) is smaller than 60 mm and the M-line (dashed green) is no more than 20 mm in length. The H-line also enables measuring organ prolapse through the “O” component of the HMO system that

corresponds to the shortest distance between the most caudal aspect of a given organ during Valsalva manoeuvre and the H-line. Figure 2 shows sagittal images at maximal Valsalva manoeuvre from a woman w/o (a) and another one w/ prolapse (b).

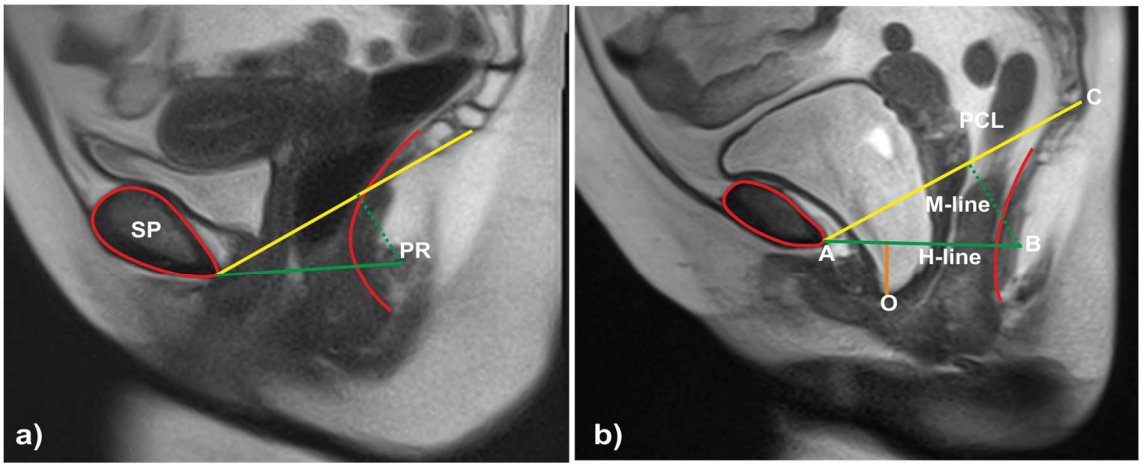

Grade	*Grading of Pelvic Floor Relaxation*		*Grading of Pelvic Organ Prolapse*
	Hiatal Enlargement (H-line) (mm)	*Pelvic Floor Descent (M-line) (mm)*	*Organ location relative to the H-line Distance to point O (mm)*
0 (normal)	<60	0-20	Above
1 (mild)	60-80	20-40	0-20
2 (moderate)	80-100	40-60	20-40
3 (severe)	≥100	≥60	≥40

Figure 2. MR images in the mid-sagittal plane acquired at maximal Valsalva manoeuvre. Women w/o (a) and w/ prolapse (b). The hiatal enlargement (H-line) and the pelvic floor descent (M-line dashed green) and organ location relative to H-line (straight orange line) are shown. The table shows the grading of pelvic floor relaxation and pelvic organ prolapse adapted by Boyadzhyan et al. (Boyadzhyan et al., 2008). PCL - pubococcygeal line; PR - *puborectalis* muscle; SP - *symphysis pubis*.

Numerical Modelling

The T2w axial images were used to build the 3D solid models of the PVM and the surrounding structures - coccyx, internal obturator muscle and the pelvic girdle. These structures were identified and segmented (see Figure 3) by applying a semi-automatic procedure using the Mimics® software v.16 (Software and Services for Biomedical Engineering, Materialise HQ, Belgium), as described by Silva et al. (Silva et al., 2016). Posteriorly, a 3D default-smoothing algorithm (based on the Laplacian 1st order function) of the Mimics software was applied.

After these procedures, the 3D solid models of PVM were imported into the Abaqus software v.2016 (Dassault Systmes Simulia Corp., Providence, RI, USA) and the finite element meshes (with hybrid tetrahedral elements - C3D4H) were created (Figure 3).

These axial images were also used to measure the thickness of the PVM at the level of the midvagina and anal canal (right and left sides) (Figures 3.a and 3.c). The measurements were made in the slice closer to the plane of minimal hiatal dimensions.

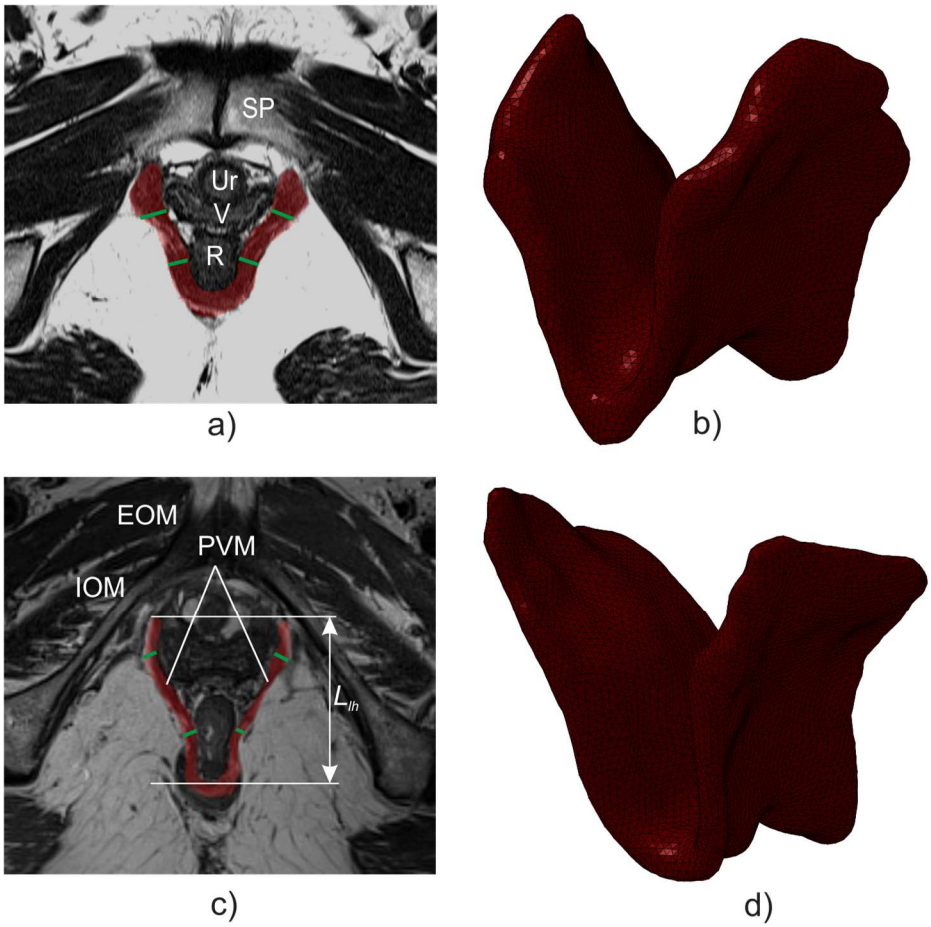

Figure 3. Magnetic Resonance images in the axial plane and finite element mesh of a woman without (a and b, respectively) and with prolapse (c and d, respectively). The thickness (right and left sides) of the *puboviscerali*s muscle (PVM) was measured at the level of the midvagina and the canal anal (EOM - external obturator muscle; IOM - internal obturator muscle; L_{lh} - length of the *levator hiatus;* PVM - *puboviscerali*s muscle; R - rectum; SP - *symphysis pubis*; Ur - urethra V - vagina).

The number of elements and nodes on the finite element meshes varied among the subjects according to the individual differences in the muscle geometry/morphology (ranging between 55,867 and 92,423 elements, and 12,167 and 20,645 nodes). For each

numerical model, the element size was set to be approximately constant throughout the geometry, resulting in a mesh with a characteristic element length of 1.4 mm. The boundary conditions were imposed to incorporate the existence of the 3D solid models of the surrounding structures - coccyx, *symphysis pubis*, internal obturator muscle – as it can be seen in the MR images (see Figure 4).

The nodes corresponding to the insertion of the PVM were considered zero-displacement nodes (Parente et al., 2008; M. P. L. Parente et al., 2009; Rubod et al., 2012). The pressure applied to the inner surface of the PVM was 4 kPa, as suggested by Noakes et al. (Noakes et al., 2008). This pressure corresponds to the approximated average supine Valsalva pressure (4.5 kPa), to which the mean resting pressure (0.5 kPa) was subtracted, as the muscles already incorporate resting tone.

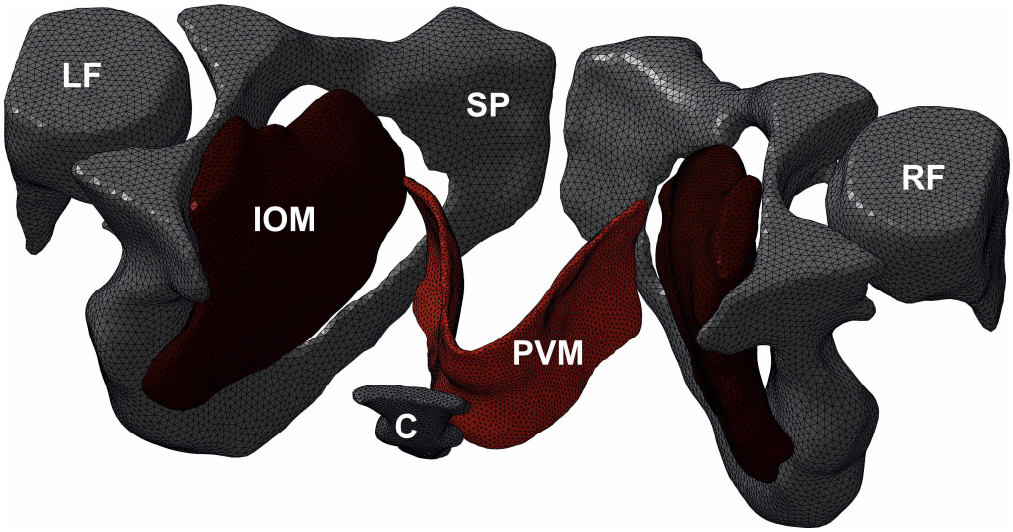

Figure 4. Finite element mesh of a woman without prolapse. The coccyx, internal obturator muscle and *symphysis pubis* were included in the model to help defining the boundary conditions. C - coccyx; IOM - internal obturator muscle; LF - left femur; PVM - *puboviscerali*s muscle; RF - right femur; SP - *symphysis pubis*.

The inverse Finite Element Analysis

The material constants for the different constitutive models - Neo-Hookean, Mooney-Rivlin and Yeoh - were determined by using the same methodology of the inverse FEA previously implemented by Silva et al. (Silva et al., 2016). In order to determine them the Python scripting Language was applied to couple the MATLAB MathWorks v.R2016a (Mathematical Computing Software, Natick, Massachusetts, USA) and the Abaqus software.

The present inverse FEA uses the Powell optimization algorithm, which has no need to calculate a gradient in order to minimize the objective function, in this case, the distance between two curves (Gao et al., 2013; Powell, 1977). It is based on the concept of conjugate directions $\mathbf{D}$, where $\mathbf{D}^i$ and $\mathbf{D}^j$ are conjugate if (Eq. 1):

$$(\mathbf{D}^i)^T \mathbf{H} \mathbf{D}^j = 0 \tag{1}$$

where $\mathbf{H}$ is the Hessian matrix containing the second-order partial derivatives. In the present work, the procedure starts by assuming $\mathbf{H}$ as the identity matrix, as illustrated by Eq. (2),

$$\mathbf{H} = \begin{bmatrix} 1 & 0 & \dots & 0 \\ 0 & 1 & \dots & 0 \\ \vdots & \vdots & \ddots & \vdots \\ 0 & 0 & \dots & 1 \end{bmatrix} \tag{2}$$

where each column of $\mathbf{H}$ represents the unidirectional search vector $\mathbf{D}^i, i = 1, n$ and in each search, the vector $\mathbf{X}$ is updated according to Eq. (3):

$$\mathbf{X}^{i} = \mathbf{X}^{i-1} + \beta_i^* \mathbf{X}^{i-1}\mathbf{D}^{i} \tag{3}$$

the constant β^* was tested with values from the vector: {-0.200, -0.150, -0.100, -0.050, -0.010, -0.001, 0.000, 0.001, 0.010, 0.050, 0.100, 0.150, 0.200}. Since the function to be optimized is the result of a finite element simulation, it is necessary to obtain the optimum value for β^* in each search direction. After that, $\mathbf{D}^i$ is replaced in the matrix $\mathbf{H}$ by $\beta_i^*\mathbf{D}^i$. Having completed the n unidirectional searches, a new conjugate search direction is created by adding all the columns of $\mathbf{H}$. This becomes the n+1 search direction (Powell, 1977), corresponding to the conjugate direction $\mathbf{D}^{n+1}$. More details can be consulted on the work of Silva et al. (Silva et al., 2016).

$$\mathbf{D}^{n+1} = \sum_{i=1}^{n} \beta_i^* \mathbf{D}^{i} \tag{4}$$

Hence the conjugate direction is obtained, a new search for the optimum set of materials constants is conducted according to Eq. (5).

$$\mathbf{X}^{n+1} = \mathbf{X}^{n} + \beta_{n+1}^* \mathbf{D}^{n+1} \tag{5}$$

The first column of $\mathbf{H}$, which represents the direction of the first search in the matrix $\mathbf{H}$, is now deleted and all the columns orders are shifted in order for the new

direction $\beta_{n+1}^{*}\mathbf{D}^{n+1}$ to be added. The entire process is repeated until convergence is satisfied and error measure is minimized Eq. (6).

So, the aim was to estimate the material constants for the different constitutive models were obtained from the vector associated to $\mathbf{X}^{n+1}$ in Eq. (5) and the error measure was based on the comparison of a set points between two curves: one corresponds to the position of the *puborectalis* muscle - the main constrictor of the pelvic floor - defined by a mid-sagittal line in the numerical model (shown in the right side of the Figure 5) for each iteration and consequent deformation, and the other curve represents its position in the dynamic mid-sagittal image acquired at Valsalva manoeuvre (left side, Figure 5). In all the iterations, the orthogonal distance between two curves defined on top of the *puborectalis* muscle, at rest and in the deformed position, was calculated.

In this work, the inverse FEA is an iterative process that updates the material constants through the computation of the *Error* measure - the value of the distance between the two compared curves:

$$Error = \sum_{i=1}^{np} \left\| d_{MRI_i} - d_{FEA_i} \right\| \tag{6}$$

where *np* is the number of points d_{MRI_i} used to define the first curve and d_{FEA_i} is the closest point projection of d_{MRI_i} on the second curve (Silva et al., 2016). The *Final Error* is described as follows:

$$Final\ Error = \frac{Error}{np} \tag{7}$$

The objective function (Eq. 8) corresponds to the normalized *Final Error*. For this normalization the *levator hiatus* length (L_{lh}) was used (see Figure 3). The stopping criteria was set to $f < 5\%$.

$$f = \frac{Final\ Error}{L_{lh}} \times 100 \tag{8}$$

The Neo-Hookean, Mooney-Rivlin and Yeoh isotropic constitutive models were applied in the numerical simulations for the PVM, similarly to previous studies simulating Valsalva manoeuvre, defecation (Janda, 2006; Lee et al., 2005; Noakes et al., 2008) and vaginal delivery (Li et al., 2008). They were chosen due to their computational simplicity, with few constants to optimize. Moreover, these models use a nonlinear relationship between stress and strain to describe incompressible hyperelastic materials, which is the most common definition for the material properties of the pelvic floor muscles. When using these constitutive models, it is assumed that the muscles are always subjected to loads and boundary conditions that cause the direction of the maximum principal stresses and strains to be aligned with the muscle fibers and that the obtained material constants only correctly characterize the muscles in this direction.

In this study, muscles were assumed as being in a passive state, in which the active component of the muscle is not considered. Additionally, in the current constitutive models used do simulate the active behavior of muscles, the active component of the

strain energy density function is not coupled with the passive component (d'Aulignac et al., 2005; Martins et al., 2013b).

The Neo-Hookean (Equation 9), Mooney-Rivlin (Equation 10) and Yeoh (Equation 11) constitutive models are characterized by:

$$W = c_1(I_1 - 3) \tag{9}$$

$$W = c_1(I_1 - 3) + c_2(I_2 - 3) \tag{10}$$

$$W = c_1(I_1 - 3) + c_2(I_1 - 3)^2 + c_3(I_1 - 3)^3 \tag{11}$$

where W is the strain energy function and c_1, c_2 and c_3 are the material constants to be determined that have dimensions of stress; I_1, I_2 and I_3 are the strain invariants of the right Cauchy-Green tensor (Noakes et al., 2008). The principal Cauchy stress is characterized in Equation 12 (Martins et al., 2006):

$$\sigma_i = J^{-1}\lambda_i \frac{\partial W}{\partial \lambda_i}, \quad i = 1, 2, 3. \tag{12}$$

where λ_i are the principal stretches and J corresponds to the isotropic incompressible (J=1) hyperelastic material.

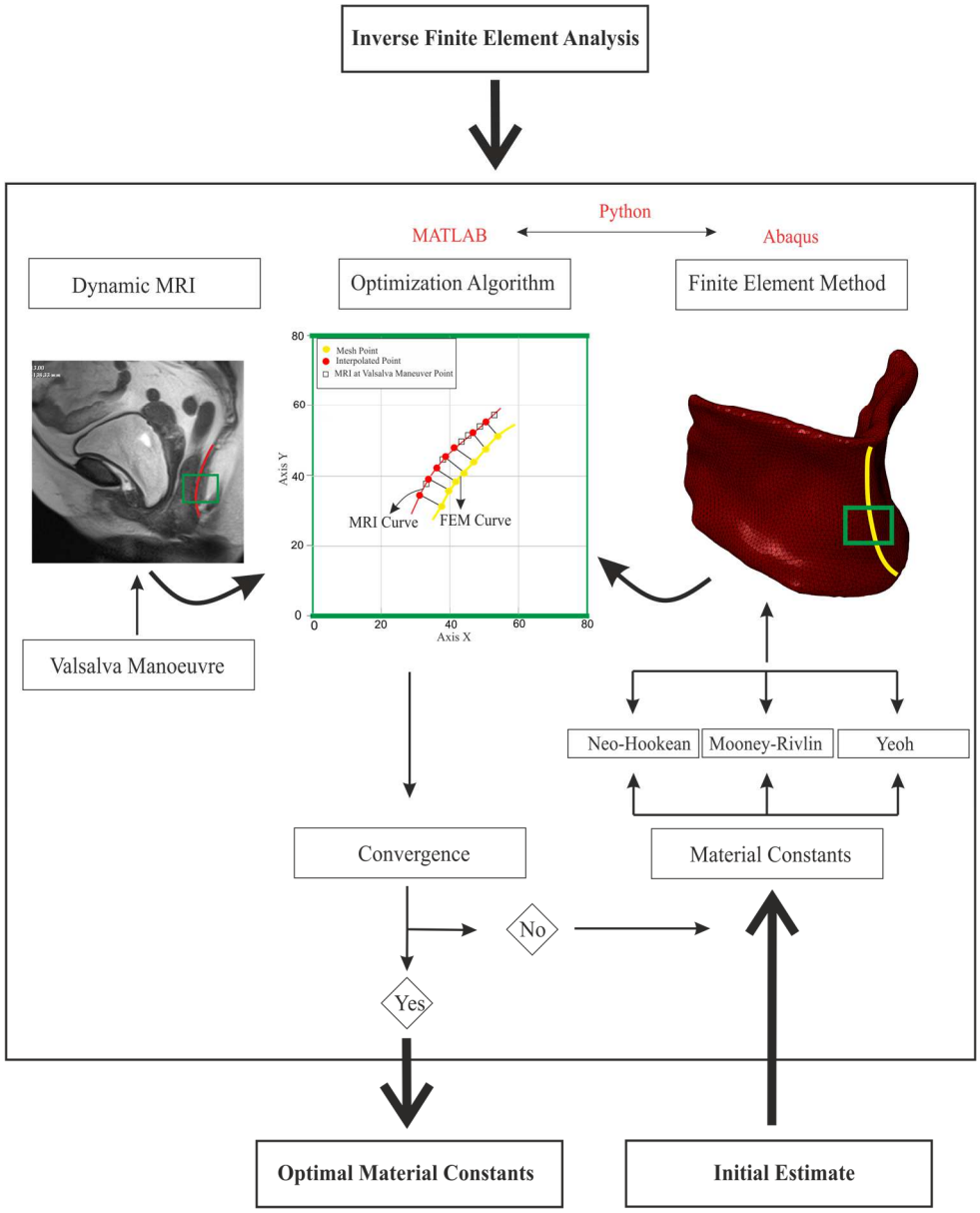

Figure 5. Flow chart of the inverse FEA. Several procedures were set to get the adjusted material constants of the Neo-Hookean, Mooney-Rivlin and Yeoh constitutive models.

Statistical analysis

All analyses were computed using IBM SPSS Statistics 23.0 software. Descriptive statistics (mean and standard deviation for continuous variables) were calculated. Mann-Whitney *U* test was used to compare the two groups (women w/ *vs.* w/o prolapse). The demographic and morphological characteristics and material constants of the three different constitutive models (Neo-Hookean, Mooney-Rivlin and Yeoh) were compared between groups to determine the precision of the results obtained through the Finite element modelling. Significance level was established as $p<0.05$.

3. Results

To further corroborate the clinical results, the POP-Q, the HMO grading system was applied. The results are summarized in Table 1 for all subjects.

Table 1. Clinical results for the two groups obtained from the measurements in MR images.

	Without pelvic organ prolapse				***With pelvic organ prolapse***				
	subj 1	*subj 2*	*subj 3*	*subj 4*	*subj 5*	*subj 6*	*subj 7*	*subj 8*	*subj 9*
Stage of prolapse	0	0	0	0	1	1	2	1	2

subj: subject.

Demographic and morphological characteristics of the women w/ and w/o POP are presented in Table 2 (shown as mean ±SD). When comparing the two groups, there was no significant difference in age, body mass index (BMI) and parity.

There was also no significant difference in muscle thickness at the level of the anal canal between the two groups, as opposite to the findings at the level of the midvagina.

Table 2. Demographic characteristics and measurements of muscle thickness in women w/ and w/o POP.

variable		*w/o POP (n=4)*	*w/ POP (n=5)*	*p value*
age		41.50±16.22	48.80±16.02	0.730
BMI		25.88±4.83	29.55±4.69	0.413
parity		1.00±1.16	1.60±0.89	0.556
thickness (mm)	**MidVa (left)**	7.70±1.84	5.31±0.53	0.016*
	MidVa (right)	7.03±1.94	4.65±0.68	0.016*
	AC (left)	5.48±1.13	4.50±1.81	0.413
	AC (right)	5.67±1.78	4.72±0.84	0.556

AC: anal canal; BMI: body mass index; MidVa: midvagina; mm: millimetres; w/ POP: with pelvic organ prolapse; w/o POP: without pelvic organ prolapse.
*statistically significant.

The estimation of the material constants evidenced a significant difference between two groups (p<0.05), with the values of women w/ prolapse showing higher values for the three different constitutive models (Table 3).

Table 3. Material constants for the pubovisceral muscle obtained for the three different constitutive models obtained through inverse FEA.

***Variable* (MPa)**		***w/o POP (n=4)***	***w/ POP (n=5)***	***P value***
Neo-Hookean	c_1	0.025±0.005	0.058±0.014	0.016*
Mooney-Rivlin	c_1	0.020±0.003	0.035±0.006	0.016*
	c_2	0.006±0.002	0.025±0.009	0.016*
Yeoh	c_1	0.019±0.003	0.0054±0.014	0.016*
	c_2	0.009±0.008	0.042±0.025	0.032*
	c_3	0.004±0.004	0.029±0.018	0.016*

w/ POP: with pelvic organ prolapse; w/o POP: without pelvic organ prolapse.
*statistically significant.

Figure 6 presents the mechanical response of the PVM from women w/o and w/ prolapse. To compare the stress-stretch mechanical response, the material constants obtained directly from Equation 12 were compared with experimental data from non-prolapsed cadaveric LA muscle (Martins, 2010), assuming similar properties along all the portions of the muscle. The curve of the Yeoh constitutive model for women w/ prolapse follows the behavior of the experimental curve. The maximum stress values are higher for prolapsed muscles for the three constitutive models when compared with controls.

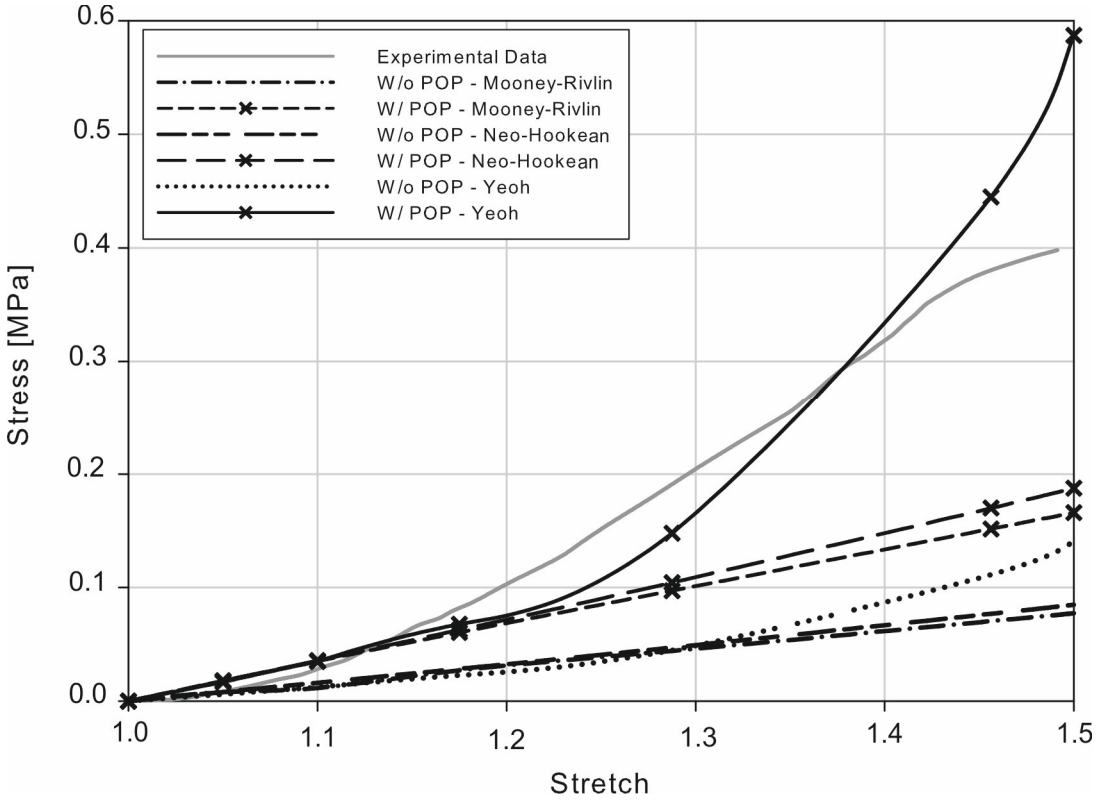

Figure 6. Stress-stretch response for passive behavior of the PVM for the different constitutive models for women w/ POP and w/o POP was compared with the experimental curve obtained by Martins et al. in normal muscle (Martins, 2010).

Figure 7 illustrates the PVM and surrounding structures at rest (a), the magnitude of displacements (b) and principal logarithmic strain (c) during Valsalva manoeuvre for a woman w/o POP. The posterior area of the PVM evidenced the greatest values of displacement (7.89 mm), using the material constants for the Mooney-Rivlin (Table 3). The principal logarithmic strain shows that the elements representing the insertion points display the highest values of deformation, along with the mid-posterior portion of the PVM.

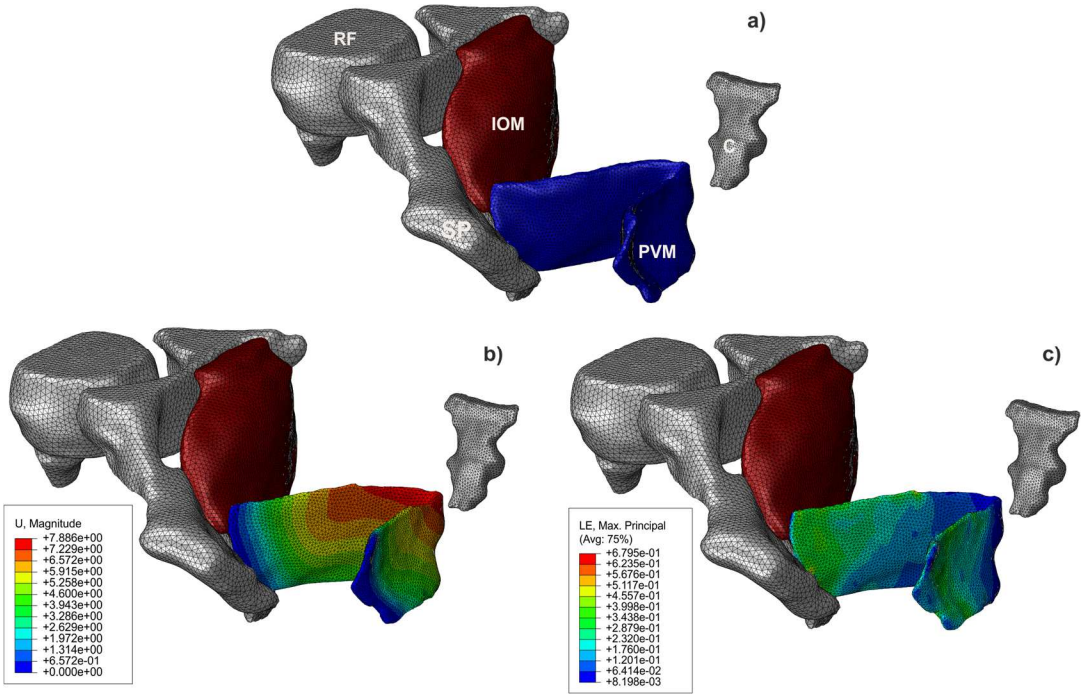

Figure 7. PVM of a woman without prolapse, at rest (a), the magnitude displacement (b) and the logarithmic strain (c) during Valsalva manoeuvre. Some of the osseous structures were eliminated for a better visualization of the muscle. C - coccyx; IOM - internal obturator muscle; PVM - *puboviscerali*s muscle; RF - right femur; SP - *symphysis pubis*.

The mean antero-posterior (AP) diameter of the *levator hiatus*, was 10 mm larger in women with prolapse both at rest and when maintaining the Valsalva manoeuvre, when compared to women without prolapse (p=0.029; p=0.029) (see Table 4).

Table 4. Antero-posterior hiatal diameter measured in the dynamic MR image.

AP Diameter		***w/o POP***	***w/ POP***	***p value***
levator hiatus (mm)	**Rest**	49.76±4.67	60.03±6.51	0.029*
	Valsalva	57.18±2.86	66.69.±4.81	0.029*

w/ POP: with pelvic organ prolapse; w/o POP: without pelvic organ prolapse.
*statistically significant.

Table 5 presents the means values of the antero-posterior displacements of the PVM in the numerical simulation *vs.* MRI. The displacements obtained in the numerical simulation were similar with the ones obtained in the dynamic MRI for the three constitutive models (p-values>0.05). When comparing the two groups, the difference in the displacements for women w/o POP and women w/ POP was approximately 36.38% for the Neo-Hooke, 31.41% for the Mooney-Rivlin and 33.32% for the Yeoh model, respectively, and the variation in the MR images was 13.79%.

Table 5. Mean values of the antero-posterior displacement of the dynamic MRI compared with the displacements of the numerical models for women w/ POP and w/o POP.

variable	MRI (mm)	Neo-Hookean (mm)	Mooney-Rivlin (mm)	Yeoh (mm)
w/o POP-AP	7.723±2.484	7.322±1.189	7.468±1.331	7.898±1.406
w/ POP-AP	6.658±4.059	4.658±2.273	5.122±2.432	5.266±2.263
p-value	0.905	0.190	0.286	0.190
percent variation (%)	13.79%	36.38%	31.41%	33.32%

w/ POP-AP: with pelvic organ prolapse – antero-posterior; w/o POP-AP: without pelvic organ prolapse – antero-posterior.

Figure 8 shows the posterior contour of the PVM to better illustrate the displacements along the mid-sagittal plane. The contour of the posterior region is drawn at rest (dashed contour) and at the position during the Valsalva manoeuvre for the same model, with material constants obtained for women w/ POP (green fill) and w/o POP (red fill) and for the three constitutive models: Neo-Hookean (a), Mooney-Rivlin (b) and Yeoh (c). The displacements obtained with the Neo-Hookean and Mooney-Rivlin were similar

and higher that the ones obtained when using the Yeoh constitutive model with the material constants for women w/ POP and w/o POP.

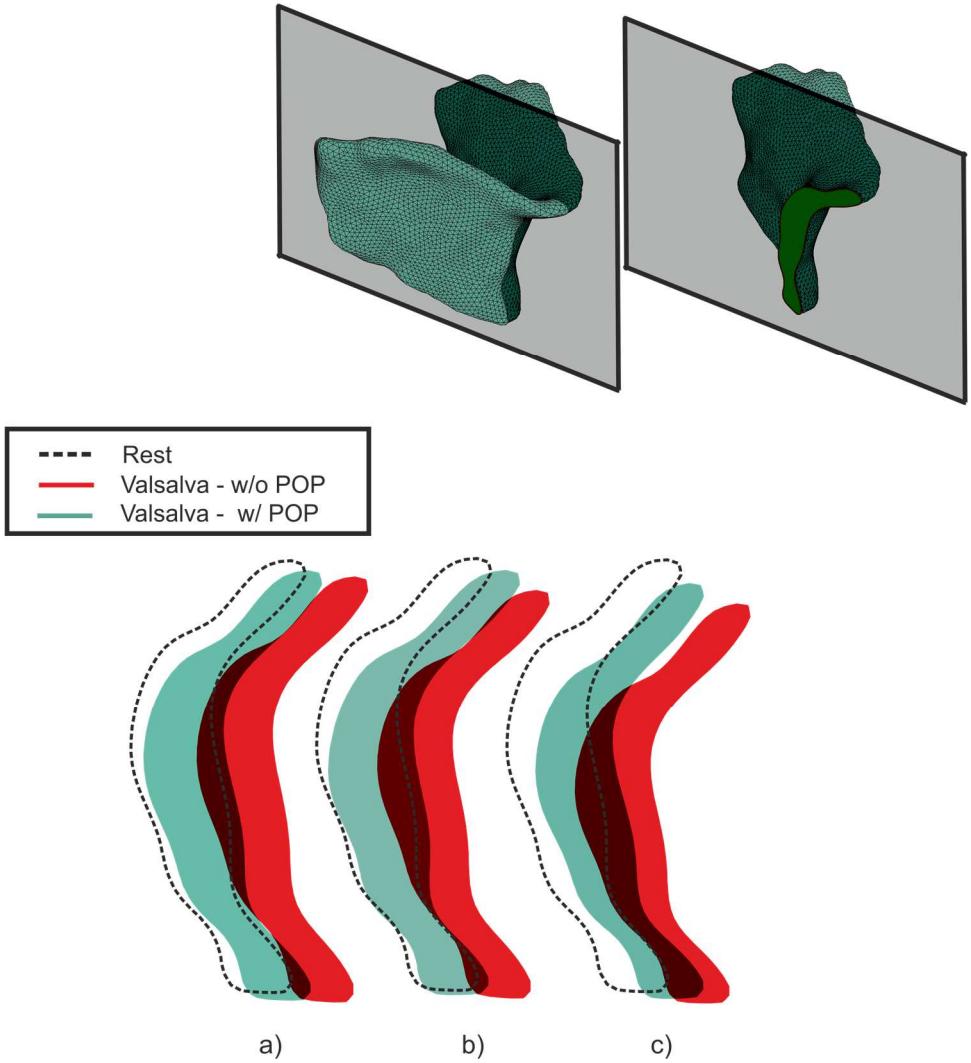

Figure 8. PVM contour for a woman without prolapse using the Neo-Hookean (a), Mooney-Rivlin (b) and Yeoh (c) constitutive models.

4. Discussion

The Valsalva manoeuvre is used to assess muscle (in)ability to prevent urethral hypermobility or organ prolapse (Ornö and Dietz, 2007). POP has been associated to LA

muscle injury and increased size of *levator hiatus* (Brandão et al., 2013; Schwertner-Tiepelmann et al., 2012), but it can also be associated to changes in collagen subtypes or connective tissue metabolism (Dietz, 2008; Kerkhof et al., 2009).

An inverse FEA was used with an optimization algorithm to understand the influence of POP on the material constants. For the three constitutive models (Neo-Hookean, Mooney-Rivlin and Yeoh) these material constants were determined, being the computational time six times longer for the Yeoh constitutive model than for the Neo-Hookean. When comparing the two groups, the ratio between the values of the material constants for women w/o and w/ prolapse was approximately 43% for the c_1 parameter of the Neo-Hookean constitutive model, 57% and 24% for c_1 and c_2 of the Mooney-Rivlin constitutive model, and 35%, 21% and 14% for c_1, c_2 and c_3 of the Yeoh constitutive model, meaning that women with prolapse presented a higher stiffness. Our findings are in line with previous experimental *in-vitro* studies with vaginal tissue showing that the elasticity module is significantly higher in the prolapsed tissue when compared with the normal tissue (Jean-Charles et al., 2010; Lei et al., 2007), but Lei et al. (Lei et al., 2007) also concluded that there are no significant differences in biomechanical properties between moderate and severe type of POP.

The difference obtained in the values of the material constants between groups can be associated to differences in muscle morphology, with women w/ POP presenting thinner muscles, as previously described by Brandão et al. (Brandão et al., 2013). The thinner muscles in women with POP can have an histological response, decreasing the total collagen content and increasing the concentration of collagen type III (Kerkhof et al., 2009). An increase in collagen type III in combination with an increase in active matrix metalloproteinases (MMP-9) is typical of prolapsed muscles that are actively

remodelling to accommodate a progressively increasing mechanical load (Kerkhof et al., 2009; Martins et al., 2013a). Also, the antero-posterior diameter of the *levator hiatus* was higher for the group of women w/ POP (Table 5), in line with previous results (Brandão et al., 2013; Clark et al., 2010; Ying et al., 2012). However, when comparing the antero-posterior displacement between two groups (w/POP and w/o POP) there was no significant difference for the numerical models using the three constitutive models and MRI (Table 6). The variation of the antero-posterior displacement between numerical model *vs.* MRI can be associated with poor cooperation of women w/POP during the dynamic MRI acquisition - the standard deviation was approximately 4.059 mm for the women with POP - or it can also be to the simplicity of the numerical models.

Since there is no significant difference for any of the demographic characteristics (age, BMI and parity) and there is no visible injury to the PVM in the MR images, the thickness differences may be due to changes in the pelvic architecture and properties of the soft tissues.

The present study has certain limitations. First, the sample size was small. Secondly, the numerical models did not include the pelvic organs and connective tissue, which would be more realistic. Thirdly, the pressure applied in the model to mimic Valsalva manoeuvre was retrieved from the literature (Noakes et al., 2008), but one cannot guarantee that the same pressure was performed by the women during the scanning. A better approximation would be achieved by means of an intracavitary measurement instrument. Finally, three different isotropic constitutive models (Neo-Hookean, Mooney-Rivlin, and Yeoh) were used to characterize the mechanical behavior of the pelvic floor muscles, but future work should include a quasi-incompressible transversely isotropic hyperelastic model (Martins et al., 1998) which could perhaps more

accurately reproduce the nonlinear stress-strain relationship and anisotropic behavior of the muscles. These muscles are anisotropic due to the presence of the muscle fibers, which play an important role in muscle stiffness. Muscle fibers directions are aligned in the longitudinal direction of the muscle, which corresponds to the direction in which the muscle is subjected to load. Muscle fibers are aligned with the loading direction, as a biological response to an optimization problem. For future works, in order to include direction of the muscle fibers, data from MR diffusion tensor imaging (DTI) can be used to estimate of overall muscle fiber directionality of the PVM, based on the water diffusivity. As referred before, muscle fibers are highly anisotropic structures and water molecules are more likely to diffuse along muscle direction. Hence, the major diffusion eigenvector can be assumed to be close to the muscle's fibers direction (Brandão et al., 2017).

Hence, despite the limitations mentioned above, the methodology used in this work allowed to determine the material constants of the PVM *in vivo* in a non-invasive manner and these results are comparable with *ex vivo* experimental results (Martins, 2010), as shown in Figure 6.

The inverse FEA coupled to MRI may enable estimating accurately the biomechanical properties of the subject-specific iteratively. It is possible to use this methodology in the clinical setting during the planning of surgical procedures for POP. Mesh implants could be used more efficiently by first characterizing the mechanical properties of the pelvic tissues and then optimizing the mesh properties, such as its stiffness, in order to reduce failure rates of surgical procedures.

In conclusion, the inverse FEA used in this study allowed establishing the material constants of the muscles in women w/ and w/o prolapse in order to simulate a more

realistic passive behavior. The present computational analysis showed that women w/ POP had stiffer muscles as described in the literature (Jean-Charles et al., 2010; Lei et al., 2007).

Conflict of interest statement

The authors declare that there is no financial, professional or other personal interest of any nature or kind in any product, service and/or company that could be constructed as influencing the position.

Acknowledgments

The authors gratefully acknowledge the funding by Ministério da Ciência Tecnologia, e Ensino Superior, FCT, Portugal, under grants SFRH/BD/89519/2012 and IF/00159/2014, and the project UID/EMS/50022/2013. The fifth author acknowledge the funding of Project NORTE-01-0145-FEDER-000022 - SciTech - Science and Technology for Competitive and Sustainable Industries, cofinanced by Programa Operacional Regional do Norte (NORTE2020), through Fundo Europeu de Desenvolvimento Regional (FEDER).

References

Barber, M.D., Bremer, R.E., Thor, K.B., Dolber, P.C., Kuehl, T.J., Coates, K.W., 2002. Innervation of the female levator ani muscles. Am. J. Obstet. Gynecol. 187, 64–71.

Boyadzhyan, L., Raman, S.S., Raz, S., 2008. Role of static and dynamic MR imaging in surgical pelvic floor dysfunction. Radiographics 28, 949–967.

Brandão, S., Da Roza, T., Mascarenhas, T., Duarte, S., Ramos, I., Parente, M., Jorge, R.N., 2013. Moment of inertia as a means to evaluate the biomechanical impact of pelvic organ prolapse. Int. J. Urol. 20, 86–92.

Brandão, S., Parente, M., Mascarenhas, T., da Silva, A.R.G., Ramos, I., Jorge, R.N., 2015. Biomechanical study on the bladder neck and urethral positions: Simulation of impairment of the pelvic ligaments. J. Biomech. 48, 217–223.

Brandão, S., Parente, M., Silva, E., Da Roza, T., Mascarenhas, T., Leitão, J., Cunha, J., Natal Jorge, R., Nunes, R.G., 2017. Pubovisceralis Muscle Fiber Architecture Determination: Comparison Between Biomechanical Modeling and Diffusion Tensor Imaging. Ann. Biomed. Eng.

Clark, N.A., Brincat, C.A., Yousef, A., DeLancey, J.O.L., 2010. Levator defects affect perineal position independently of prolapse status. Am J Obs. Gynecol. 203, 595.e17-595.e22.

d'Aulignac, D., Martins, J. a C., Pires, E.B., Mascarenhas, T., Jorge, R.M.N., 2005. A shell finite element model of the pelvic floor muscles. Comput. Methods Biomech. Biomed. Engin. 8, 339–347.

DeLancey, J., Morgan, D., Fenner, D., Kearney, R., Guire, K., Miller, J., Hussain, H., Umek, W., Hsu, Y., Ashton-Miller, J., 2007. Comparison of levator ani muscle defects and function in women with and without pelvic organ prolapse. Obs. Gynecol. 109, 295–302.

Dietz, H.P., 2008. The aetiology of prolapse. Int. Urogynecol. J. Pelvic Floor Dysfunct. 19, 1323–1329.

Dietz, H.P., Shek, C., Clarke, B., 2005. Biometry of the pubovisceral muscle and levator hiatus by three-dimensional pelvic floor ultrasound. Ultrasound Obstet. Gynecol. 25, 580–585.

Gao, W., Liu, S., Huang, L., 2013. A novel artificial bee colony algorithm with Powell's method. Appl. Soft Comput. 13, 3763–3775.

Hendrix, S.L., Clark, A., Nygaard, I., Aragaki, A., Barnabei, V., McTiernan, A., 2002. Pelvic organ prolapse in the women's health initiative: Gravity and gravidity. Am. J. Obstet. Gynecol. 186, 1160–1166.

Hsu, Y., Summers, A., Hussain, H.K., Guire, K.E., Delancey, J.O.L., 2006. Levator plate angle in women with pelvic organ prolapse compared to women with normal support using dynamic MR imaging. Am. J. Obstet. Gynecol. 194, 1427–1433.

Janda, S., 2006. Biomechanics of the pelvic floor musculature. PhD. Thesis. Technische Universiteit Delft.

Janda, S., Van Der Helm, F.C.T., De Blok, S., 2003. Measuring morphological parameters of the pelvic floor for finite element modelling purposes. J. Biomech. 36, 749–757.

Jean-Charles, C., Rubod, C., Brieu, M., Boukerrou, M., Fasel, J., Cosson, M., Clay, J.-C., Rubod, C., Brieu, M., Boukerrou, M., Fasel, J., Cosson, M., 2010. Biomechanical properties of prolapsed or non-prolapsed vaginal tissue: impact on genital prolapse surgery. Int. Urogynecol. J. 21, 1535–1538.

Kerkhof, M.H., Hendriks, L., Brölmann, H. a M., 2009. Changes in connective tissue in patients with pelvic organ prolapse--a review of the current literature. Int. Urogynecol. J. Pelvic Floor Dysfunct. 20, 461–474.

Kuncharapu, I., Majeroni, B.A., Johnson, D.W., 2010. Pelvic organ prolapse. Am. Fam. Physician 81, 1111–1117.

Lee, S., Darzi, A., Yang, G., 2005. Subject Specific Finite Element Modelling of the Levator Ani. Med. Image Comput. Comput. Interv. 3749, 360–367.

Lei, L., Song, Y., Chen, R., 2007. Biomechanical properties of prolapsed vaginal tissue in pre- and postmenopausal women. Int. Urogynecol. J. Pelvic Floor Dysfunct. 18, 603–607.

Li, X., Kruger, J.A., Chung, J.H., Nash, M.P., Nielsen, P.M.F., 2008. Modelling childbirth: Comparing athlete and non-athlete pelvic floor mechanics. Med Image Comput Comput - Assist Interv. 11, 750–757.

Martins, J.A.C., Pires, E.B., Salvado, R., Dinis, P.B., 1998. A numerical model of passive and active behavior of skeletal muscles. Comput. Methods Appl. Mech. Eng. 151, 419–433.

Martins, P.A.L., 2010. Experimental and numerical studies of soft biological tissues. PhD. Thesis. Faculty of Engineering, University of Porto, Portugal.

Martins, P., Jorge, R.N., Ferreira, A., 2006. A Comparative Study of Several Material Models for Prediction of Hyperelastic Properties: Application to Silicone-Rubber and Soft Tissues. Strain 42, 135–147.

Martins, P., Lopes Silva-Filho, A., Rodrigues Maciel Da Fonseca, A.M., Santos, A., Santos, L., Mascarenhas, T., Natal Jorge, R.M., Ferreira, A.J.M., 2013a. Biomechanical properties of vaginal tissue in women with pelvic organ prolapse. Gynecol. Obstet. Invest. 75, 85–92.

Martins, P., Silva-Filho, A.L., Fonseca, A.M.R.M., Santos, A., Santos, L., Mascarenhas, T., Jorge, R.M.N., Ferreira, A.M., 2013b. Strength of round and uterosacral ligaments: a biomechanical study. Arch. Gynecol. Obstet. 287, 313–8.

Noakes, K.F., Pullan, A.J., Bissett, I.P., Cheng, L.K., 2008. Subject specific finite elasticity simulations of the pelvic floor. J. Biomech. 41, 3060–3065.

Ornö, A.K., Dietz, H.P., 2007. Levator co-activation is a significant confounder of pelvic organ descent on Valsalva maneuver. Ultrasound Obstet. Gynecol. 30, 346–350.

Parente, M.P., Jorge, R.M.N., Mascarenhas, T., Fernandes, A.A., Martins, J.A.C., 2009a. The influence of an occipito-posterior malposition on the biomechanical behavior of the pelvic floor. Eur. J. Obstet. Gynecol. Reprod. Biol. 144, S166–S169.

Parente, M.P., Natal Jorge, R., Mascarenhas, T., Fernandes, A., Martins, J., 2009b. The influence of the material properties on the biomechanical behavior of the pelvic floor muscles during vaginal delivery. J. Biomech. 42, 1301–1306.

Parente, M.P., Natal Jorge, R., Mascarenhas, T., Fernandes, A., Martins, J., 2008. Deformation of the pelvic floor muscles during a vaginal delivery. Int. Urogynecol. J. Pelvic Floor Dysfunct. 19, 65–71.

Powell, M.J.D., 1977. Restart procedures for the conjugate gradient method. Math. Program. 12, 241–254.

Rubod, C., Boukerrou, M., Brieu, M., Jean-Charles, C., Dubois, P., Cosson, M., 2008. Biomechanical properties of vaginal tissue: Preliminary results. Int. Urogynecol. J. Pelvic Floor Dysfunct. 19, 811–816.

Rubod, C., Brieu, M., Cosson, M., Rivaux, G., Clay, J.C., De Landsheere, L., Gabriel, B., 2012. Biomechanical properties of human pelvic organs. Urology 79, 968.e17-968.e22.

Saleme, C.S., Parente, M.P.L., Natal Jorge, R.M., Pinotti, M., Silva-Filho, A.L., Roza, T., Mascarenhas, T., Tavares, J.M.R.S., 2011. An approach on determining the displacements

of the pelvic floor during voluntary contraction using numerical simulation and MRI. Comput. Methods Biomech. Biomed. Engin. 14, 365–370.

Schwertner-Tiepelmann, N., Thakar, R., Sultan, A.H., Tunn, R., 2012. Obstetric levator ani muscle injuries: Current status. Ultrasound Obstet. Gynecol. 39, 372–383.

Silva, M., Brandao, S., Parente, M., Mascarenhas, T., Natal Jorge, R., 2016. Establishing the biomechanical properties of the pelvic soft tissues through an inverse finite element analysis using magnetic resonance imaging. Proc. Inst. Mech. Eng. Part H J. Eng. Med. 230, 298–

Tumbarello, J.A., Hsu, Y., Lewicky-Gaupp, C., Rohrer, S., DeLancey, J.O.L., 2010. Do repetitive Valsalva maneuvers change maximum prolapse on dynamic MRI? Int. Urogynecol. J. Pelvic Floor Dysfunct. 21, 1247–1251.

Ying, T., Li, Q., Xu, L., Liu, F., Hu, B., 2012. Three-dimensional ultrasound appearance of pelvic floor in nulliparous women and pelvic organ prolapse women. Int. J. Med. Sci. 9, 894–900.

Part B - Article 4

Characterisation of the Passive and Active Material Parameters of the *Puboviscerali*s Muscle using an Inverse Numerical Method

M.E.T. Silva[a], M.P.L. Parente[a], S. Brandão[a,b] , T. Mascarenhas[c],

R.M. Natal Jorge[a]

[a]LAETA, INEGI, Faculty of Engineering, University of Porto, Porto, Portugal
[b]Department of Radiology, Centro Hospitalar de São João-EPE, Faculty of Medicine, University of Porto, Porto, Portugal
[c]Department of Gynecology and Obstetrics, Centro Hospitalar de São João-EPE, Faculty of Medicine, University of Porto, Porto, Portugal

Submitted to: Journal of Biomechanics (under review), December 2016.

Abstract

The mechanical characteristics of the female pelvic floor are relevant to understand pelvic floor dysfunctions, and how they are related with changes in their biomechanical behaviour. Urinary incontinence (UI) and pelvic organ prolapse (POP) are the most common pathologies, which can be associated with changes in the mechanical properties of the supportive structures in the female pelvic cavity. The related conditions have been studied through different methods, from experimental tensile tests using tissues from fresh female cadavers or tissues collected at the time of a transvaginal hysterectomy procedure and imaging techniques.

In this work, an inverse finite element analysis (FEA) was used to understand the passive and active behaviour of the *pubovisceralis* muscle (PVM) during Valsalva manoeuvre and muscle active contraction, respectively. Individual numerical models of women without pathology, with stress urinary incontinence (SUI) and with POP were built based on magnetic resonance images, including the PVM and surrounding structures.

The passive and active material parameters for a constitutive model were estimated for the three groups, and were found to be significantly higher for the women with POP when compared with the other two groups. The PVM of women with POP showed the highest stiffness. Additionally, the influence of these parameters was analysed by evaluating their stress-strain, and force-displacements response. The force produced by the PVM in women with POP was 47% and 82% higher when compared to women without pathology and with SUI, respectively.

The inverse FEA allowed estimating the material parameters of the PVM using input information acquired non-invasively.

Keywords Pelvic floor dysfunctions, magnetic resonance imaging, numerical simulation, material parameters, constitutive model, inverse finite element analysis.

1. Introduction

Urinary incontinence (IU) and pelvic organ prolapse (POP) are clinical conditions described in the literature as pelvic floor dysfunctions (PFD). They relate to weakening or injury in the support structures, such as the pelvic floor muscles (PFM), ligaments or endopelvic fascia. In the United States 24% of women are affected by one of these and it is estimated that the number of women with PFD will increase from 28.1 million in 2010 to 43.8 million in 2050 (Memon and Handa, 2013). Moreover, 11% of the women will require corrective surgery for dysfunction at least once in their lifetime (Luo et al., 2014). Re-operation rates are around 30%, and there is also evidence of reduced time interval between repeated procedures (Segal et al., 2012). The PFD impair the quality of life for many women, imply high costs, and represent a major public health problem due a high prevalence (Kiyosaki et al., 2012). Known risk factors associated with UI and POP are increased age, hormonal changes, pregnancy or vaginal delivery (Schwertner-Tiepelmann et al., 2012). Stress urinary incontinence (SUI) - the involuntary urinary leakage associated with increase of the intra-abdominal pressure (IAP) (Bø, 2012; Peng et al., 2015), on effort, exertion and coughing (Abrams et al., 2002; Thyer et al., 2008) - relates with weakness of the PFM, but often also with poor function or decreased strength of the urethral sphincter, not always in the presence of muscle PFM injury (McGuire, 2004).

While the PFM maintain fecal, urinary continence and active support the pelvic organs by means of contraction (Verelst and Leivseth, 2007) - the passive support of the pelvic floor is mostly provided by the connective tissue of the endopelvic fascia and

pelvic ligaments. The difficulty in maintaining organ support and levator hiatus closure may result from muscle disorders along with laxity of the connective tissue (Hoyte et al., 2001).

During Valsalva manoeuvre - increased IAP and muscle relaxation - some degree of hiatal widening is seen, as well as the opening of the anorectal angle, which is accompanied by some degree of verticalization of the levator plate (Raizada and Mittal, 2008).

Magnetic resonance imaging (MRI) is often used to correlate imaging findings with clinical evidence of PFD (Hoyte et al., 2001), and allows obtaining anatomical and functional imaging of the PFM, such as quantifying the upward and anterior movement of the anorectal junction to close the *levator hiatus* (Brandão et al., 2015).

Computational models based in the finite element method (FEM) have been used to study the biomechanical behavior of the PFM, during vaginal delivery (Parente et al., 2010b, 2008; Silva et al., 2015), Valsalva manoeuvre (Noakes et al., 2008) or during contraction (Saleme et al., 2011), applying material properties obtained from experimental data in in vitro conditions.

In a recent paper, (Silva et al., 2016) implemented the inverse finite element analysis (FEA) to estimate the biomechanical properties of the PFM *in vivo*. This methodology allowed studying muscle passive behavior during Valsalva manoeuvre. However, it is of great interest to also model active muscle contraction, since an inefficient muscle contraction often leads to urine loss in some situations such as physical activity practice and sneezing.

In that sense, the aim of the present study was to estimate the material parameters of the PFM and the contribution of the active and passive muscle fibers for muscle

mechanical behavior. Three groups were included for this analysis: asymptomatic, incontinent and prolapsed women. The numerical simulations of Valsalva manoeuvre and muscle contraction were performed, applying a quasi-incompressible transversely isotropic hyperelastic constitutive model - to reproduce more accurately the PFM nonlinear stress-strain relationship and anisotropic behavior - and also the inverse FEA. The in vivo biomechanical properties of the pelvic floor muscles for a specific subject can be crucial to choose (or to design) personalized implant meshes.

2. Methods

Twelve women participated in this study. They were divided in groups after gynaecological evaluation (4 with SUI, 5 with POP and 3 controls). Demographic characteristics (age, body mass index (BMI) and parity) were also collected.

Women were scanned for pelvic MRI in the supine position using a 3T scanner (Magnetom® Tim Trio, Siemens Medical Solutions, Erlangen, Germany). Static multiplanar T2-w were acquired. In addition, mid-sagittal dynamic images were also obtained at rest, during Valsalva manoeuvre and muscle contraction.

Women were instructed on how to perform proper muscle contraction and Valsalva manoeuvre by a physiotherapist. The dynamic images at maximal Valsalva manoeuvre and muscle contraction were obtained in the mid-sagittal plane, approximately every 2.0 s for a 10 s-period (5 images). Three successive sets of these dynamic images were acquired with a 3 min interval.

An experienced observer revised the datasets to evaluate both morphology and signal intensity of the pelvic structures and PFM, and there was no evidence of injury. Then, the best image datasets were selected based on the most evident vertical descent of the organs and wider *levator hiatus* to represent maximal Valsalva manoeuvre. To represent muscle contraction, the one with both shorter hiatal sagittal diameter and also the more reduced anorectal angle was chosen (Rostaminia et al., 2015). These changes in the *levator hiatus* size are predominantly related to the *puborectalis* muscle (the main contributor to the active contractile forces (Verelst and Leivseth, 2007).

Figure 1 shows sagittal images acquired during maximal Valsalva manoeuvre (a), at rest (b) and maximum muscle contraction (c), from three women - one asymptomatic, one incontinent and other with POP. During Valsalva manoeuvre hiatal widening, opening of the, and verticalization of the *levator plate* can be seen, whilst during muscle contraction, the *levator hiatus* diameter and the anorectal angle are substantially shortened.

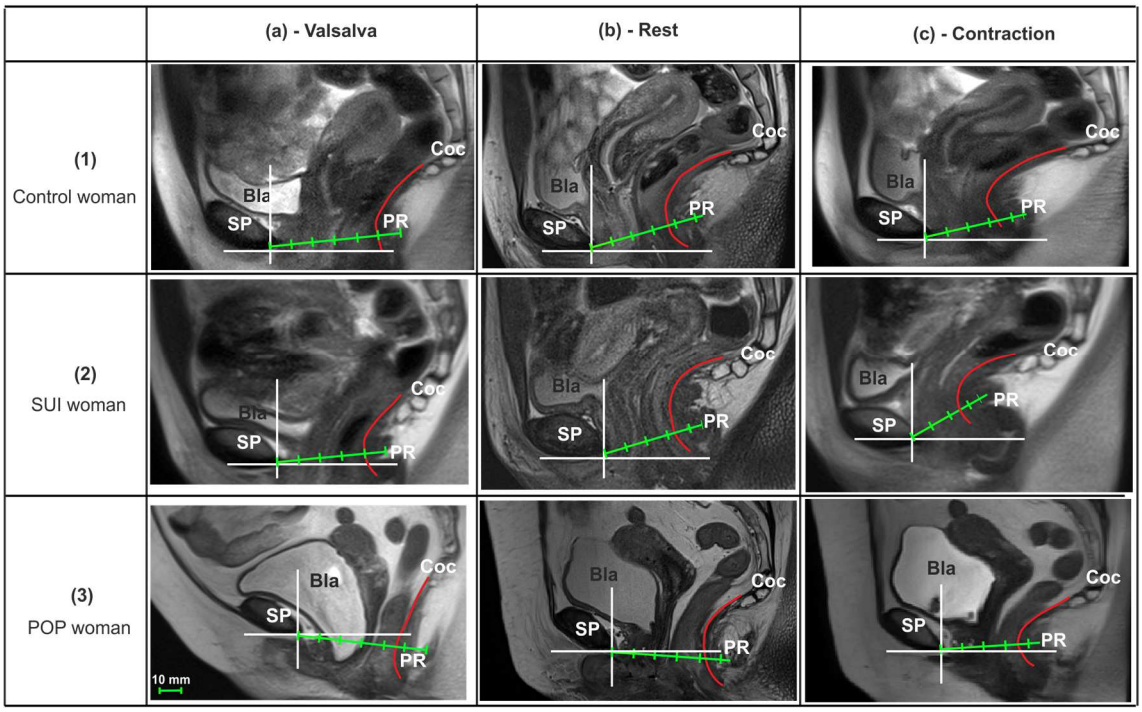

Figure 1. Mid-sagittal dynamic images of a control (1), incontinent (2) and one woman with POP (3). Images were acquired at Valsalva manoeuvre (a), at rest (b) and at muscle maximum contraction (c). The antero-posterior *levator hiatus* diameter (green line with scale) is shown for the 3 conditions. Bla - bladder; Coc - coccyx; PR - *puborectalis* muscle; SP - *symphysis pubis*.

To quantify the changes in the *levator hiatus* and to compare them with the results of the numerical simulations, horizontal and vertical axes were drawn crossing the inferior and posterior border of the *symphysis pubis*. The green line with scale shows the antero-posterior hiatal diameter, between the *symphysis pubis* and the *puborectalis* muscle. The difference in the hiatal diameter between rest *vs.* Valsalva and rest *vs.* contraction are considered as representing the PFM antero-posterior and postero-anterior displacements, respectively.

Biomechanical models

The finite element models of the PFM and surrounding structures - *symphysis pubis*, coccyx and internal obturator muscle (IOM) - were built from the T2-w axial images. For the purposes image segmentation, two of the three portions of the *levator ani* were considered (the *pubococcygeus* and *puborectalis* muscles, frequently referred together as the *pubovisceralis* muscle (PVM)) (Herschorn, 2004), since they cannot be easily distinguished.

The 3D geometrical models of these structures were created using a semi-automatic process, *via* the Mimics Innovation Suite v. 17 (Materialise, Leuven, Belgium) software. An initial pixel intensity threshold was set to obtain the contours of the PVM and surrounding structures, generating their 3D volume. Additional refinements were hand-made using the source T2-w images as reference. The resulting 3D triangulated surface model was generated from the volumes, and then the Mimics 3D default-smoothing algorithm (based on the Laplacian 1st order function) was applied.

The triangulated 3D surface models of the PVM were imported to the Abaqus software v.2016 (Dassault Systemes Simulia Corp., Providence, RI, USA) to create the finite element model for each woman. The finite element meshes were generated using hybrid linear tetrahedral elements (Abaqus C3D4H), and the number of nodes and elements varied among the subjects according to the morphology of the muscles (ranging between 54,639 and 93,733 elements, and 12,234 and 19,535 nodes). The test of numerical convergence was included in the section 1 of the Appendix). Additionally, the element size set was approximately constant throughout the geometry, resulting in a mesh with a characteristic element length of 1.4 mm.

The 3D geometric models of the surrounding structures were added to the model of the PVM, both for visualization purposes and to help in correctly defining the boundary conditions. These were imposed to the PVM to incorporate its insertion points in the *symphysis pubis*, internal obturator fascia and coccyx (Figure 2). The nodes along the anterior borders of the PVM were considered fixed, and in the supero-posterior portion the PVM the nodes were kept unconstrained in the supero-inferior and antero-posterior directions to allow reproducing the coccygeal movements (Bø et al., 2001).

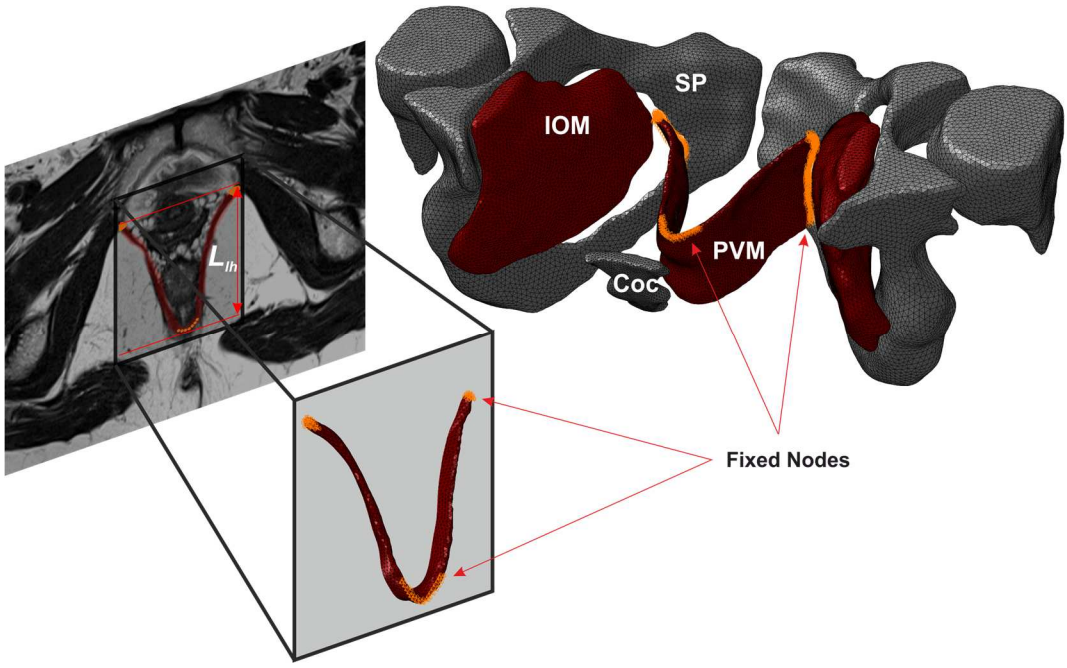

Figure 2. Definition of the boundary conditions (orange dots) mimicking muscle attachments to the surrounding structures. Coc - coccyx; IOM - internal obturator muscle; L_{lh} - length of the *levator hiatus*; PVM - *pubovisceralis* muscle; SP - *symphysis pubis*.

Constitutive model

Assuming the PVM as a highly hydrated tissue, a quasi-incompressible behavior was assumed. Thus, the constitutive model adopted was a modified form of the incompressible transversely isotropic hyperelastic model, proposed by (Martins et al., 1998), as in the work of the (Parente et al., 2009). This hyperelastic model was used by others authors, to simulate the PFM contraction, comparing the numerical displacements with data from dynamic sagittal images (Roza et al., 2015; Saleme et al., 2011), and to study the biomechanical behavior of the PFM during vaginal delivery (Parente et al., 2010a, 2009).

For the constitutive model used, the strain energy per unit volume of the reference configuration can be written using the following equation:

$$U = U_I\left(\bar{I}_1^C\right) + U_f\left(\bar{\lambda}_{f,\alpha}\right) + U_J\left(J\right) \tag{1}$$

where, U_I is the strain energy related with deformation of the isotropic matrix embedding the muscle fibers, defined as:

$$U_I = c\left\{\exp\left[b\left(\bar{I}_1^C - 3\right)\right] - 1\right\}\ , \tag{2}$$

and U_f is the strain energy related with each muscle fiber, considering a passive elastic part, U_{PE}, and an active part, U_{SE}, due to contraction.

$$U_f = \overbrace{A\left\{\exp\left[a\left(\bar{\lambda}_f - 1\right)^2\right] - 1\right\}}^{U_{PE}} + \overbrace{T_0^M \int_1^{\bar{\lambda}_f} f_{SE}\left(\lambda^M, \alpha\right) d\lambda^M}^{U_{SE}}, \tag{3}$$

U_J is the term of the strain energy associated with the volume change.

$$U_J = \frac{1}{D}\left(J - 1\right)^2 . \tag{4}$$

In these definitions, c, b, A, a, D and T_0^M are constants, $\bar{I}_1^C$ is the first invariant of the right Cauchy-Green strain tensor, $\mathbf{C}$, with the volume change eliminated, i.e.

$$\bar{I}_1^C = \operatorname{tr}\bar{\mathbf{C}} = \operatorname{tr}\left(\bar{\mathbf{F}}^T\bar{\mathbf{F}}\right) = J^{-\frac{2}{3}} \operatorname{tr}\mathbf{C} \tag{5}$$

$$\bar{\lambda}_f = \sqrt{\mathbf{N}^T\bar{\mathbf{C}}\mathbf{N}} = \sqrt{\bar{\mathbf{C}} : \left(\mathbf{N} \otimes \mathbf{N}\right)} \tag{6}$$

It represents the fiber stretch ratio in the direction $\mathbf{N}$ of the undeformed fiber and $\otimes$ denotes the tensor product. In Eq. (5), $\bar{\mathbf{F}}$ is the deformation gradient with the volume change eliminated and J the volume change. For the function $f_{SE}\left(\lambda^M, \alpha\right)$ in Eq. (6) the following expression was used:

$$f_{SE} = \alpha \begin{cases} 1-4\left(\lambda^{M}-1\right)^{2}, & \text{for } 0.5 < \lambda^{M} < 1.5 \\ 0, & \text{otherwise} \end{cases} \tag{7}$$

which means that for values of $0.5 \geq \lambda^{M} \geq 1.5$ the muscle produces no energy. The level of activation is controlled by the internal variable $\alpha \in [0,1]$. In this study we simulated maximal muscle contraction, that is $\alpha = 1$.

Based on the constitutive equations governing the material response at a continuum level the stress tensor, $\boldsymbol{\sigma}$, and the associated material tangent, $\mathbf{H}$, must be provided for numerical calculations. However, to implement the constitutive model in the Abaqus it is mandatory to define the spatial tangent tensor, $\mathbf{h}$. In particular, the Cauchy stress tensor and the tangent stiffness matrix using the Jaumann rate of Cauchy stress are given by (Crisfield, 2001).

$$\boldsymbol{\sigma} = \frac{1}{J}\mathbf{F}\mathbf{S}\mathbf{F}^{T} \tag{8}$$

$$\mathbf{h}_{ijkl} = J\left(\mathbf{H}_{IJKL} + \boldsymbol{\sigma}_{ij}\delta_{kl}\right), \tag{9}$$

In Eq. (8) $\mathbf{S}$ is the second Piola-Kirchhoff stress tensor given by

$$\mathbf{S} = \frac{\partial U}{\partial \mathbf{E}} \tag{10}$$

where $\mathbf{E}$ is the Green-Lagrange strain tensor.

In order to obtain the muscle fibers directions, the methodology described in (Brandão et al., 2015) works was followed, where it is assumed that the muscle fibers are

aligned with the maximum principal stress directions, when a physiological load is applied to the model.

To reproduce the muscle passive behavior during Valsalva manoeuvre, a pressure of 4 kPa was applied to its inner surface, following the methodology described by (Noakes et al., 2008).

To check the usefulness of the established material parameters for the passive and active behavior established using inverse FEA, a complete cycle of muscle deformation, based on the cylindrical model, was performed (details can be found in Appendix in the section 3). By using a simplified cylindrical model, it is possible to test the generated muscle forces with only passive behavior or only active behavior or passive plus active behavior.

Inverse Finite element analysis

To estimate the material parameters of the quasi-incompressible transversely isotropic hyperelastic model for the passive behavior (c, b, A and α) and active behavior (T_0^M) an inverse FEA was used. This methodology uses the Python scripting language - updating the displacements of the finite element models of the PVM - to couple the MATLAB MathWorks v.R2016a (Mathematical Computing Software, Natick, Massachusetts, USA) and the Abaqus software.

The Powell's algorithm allows obtaining the suited set of material parameters, in order to minimize the objective function (Eq. 14), obtained from the distance between two curves obtained for each one of the subjects. The first curve represents the position

of the *puborectalis* muscle in the finite element model, and the second curve represents a set of points defining the *puborectalis* muscle in the dynamic mid-sagittal image (see Figure 3). In this study, two inverse FEA were made: one to obtain the material parameters for the passive behavior during Valsalva manoeuvre and the other to obtain the material parameter T_0^M for the active behavior during muscle contraction.

The sum of all the distances represents the *Error* between the two curves (Eq. 12).

$$Func = \sum_{i=1}^{np} \left\| d_{MRI_i} - d_{FEA_i} \right\| \tag{12}$$

Where *np* is the number of points d_{MRI_i} is used to define the first curve and d_{FEA_i} is the closest point projection of d_{MRI_i} on the second curve (Silva et al., 2016). The *Final Error* is described as follows:

$$Final\ Error = \frac{Error}{np} \tag{13}$$

The objective function (Eq. 14) corresponds to the normalized *Final Error*. For this normalization the *levator hiatus* length (L_{lh}) was used (see Figure 2). The stopping criteria was set to $f < 5\%$.

$$f = \frac{Final\ Error}{L_{lh}} \times 100 \tag{14}$$

Figure 3 shows the flow chart of the optimization scheme to obtain the material parameters for the passive behavior and for the active behavior.

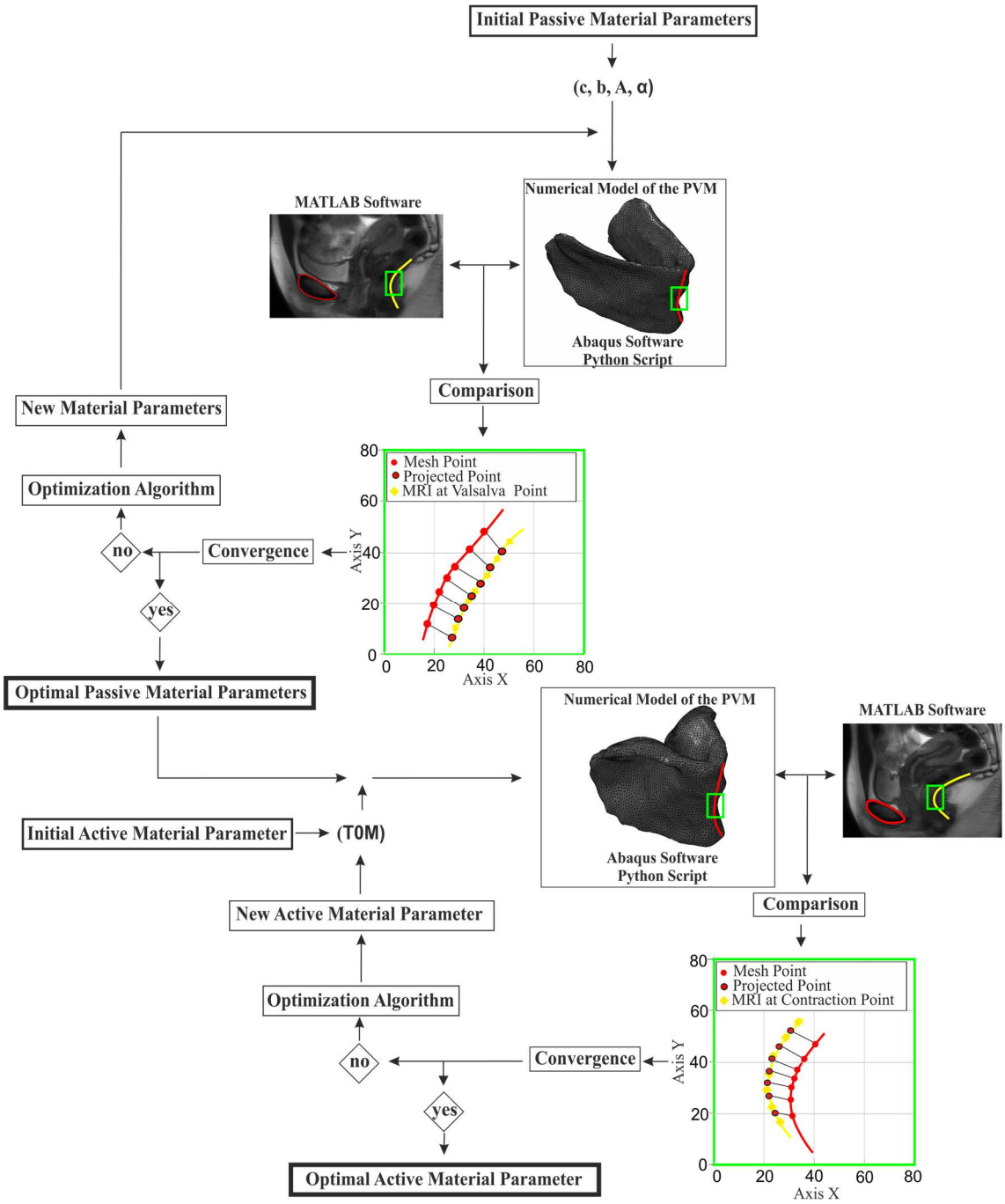

Figure 3. Flow chart of the optimization scheme to determine the material parameters for the passive and active behavior.

Statistical analysis

All analyses were computed using IBM SPSS Statistics 23.0 software and *p*-value <0.05 was considered to be significant. The continuous variables were described by the mean value ± standard deviation (SD). The demographic and morphological characteristics and the material parameters for the passive and active behavior were compared between groups by using the Kruskal Wallis test.

3. Results

Demographic characteristics and hiatal diameter measured in the mid-sagittal MR images of the control group, incontinent and women with POP are presented in Table 1. When comparing the three groups, there was only significant difference in parity and in the hiatal diameter at muscle contraction.

Table 1. Demographic characteristics and antero-posterior displacement measured in the dynamic MR image for the three groups.

variables	*CG (n=3)*	*IG (n=4)*	*POPG (n=5)*	*p-value*
age	28.330±8.505	30.500±21.672	48.800±16.022	0.163
BMI	21.788±1.412	22.225±4.134	27.382±3.104	0.090
parity	0.000±0.000	0.500±1.000	1.600±0.894	0.039*

AP-diam - antero-posterior diameter; CG - control group; IG - incontinent group; POPG - pelvic organ prolapse group.
*statistically significant.

Table 1. (cont.) Demographic characteristics and antero-posterior displacement measured in the dynamic MR image for the three groups.

variables		*CG (n=3)*	*IG (n=4)*	*POPG (n=5)*	*p-value*
AP-diam [mm]	**Rest**	48.230±5.895	50.905±7.025	60.120±7.828	0.115
	Contraction	43.016±3.394	45.952±7.489	55.426±7.667	0.049*
	Valsalva	54.237±9.385	56.320±7.860	64.252±8.321	0.228

AP-diam - antero-posterior diameter; CG - control group; IG - incontinent group; POPG - pelvic organ prolapse group.
*statistically significant.

Table 2 presents the mean values of the antero-posterior and postero-anterior muscle displacements (for Valsalva manoeuvre and contraction, respectively) measured in the dynamic MRI and in the numerical models, for the three groups. For both conditions, the displacements for the incontinent group are significantly smaller than other two groups (AP - disp variation for Valsalva manoeuvre: 8.39% for CG, 15.89% for IG and 5.49% for POPG; PA - disp variation for muscle contraction: 21.88% for CG, 11.73% for IG and 25.96% for POPG). However, taking into account the error based on the antero-posterior diameter which is a clinical measurement (the length of the green line with scale represented in the Figure 1), the values are very similar for the two conditions and for all the groups (AP - diam Error for Valsalva manoeuvre: 1.04% for CG, 2.01% for IG and 1.11% for POPG; AP - diam Error for muscle contraction: 3.02% for CG, 1.29% for IG and 2.74% for POPG).

Table 2. Mean values of antero-posterior and postero-anterior muscle displacements measured in the dynamic MRI, and compared with the ones obtained from the numerical models.

Variable	CG (n=3)	IG (n=4)	POPG (n=5)	*p-value*
Valsalva Manoeuvre				
MRI - AP-disp (mm)	6.007±4.405	5.415±0.977	4.132±1.974	0.349
NM - AP-disp (mm)	5.503±3.661	6.438±0.525	4.372±0.752	0.125
AP - disp variation (%)	8.39%	15.89%	5.49%	
AP - diam Error (%)	1.04%	2.01%	1.11%	
Muscle Contraction				
MRI - PA-disp (mm)	5.213±2.224	4.952±0.493	4.694±1.812	0.808
NM - PA-disp (mm)	6.673±1.157	5.610±0.921	6.340±0.903	0.379
PA - disp variation (%)	21.88%	11.73%	25.96%	
AP - diam Error (%)	3.02%	1.29%	2.74%	

AP-disp - antero-posterior displacement during Valsalva manoeuvre; CG - control group; IG - incontinent group; NM - numerical model; POPG - pelvic organ prolapse group; PA-disp - postero-anterior displacement during muscle contraction

Table 3 presents the mean values of the material parameters. The passive material Table 3 presents the mean values of the material parameters obtained from the numerical simulation. The passive material parameters for the group with POP were higher than those of the other two groups. The matrix parameters (c and b) and fiber parameters (A and α) were 12% and 17%, and 12% and 2% higher when compared with the ones of the women without pathology, and 64% and 33%, and 51% and 24% higher than those of the incontinent women, respectively, with significant differences. The active material

parameter (T_0^M) was approximately 61% and 84% higher than that of the control and incontinent group, respectively.

Table 3. Mean values of the material parameters for the passive and active behaviour obtained for the three groups.

variables	CG (n=3)	IG (n=4)	POPG (n=5)	*p-value*
c [MPa]	0.022±0.010	0.009±0.002	0.025±0.005	0.022*
b	1.510±0.239	1.227±0.057	1.824±0.195	0.013*
A [MPa]	0.036±0.011	0.020±0.001	0.041±0.003	0.022*
α	0.634±0.134	0.488±0.006	0.647±0.021	0.022*
T_0^M **[MPa]**	0.115±0.034	0.046±0.019	0.296±0.261	0.013*

CG - control group; IG - incontinent group; POPG - pelvic organ prolapse group.
*statistically significant.

Figure 4 shows the mechanical response of the uniaxial stress-stretch response from controls, incontinent and women with POP to compare the passive material parameters obtained in the present study (listed in Table 3) with the ones obtained by means of numerical simulation by (Parente et al., 2009), using experimental data of (Janda, 2006).

Using the material parameters of the present study, the PVM of the women with POP evidenced higher values for the stress when compared to the ones of (Parente et al., 2009), but the same profile of the stiffer material curve.

Additionally, the curves obtained, using the material parameters obtained in this work, were compared with experimental data from non-prolapsed cadaveric *levator ani* (Martins, 2010), assuming similar properties along all the portions of the muscle. The experimental curve is in the line of the one of the group of women with POP.

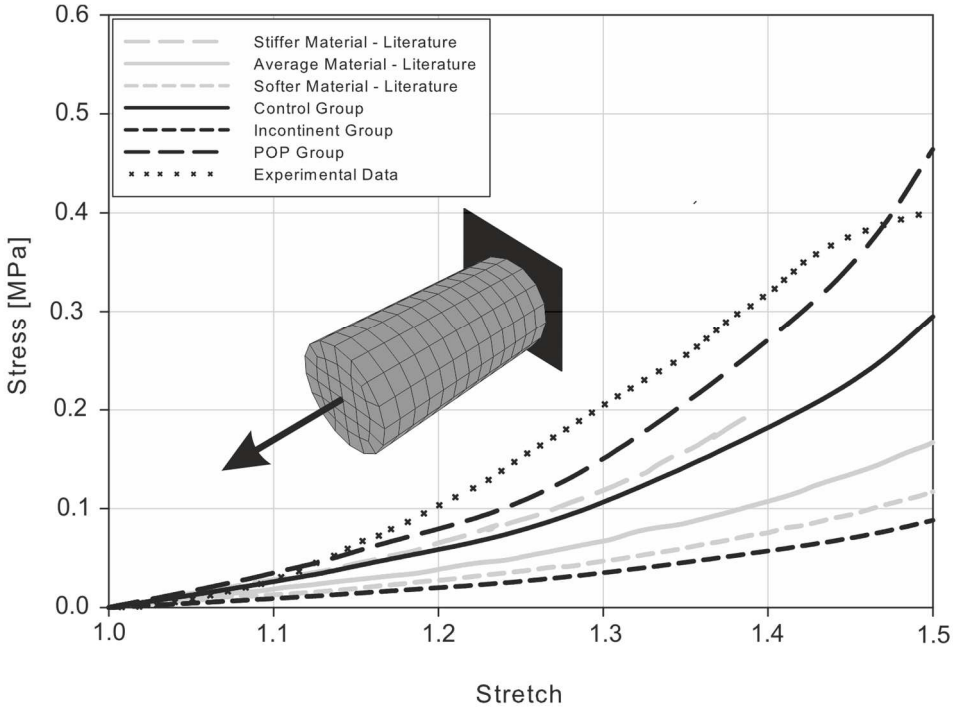

Material	*c (MPa)*	*b*	*A (MPa)*	*a*	*Numerical data*
Softer	0.0130	1.173	0.0196	0.6215	Parente et al. (2009)
Average	0.0185	1.173	0.0280	0.6215	
Stiffer	0.0200	1.75	0.0420	0.6215	

Figure 4. Uniaxial stress-stretch response for passive material parameters of the PVM for the different material parameters with numerical (Parente et al., 2009) and experimental (Martins, 2010) data of the literature.

The maximum force (Figure 5) produced by the muscle during the deformation cycle was higher for the prolapsed group and lower for the incontinent group

(approximately 97 N and 17 N, respectively).

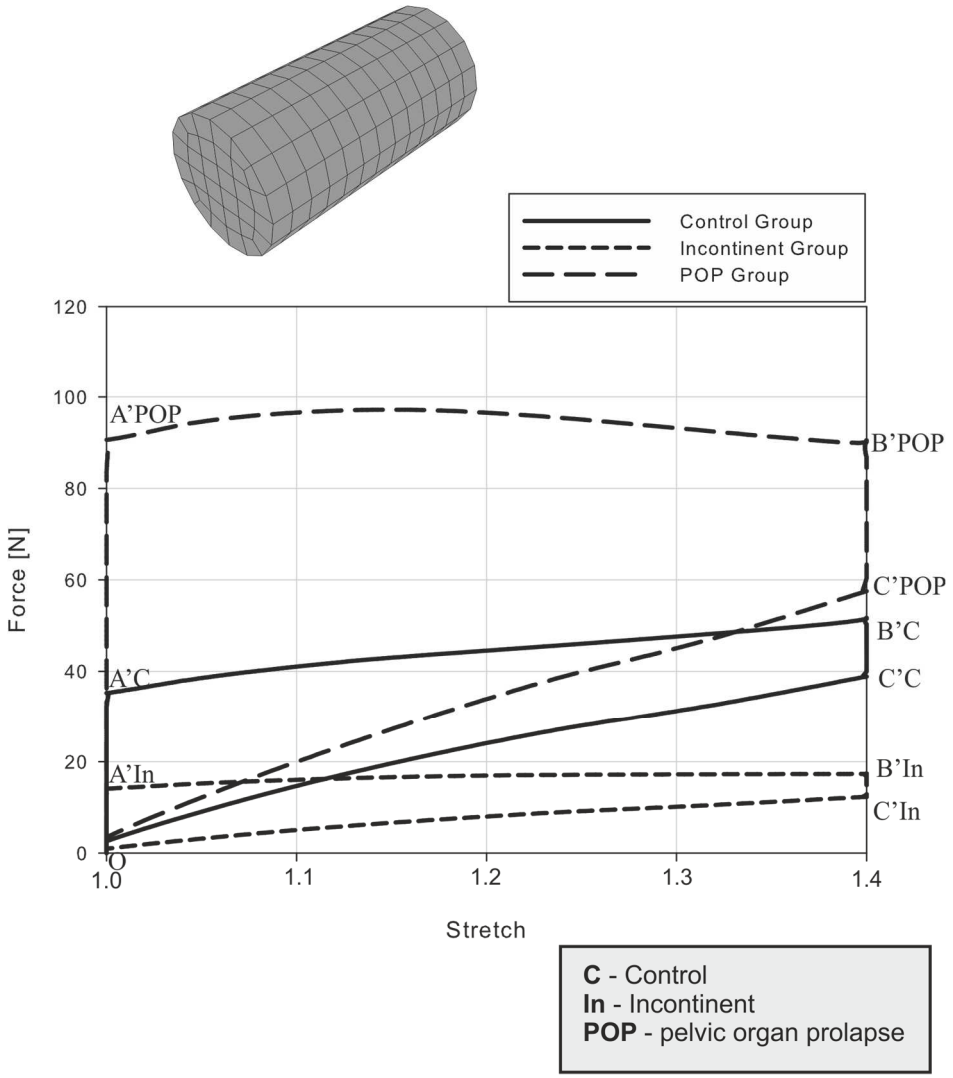

Figure 5. Cycle of muscle deformation for the control, incontinent and prolapsed groups.

The output for antero-posterior displacements and postero-anterior retrieved from the numerical simulation is represented in Figure 6 for three women: control, SUI and POP. The asymptomatic woman presented a maximum antero-posterior displacement (3.763 mm) lower than the ones with SUI (6.402 mm) and with POP (5.891 mm). During active contraction, the woman with POP presents a maximum postero-anterior displacement lower than the women without pathology and with SUI.

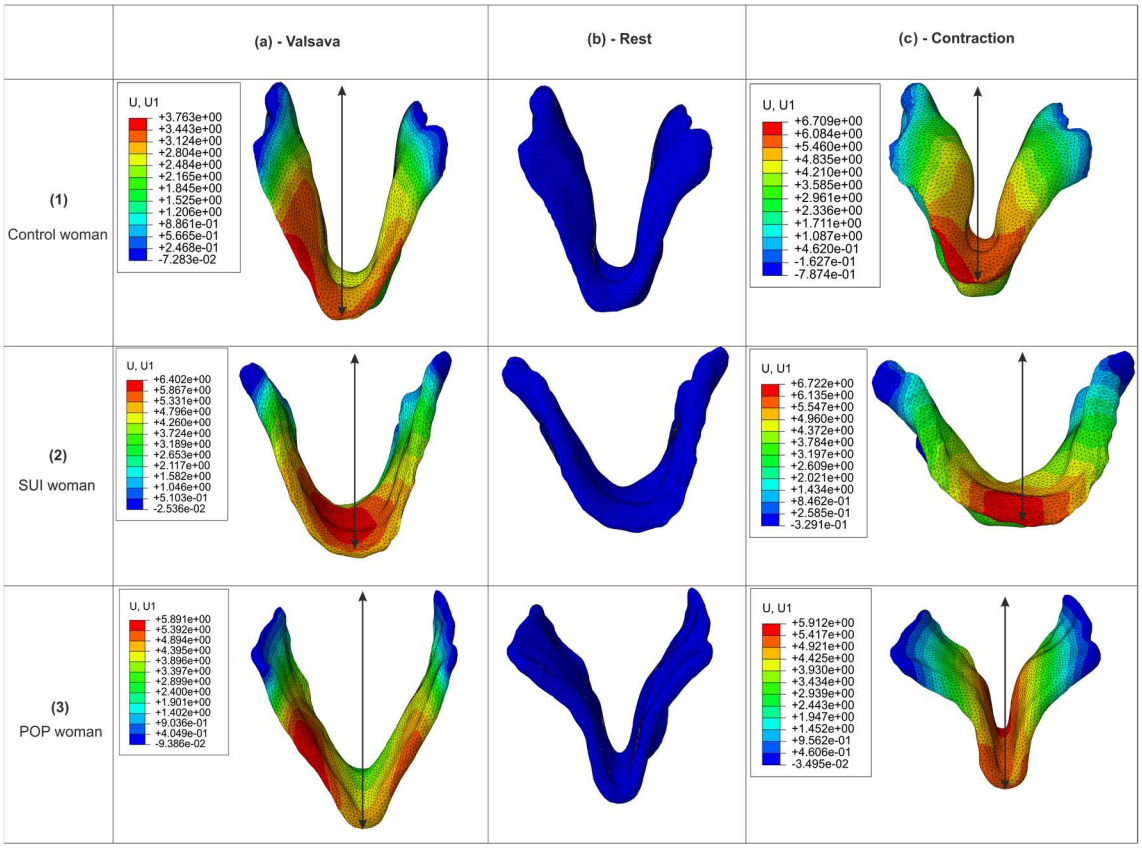

Figure 6. Numerical model of the PVM of a control (1), incontinent (2) and a woman with prolapse (3), during Valsalva manoeuvre (a), at rest (b) and during contraction (c). The black line denotes the axis of antero-posterior and postero-anterior displacements (in mm).

The Figure 7 shows the numerical model of the PVM overlaid with the mid-sagittal slices acquired at rest, during Valsalva manoeuvre and during muscle contraction.

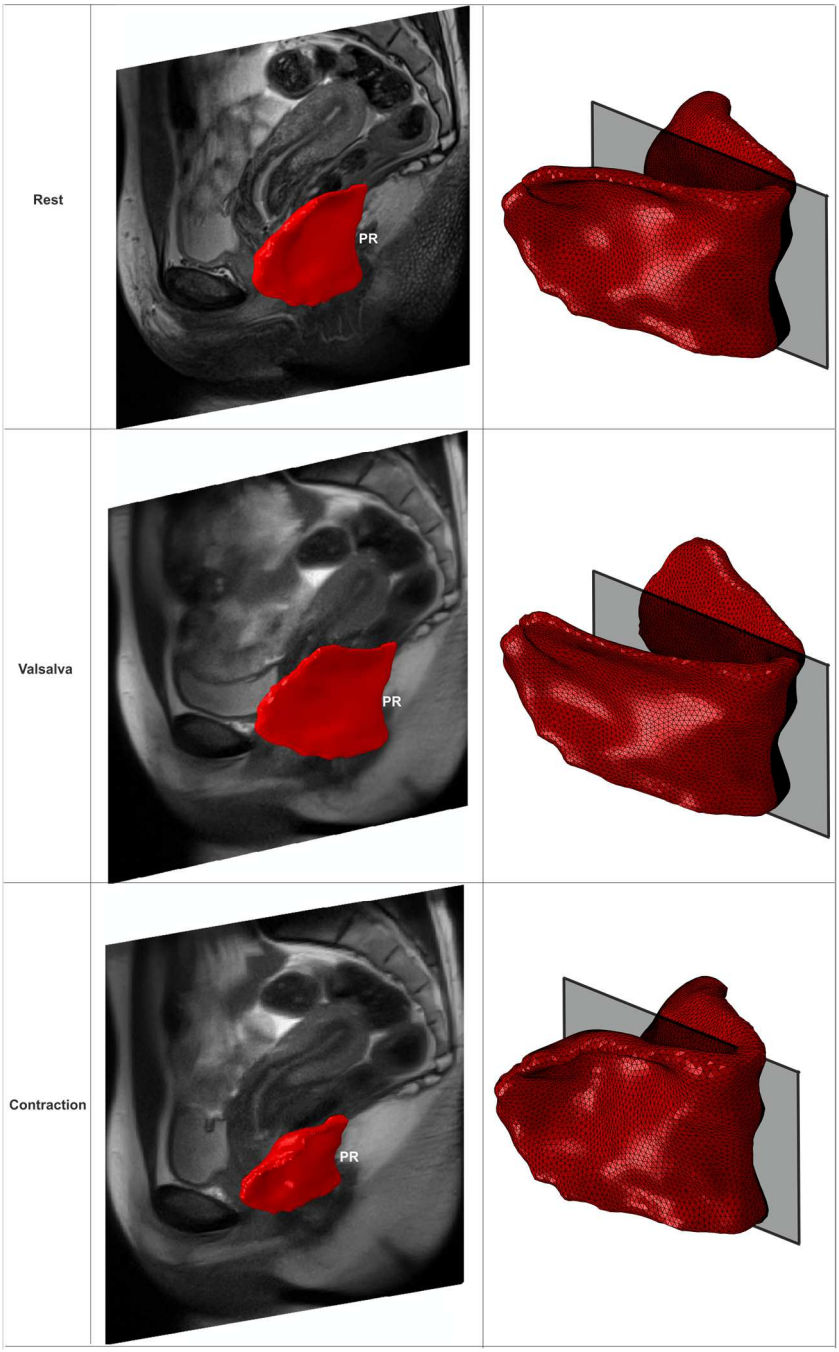

Figure 7. PVM overlaid with the mid-sagittal slices acquired at rest, during Valsalva manoeuvre and during muscle contraction

4. Discussion

The biomechanical properties of the PFM have been studied through experimental *in vitro* studies, but there are few in tissues retrieved from women with POP and SUI, and furthermore the conclusions are controversial. In this regard, (Martins, 2010) found that tensile strength and tangent *modulus* of *levator ani* muscle extracted from cadaveric tissue without POP was significantly smaller when compared to bladder wall, vaginal tissue and round and uterosacral ligaments, but not comparing with pathological muscles. This is consistent with tissue morphology because muscle fibers are highly oriented. Additionally, (Jean-Charles et al., 2010) concluded that the vaginal tissue of female cadavers without POP (mean age was approximately 76 years) present lower stiffness than that prolapsed women with less age (mean age was approximately 66 years).

In this work, we used an inverse FEA to estimate the passive and active material parameters of a constitutive model applied to the PVM. This appears to be a promising methodology for estimating the material properties using non-invasive input information from MRI. For both the passive and active behavior, the material parameters are significantly higher for women with POP than for the ones of the other groups. The difference was approximately **(1)** (POP *vs.* SUI): 64% for the *c*, 33% for the *b*, 51% for the *A*, 24% for the α, and 84% for the T_0^M ; **(2)** (POP *vs.* control): 12% for the *c*, 17% for the *b*, 12% for the *A*, 2% for the α, and 61% for the T_0^M ; **(3)** (control *vs.* SUI): 59% for the *c*, 19% for the *b*, 44% for the *A*, 23% for the α, and 60% for the T_0^M .

The inverse FEA showed that, in spite of the relatively small sample size and having only statistical differences in parity, the PVM of women with POP are stiffer than

that of women without pathology and women with SUI. The higher values of the passive parameters in prolapsed women can be explained by the lower total collagen content and increased concentration of collagen type III in the connective tissues [33], which affects the extracellular matrix.

An increase in collagen type III in combination with an increase in active matrix metalloproteinases (MMP-9) is typical of prolapsed muscles that are actively remodelling to accommodate a progressively increasing mechanical load (Kerkhof et al., 2009; Martins et al., 2013).

However, the ability of the skeletal muscle to sustain contractile activity also depends on the type of the muscle fiber, slow-twitch (type I) or fast-twitch (type II). Type I fibers contract slowly and type II usually perform powerful contractions, exerting 20% more force than type I (Marques et al., 2010). The maximum muscular contraction occurs when tension is generated within the sarcomere by maximum overlap of actin and myosin filaments. PFD affects muscle fiber length and contractile forces, and distensile and stiff muscle fibers have decreased ability to generate power (Marques et al., 2010). In prolapsed women, muscle fibers are distended, which contributes to poor outcomes with exercise and conservative treatment, and prevents proper filament overlap to occur when initiating muscle contraction (Marques et al., 2010). The simulations were run with 100% of muscle activation, and the higher T_0^M obtained for the prolapsed women, that is, the tension produced by the muscle at resting length, can be associated with muscle effort to constantly and properly support the pressure against the pelvic floor.

The higher value can also relate to muscle fiber diameters. One study showed that women with rectal prolapse and/or anal incontinence demonstrated an increase in 21%

and 61% in the diameters of type I and type II fibers of the *levator ani* muscle, respectively, when compared with controls (Beersiek et al., 1979).

For incontinent women, the lower passive parameters - as consequence of softer muscles - may be explained by a significant reduction of type III collagen, which is not due to a decreased production of collagen but due to increased degradation of nascent collagen (Patel et al., 2007). (Verelst and Leivseth, 2007) concluded that incontinent women have a decreased in active force and stiffness that can be associated with muscular weakness. Furthermore, (Zhu et al., 2005) also showed that incontinent women have increased number of fibers, but significantly narrower than that of the controls.

The numerical simulation performed with the cylinder (Figure 5) allowed verifying the influence of the material parameters on the active behavior of the muscle and its influence on the generated force. The higher and lower material parameters in prolapsed and incontinent women reflect higher and lower generated forces, respectively, when compared to asymptomatic women, which can be explained by the diameter of the muscle fibers.

Incontinent and prolapsed women have a higher antero-posterior diameter of the *levator hiatus* than asymptomatic women as previously described (Brandão et al., 2013; Ying et al., 2012). The antero-posterior and postero-anterior displacements measured in the MRI *vs.* numerical models were significantly smaller for prolapsed group. This can be associated with a significantly increased of the *hiatus* antero-posterior diameter.

Despite the limitations abovementioned, the uniaxial stress-stretch response (Figure 4) presented shows that our results can be compared with the numerical and experimental data existent in the literature (Martins, 2010; Parente et al., 2009), that is, the passive material parameters of the asymptomatic group are located between the stiffer

and softer material parameters. However, the curve characterizing prolapsed tissue follows the experimental curve from non-prolapsed cadaveric *levator ani* muscle (Martins, 2010). This can be explained by the way tissues are collected and their properties, and therefore comparison to *in vivo* healthy tissues is difficult (Baah-Dwomoh et al., 2016).

To properly interpret our findings, it is important to consider the limitations and simplifications involved. The sample is not so big. The numerical models did not include the connective tissues (fascia and ligaments) and pelvic organs, which would be more realistic. Finally, in this study, we assumed that the muscle fiber direction are aligned to the maximal principal stress direction obtained when applying a distributed pressure on the inner surface of the PVM, being this criteria assumed by different authors (Martins et al., 1998; Parente et al., 2009). However, recently, (Brandão et al., 2017) evaluated the concurrence between the representation of the PVM fibers obtained from diffusion tensor imaging (DTI) and the directions of the maximum principal stress established by numerical models, concluding that the directions were dissimilar between the two methods in some circumstances, mainly close to the boundary conditions. Hence, this procedure presents some difficulties, being associated with the complex anatomical architecture of the studied region. However, for future works, the use of this procedure can be an useful methodology to be considered.

In conclusion, the inverse FEA seems to be an important tool to estimate the material parameters of the PVM for the different conditions, and shows promising results for subject-specific analyses, with the advantage of being completely non-invasive with information is provided by the MR images. The results obtained are comparable with numerical/*ex vivo* experimental results. Establishing the biomechanical properties of

living tissues through the inverse FEA can in the future avoid the use of *ex vivo* tissues collected *postmortem*, hysterectomy or aspiration experiments during surgical proceedings (Jean-Charles et al., 2010; Kauer et al., 2002; Lei et al., 2007). In addition, we believe this procedure will be essential to optimize the mesh implants, which will reduce the re-operation rates.

Conflict of interest statement

The authors declare that there is no financial, professional or other personal interest of any nature or kind in any product, service and/or company that could be constructed as influencing the position.

Acknowledgments

The authors gratefully acknowledge the funding by Ministério da Ciência Tecnologia, e Ensino Superior, FCT, Portugal, under grants SFRH/BD/89519/2012 and IF/00159/2014, and the project UID/EMS/50022/2013. The fifth author acknowledge the funding of Project NORTE-01-0145-FEDER-000022 - SciTech - Science and Technology for Competitive and Sustainable Industries, cofinanced by Programa Operacional Regional do Norte (NORTE2020), through Fundo Europeu de Desenvolvimento Regional (FEDER).

References

Abrams, P., Cardozo, L., Fall, M., Griffiths, D., Rosier, P., Ulmsten, U., Van Kerrebroeck, P., Victor, A., Wein, A., 2002. The standardisation of terminology in lower urinary tract function: Report from the standardisation sub-committee of the International Continence Society. Neurourology and Urodynamics 21, 37–49.

Baah-Dwomoh, A., McGuire, J., Tan, T., De Vita, R., 2016. Mechanical Properties of Female Reproductive Organs and Supporting Connective Tissues: A Review of the Current State of Knowledge. Applied Mechanics Reviews 68, 60801.

Beersiek, F., Parks, A.G., Swash, M., 1979. Pathogenesis of ano-rectal incontinence: a histometric study of the anal sphincter musculature. J Neurol Sci 42, 111–127.

Bø, K., 2012. Pelvic floor muscle training in treatment of female stress urinary incontinence, pelvic organ prolapse and sexual dysfunction. World Journal of Urology 30, 437–443.

Bø, K., Lilleås, F., Talseth, T., Hedland, H., 2001. Dynamic MRI of the pelvic floor muscles in an upright sitting position. Neurourol Urodyn. 20, 167–174.

Brandão, F.S., Parente, M.P., Rocha, P.A., Saraiva, M.T., Ramos, I.M., Natal Jorge, R.M., 2015. Modeling the contraction of the pelvic floor muscles. Comput Methods Biomech Biomed Engin. 8, 1–10.

Brandão, S., Da Roza, T., Mascarenhas, T., Duarte, S., Ramos, I., Parente, M., Jorge, R.N., 2013. Moment of inertia as a means to evaluate the biomechanical impact of pelvic organ prolapse. International Journal of Urology 20, 86–92.

Brandão, S., Parente, M., Silva, E., Da Roza, T., Mascarenhas, T., Leitão, J., Cunha, J., Natal Jorge, R., Nunes, R.G., 2017. Pubovisceralis Muscle Fiber Architecture Determination: Comparison Between Biomechanical Modeling and Diffusion Tensor Imaging. Annals of Biomedical Engineering.

Crisfield, M., 2001. Non-linear Finite Element Analysis of Solids and Structures, Volume 2 - Advanced Topics, Wiley, Imp. ed. London.

Herschorn, S., 2004. Female pelvic floor anatomy: the pelvic floor, supporting structures, and pelvic organs. Reviews in urology 6, S2–S10.

Hoyte, L., Schierlitz, L., Zou, K., Flesh, G., Fielding, J.R., 2001. Two- and 3-dimensional MRI

comparison of levator ani structure, volume, and integrity in women with stress incontinence and prolapse. American Journal of Obstetrics and Gynecology 185, 11–19.

Janda, S., 2006. Biomechanics of the pelvic floor musculature. PhD. Thesis. Technische Universiteit Delft.

Jean-Charles, C., Rubod, C., Brieu, M., Boukerrou, M., Fasel, J., Cosson, M., Clay, J.-C., Rubod, C., Brieu, M., Boukerrou, M., Fasel, J., Cosson, M., 2010. Biomechanical properties of prolapsed or non-prolapsed vaginal tissue: impact on genital prolapse surgery. International urogynecology journal 21, 1535–1538.

Kauer, M., Vuskovic, V., Dual, J., Szekely, G., Bajka, M., 2002. Inverse finite element characterization of soft tissues. Medical image analysis 6, 275–87.

Kerkhof, M.H., Hendriks, L., Brölmann, H. a M., 2009. Changes in connective tissue in patients with pelvic organ prolapse--a review of the current literature. International urogynecology journal and pelvic floor dysfunction 20, 461–474.

Kiyosaki, K., Ackerman, L., Histed, S., Sevilla, C., Eilber, K., Maliski, S., Anger, J., 2012. Patient understanding of Pelvic floor disoders: What women Want to Know. Female Pelvic Med Reconstr Surg 18, 137–142.

Lei, L., Song, Y., Chen, R., 2007. Biomechanical properties of prolapsed vaginal tissue in pre- and postmenopausal women. International urogynecology journal and pelvic floor dysfunction 18, 603–607.

Luo, J., Smith, T.M., Ashton-Miller, J. a, Delancey, J.O.L., 2014. In Vivo Properties of Uterine Suspensory Tissue in Pelvic Organ Prolapse. Journal of biomechanical engineering 136, 1–6.

Marques, A., Stothers, L., Macnab, A., 2010. The status of pelvic floor muscle training for women. Can Urol Assoc J 4, 419–24.

Martins, J.A.C., Pires, E.B., Salvado, R., Dinis, P.B., 1998. A numerical model of passive and active behavior of skeletal muscles. Computer Methods in Applied Mechanics and Engineering 151, 419–433.

Martins, P.A.L., 2010. Experimental and numerical studies of soft biological tissues. PhD. Thesis. Faculty of Engineering, University of Porto, Portugal.

Martins, P., Jorge, R.N., Ferreira, A., 2006. A Comparative Study of Several Material Models for Prediction of Hyperelastic Properties: Application to Silicone-Rubber and Soft Tissues.

Strain 42, 135–147.

Martins, P., Lopes Silva-Filho, A., Rodrigues Maciel Da Fonseca, A.M., Santos, A., Santos, L., Mascarenhas, T., Natal Jorge, R.M., Ferreira, A.J.M., 2013. Biomechanical properties of vaginal tissue in women with pelvic organ prolapse. Gynecologic and Obstetric Investigation 75, 85–92.

McGuire, E.J., 2004. Pathophysiology of Stress Urinary Incontinence. Reviews in urology 6, S11–S17.

Memon, H.U., Handa, V.L., 2013. Vaginal childbirth and pelvic floor disorders. Women's Health 9, 265–277.

Noakes, K.F., Pullan, A.J., Bissett, I.P., Cheng, L.K., 2008. Subject specific finite elasticity simulations of the pelvic floor. Journal of biomechanics 41, 3060–3065.

Parente, M.P., Natal Jorge, R., Mascarenhas, T., Fernandes, A., Martins, J., 2009. The influence of the material properties on the biomechanical behavior of the pelvic floor muscles during vaginal delivery. Journal of Biomechanics 42, 1301–1306.

Parente, M.P., Natal Jorge, R., Mascarenhas, T., Fernandes, A., Martins, J., 2008. Deformation of the pelvic floor muscles during a vaginal delivery. International Urogynecology Journal and Pelvic Floor Dysfunction 19, 65–71.

Parente, M.P., Natal Jorge, R., Mascarenhas, T., Silva-Filho, A., 2010a. The Influence of Pelvic Muscle Activation During Vaginal Delivery. Obstet Gynecol. 115, 804–808.

Parente, M.P., Natal Jorge, R.M., Mascarenhas, T., Fernandes, A. a., Silva-Filho, A.L., 2010b. Computational modeling approach to study the effects of fetal head flexion during vaginal delivery. American Journal of Obstetrics and Gynecology 203, 217.e1-217.e6.

Patel, P.D., Amrute, K. V., Badlani, G.H., 2007. Pelvic organ prolapse and stress urinary incontinence: A review of etiological factors. Indian J Urol. 23, 135–141.

Peng, Y., Khavari, R., Nakib, N.A., Stewart, J.N., Boone, T.B., Zhang, Y., 2015. The Single-Incision Sling to Treat Female Stress Urinary Incontinence: A Dynamic Computational Study of Outcomes and Risk Factors. Journal of Biomechanical Engineering 137, 91007.

Raizada, V., Mittal, R.K., 2008. Pelvic Floor Anatomy and Applied Physiology. Gastroenterol Clin North Am 37, 493–497.

Rostaminia, G., Peck, J., Quiroz, L., Shobeiri, S.A., 2015. Levator plate upward lift and levator

muscle strength. J Ultrasound Med. 34, 1787–1792.

Roza, T. Da, Brandão, S., Oliveira, D., Mascarenhas, T., Parente, M., Duarte, J.A., Jorge, R.N., 2015. Football practice and urinary incontinence: Relation between morphology, function and biomechanics. Journal of Biomechanics 48, 1587–1592.

Saleme, C.S., Parente, M.P.L., Natal Jorge, R.M., Pinotti, M., Silva-Filho, A.L., Roza, T., Mascarenhas, T., Tavares, J.M.R.S., 2011. An approach on determining the displacements of the pelvic floor during voluntary contraction using numerical simulation and MRI. Computer methods in biomechanics and biomedical engineering 14, 365–370.

Schwertner-Tiepelmann, N., Thakar, R., Sultan, A.H., Tunn, R., 2012. Obstetric levator ani muscle injuries: Current status. Ultrasound in Obstetrics and Gynecology 39, 372–383.

Segal, S., Arya, L.A., Smith, A.L., 2012. Functional Outcomes for Incontinence and Prolapse Surgery. Current Bladder Dysfunction Reports 7, 179–186.

Silva, M., Brandao, S., Parente, M., Mascarenhas, T., Natal Jorge, R., 2016. Establishing the biomechanical properties of the pelvic soft tissues through an inverse finite element analysis using magnetic resonance imaging. Proceedings of the Institution of Mechanical Engineers, Part H: Journal of Engineering in Medicine 230, 298–309.

Silva, M.E.T., Oliveira, D. a., Roza, T.H., Brandão, S., Parente, M.P.L., Mascarenhas, T., Natal Jorge, R.M., 2015. Study on the influence of the fetus head molding on the biomechanical behavior of the pelvic floor muscles, during vaginal delivery. Journal of Biomechanics 48, 1600–1605.

Thyer, I., Shek, C., Dietz, H.P., 2008. New imaging method for assessing pelvic floor biomechanics. Ultrasound in obstetrics & gynecology : the official journal of the International Society of Ultrasound in Obstetrics and Gynecology 31, 201–205.

Verelst, M., Leivseth, G., 2007. Force and Stiffness of the Pelvic Floor as Function of Muscle Length : A Comparison Between Women With and Without Stress Urinary Incontinence. Neurourology and Urodynamics 857, 852–857.

Ying, T., Li, Q., Xu, L., Liu, F., Hu, B., 2012. Three-dimensional ultrasound appearance of pelvic floor in nulliparous women and pelvic organ prolapse women. International Journal of Medical Sciences 9, 894–900.

Zhu, L., Lang, J.H., Chen, J., Chen, J., 2005. Morphologic study on levator ani muscle in patients with pelvic organ prolapse and stress urinary incontinence. International Urogynecology

Journal and Pelvic Floor Dysfunction 16, 401–404.

Appendix

Test of numerical convergence

The finite element mesh used for the *puboviscerali*s muscle was tested for convergence by comparing the results with more refined meshes (double number of elements) and less refined meshes (half the number of elements) and no significant differences were found in the magnitude of the displacements (Figure 1).

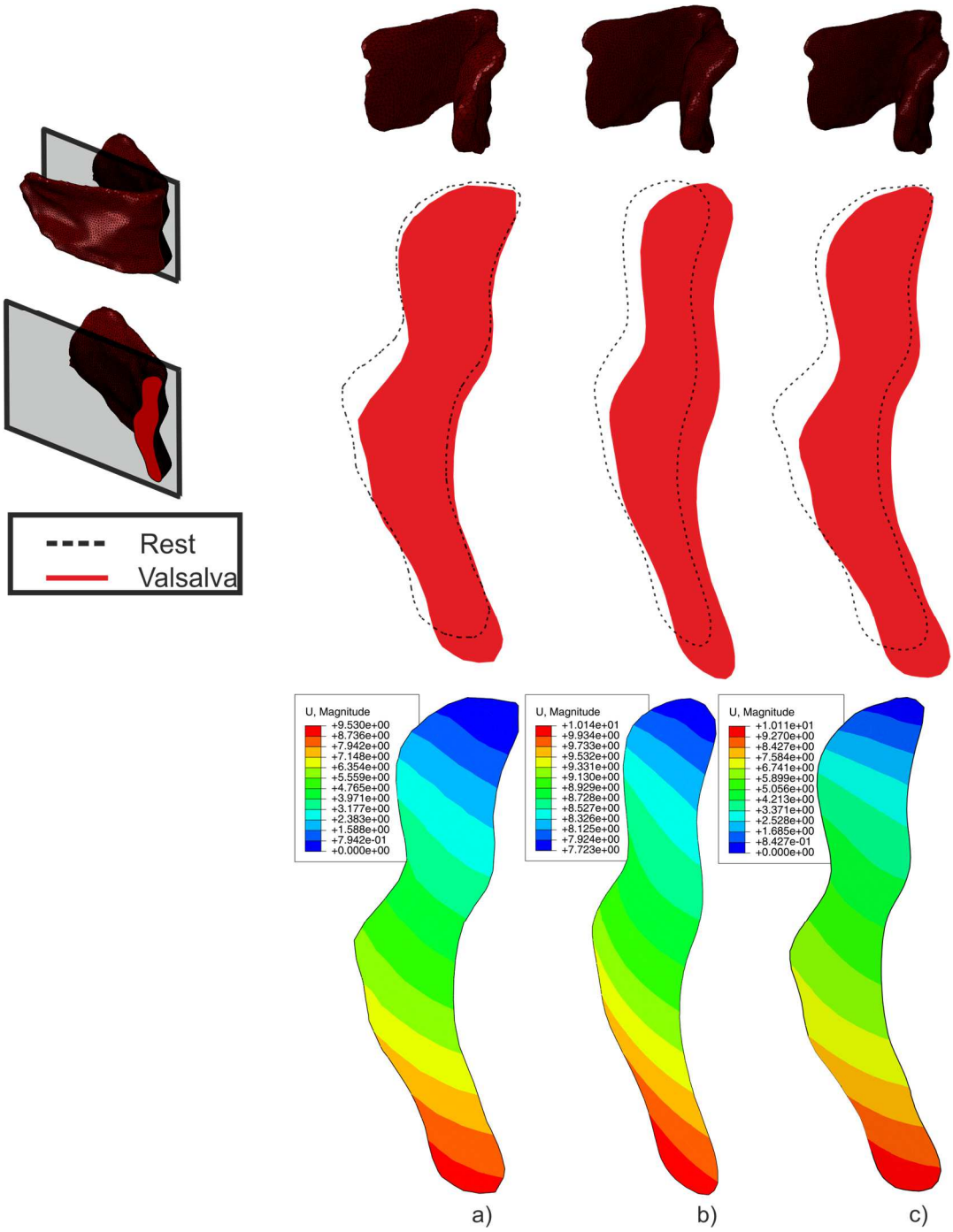

Figure 1. Displacement magnitude for 3 different meshes used to perform the numerical convergence study. a) - more sparse, b) - normal (used to obtain results) and c) - less sparse.

Contributions for the stresses

In order to show the different contributions for the stresses, from the different terms of the strain energy function (isotropic matrix, passive and active fibers), an unitary cube, containing fibers aligned with the *x* direction is considered.

To obtain a stress state corresponding to an uniaxial tension test, by using the methodology described in (Martins et al., 2006), the following deformation gradient [**F**] is used.

$$[\mathbf{F}] = \begin{bmatrix} \lambda & 0 & 0 \\ 0 & \frac{1}{\sqrt{\lambda}} & 0 \\ 0 & 0 & \frac{1}{\sqrt{\lambda}} \end{bmatrix} \qquad (1)$$

This deformation gradient allows to remove the volumetric contribution for the stresses, since *J=1*.

Using the material parameters obtained by (Parente et al., 2009) $c = 0.0185$ MPa, $b = 1.173$, $A = 0.0280$ MPa, $\alpha = 0.6215$ and $T_0^M = 0.682$ MPa, and assuming that the cube is being stretched along the direction of the fibers and that the muscle is activated (α=1), by varying λ_f between 0.2 and 1.8, the stress curves shown in Figure 2 are obtained.

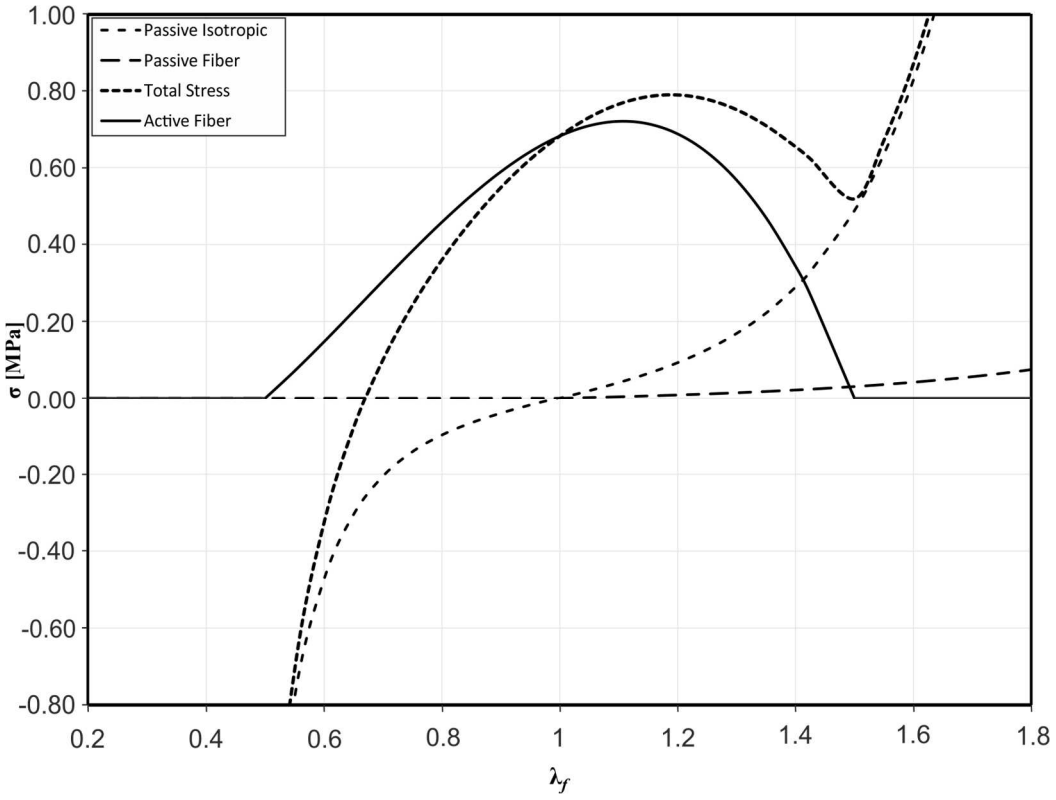

Figure 2. Total stress and its components: isotropic, passive and active stress of the fibers with respect to λ_f, using material parameters determined by (Parente et al., 2009).

Cycle of muscle deformation

Figure 3.a shows the numerical model was created with 196 nodes and 104 hybrid linear tetrahedral elements (Abaqus C3D8H), to simulate the muscle deformation cycle. The boundary conditions were defined so that the axial displacements at the left end of the cylinder were fixed whereas the transversal displacements at the same end were free. To obtain the complete cycle of muscle deformation four steps were performed (Figure 3):

(1) O to A: isometric activation, where the muscle length is kept constant and the muscle is activated;

(2) A to B: stretching with constant active stress, where the activation level is kept constant and the muscle length is increased;

(3) B to C: isometric unactivation, where the le the length is kept constant and the muscle is unactivated;

(4) C to O: passive unstretching, where the muscle is kept in passive and the muscle length is decreased.

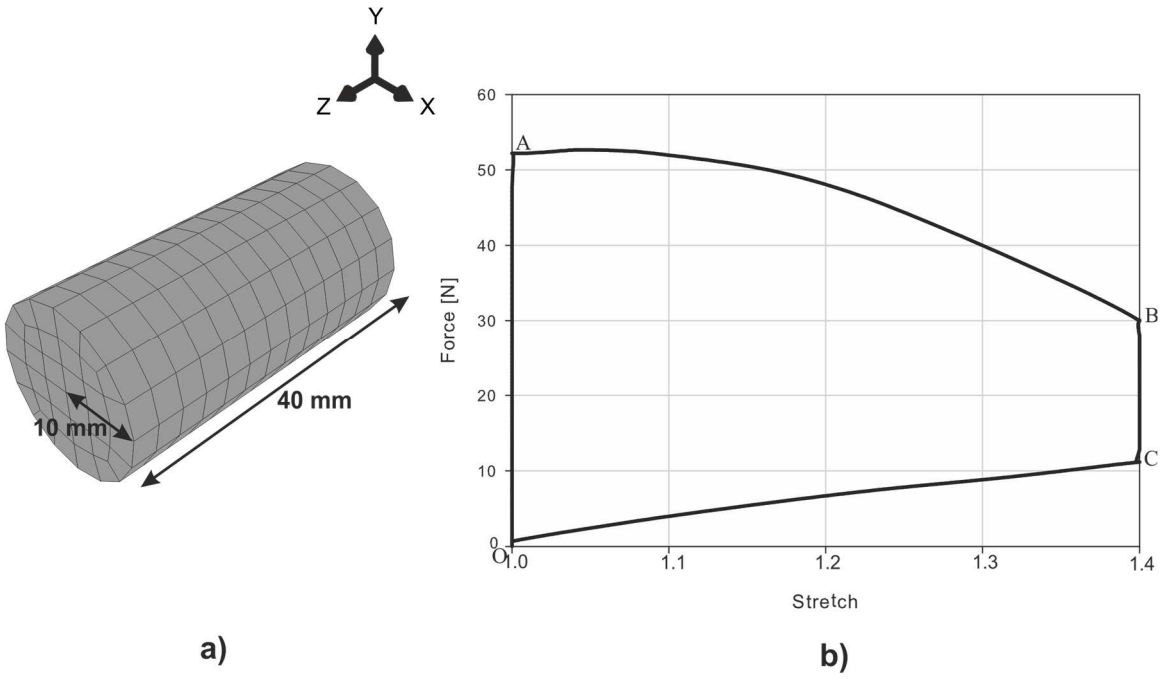

Figure 3. Finite element model (a) and Cycle of muscle deformation (b).

Part B - Article 5

Characterising the Biomechanical Properties of *Pubovisceralis* Muscle using a Genetic Algorithm and the Finite Element Method

M.E.T. Silva[a], M.P.L. Parente[a], S. Brandão[a,b] , T. Mascarenhas[c],

R.M. Natal Jorge[a]

[a]LAETA, INEGI, Faculty of Engineering, University of Porto, Porto, Portugal
[b]Department of Radiology, Centro Hospitalar de São João-EPE, Faculty of Medicine, University of Porto, Porto, Portugal
[c]Department of Gynecology and Obstetrics, Centro Hospitalar de São João-EPE, Faculty of Medicine, University of Porto, Porto, Portugal

Submitted to: Journal of Inverse Problems in Science and Engineering (under review), December 2016.

Abstract

To understand disorders in the pelvic cavity associated to the pelvic floor muscles, using computational models, it is fundamental to know the biomechanical properties of these muscles. For this purpose, we implemented an optimization scheme, involving a Genetic algorithm (GA) and an inverse finite element analysis (FEA), in order to estimate the material properties of the *pubovisceralis* muscle (PVM). The datasets of five women were included in this non-invasive analysis. The material constants obtained were compared with the ones established through a similar optimization scheme, using the Powell's algorithm. To validate the values of the material constants that characterise the passive behaviour of the PVM, the displacements obtained *via* the numerical models with both methods were compared with dynamic mid-sagittal images acquired during Valsalva manoeuvre.

The numerical models of the PVM were built from axial magnetic resonance images (MRI), and the hyperplastic Mooney-Rivlin constitutive model was used. The material constants (c_1 and c_2) were higher for the GA than for the Powell's algorithm, but when comparing the magnitude of the displacements [mm] of the PVM there was only a 5% difference, and 4% for the principal logarithmic strain.

The GA allows estimating the *in vivo* biomechanical properties of the PVM of different subjects, requiring a lower number of simulations when compared to the Powell's algorithm.

Keywords: *Pubovisceralis* muscle, Biomechanical Properties, Magnetic Resonance Imaging, Genetic algorithm, Computational Models.

1. Introduction

The pelvic floor muscles (PFM) have been studied by several authors through computational models. The main goal is to understand their mechanical behaviour under different loading and boundary conditions (Noakes et al., 2008; Parente et al., 2008; Roza et al., 2015; Silva et al., 2016), and the disorders associated with their dysfunction. The finite element method (FEM) has proven to be a valuable tool to understand the behaviour of the pelvic soft tissues, and allows determining: (1) muscles strain and stress, reaction forces and stretch during the passage of the fetus (Noakes et al., 2008; Parente et al., 2008, 2010; Silva et al., 2015), (2) the displacements of the PFM during voluntary contraction (F. S. Brandão et al., 2015; Roza et al., 2015) or Valsalva manoeuvre (Lee et al., 2005; Noakes et al., 2008; Silva et al., 2016), (3) the mechanisms underlying cystocele formation (Chen et al., 2009), among other applications.

Due to its high anatomical detail, magnetic resonance imaging (MRI) is widely used to identify and segment the pelvic organs and muscles. This information is used subsequently in the modelling process, to obtain the 3D geometrical models. The PFM includes the coccygeus, ileococcygeuos, pubococcygeus, and puborectalis muscles, the latter two are frequently segmented together and referred to as the pubovisceralis muscle (PVM) (Herschorn, 2004).

Through dynamic MRI it is possible to visualize and quantify the mobility of the PFM, and the changes in the *levator hiatus* during contraction, Valsalva manoeuvre or defecation. The *levator hiatus* enlarges during Valsalva manoeuvre and becomes smaller

in contraction due to the shortening and elevation of the PVM (Herschorn, 2004; Noakes et al., 2008).

To understand the biomechanics of the PFM, the constitutive laws have a crucial role. Hyperelastic models (Neo-Hookean, Mooney-Rivlin, Yeoh, among others) (Martins et al., 2006) have been extensively used due to their nonlinear behaviour (Lee et al., 2005; Noakes et al., 2008; Silva et al., 2016). The material constants applied are often adjusted to experimental data, obtained from uniaxial and biaxial tensile tests on tissues collected from fresh cadavers or from hysterectomy procedures. Ethical reasons make it impossible to perform live-subject analysis (Jean-Charles et al., 2010; Lei et al., 2007; Rubod et al., 2008).

An inverse FE Analysis (FEA) allows accurate estimation of the parameters of the material model for a specific subject, both invasively (Kauer et al., 2002) or non-invasively (Silva et al., 2016). (Kauer et al., 2002) used tissue aspiration to estimate *in vivo* soft tissue material model parameters using the FEM together with the Levenberg-Marquardt algorithm. Additionally, (Silva et al., 2016) used the FEM together with the Powell's algorithm to minimize the objective function with the purpose of establishing a non-invasive methodology to determine the material constants more suited to replicate muscle behaviour during Valsalva manoeuvre, when using the Mooney-Rivlin constitutive model.

These Levenberg-Marquardt and Powell's algorithms are considered local search methods, but there are other algorithms for solving inverse problems, i.e., global search methods, also known as Genetic algorithms (GA) (Khalil et al., 2006; Meier et al., 2007). The focus of the global search algorithms is to find maximum or minimum overall input values and to reduce the computational time while for the local algorithms the objective

is to find a local minimum or maximum. The GA - an optimization algorithm inspired by natural evolution - has been already used in combination with the FEM to estimate the elasticity of vascular soft tissue (Khalil et al., 2006), and to evaluate the different snatch motions of five body joints: ankle, knee, hip, shoulder and elbow (Lenjan-Nejadian and Rostami, 2010).

The aim of this work was to estimate *in vivo* the biomechanical properties of the PVM for a group of women without pelvic floor dysfunction. To simulate the passive behaviour of the PVM, the FEM was used, and the Mooney-Rivlin constitutive model was applied to describe its nonlinear behaviour. The GA was implemented to obtain the material parameters, which were compared with the ones from the inverse FEA using the Powell's algorithm. Dynamic images acquired at Valsalva manoeuvre were used to validate the displacement magnitude obtained with both methods.

2. Methods

Five women with no complaints or clinical findings indicating pelvic floor dysfunction participated in this study. Demographic characteristics were collected - mean age was 35.5 years and mean body mass index (BMI) was 24.0 Kg/m^2. These women were scanned for a pelvic MRI. Sagittal, and axial T2w images were acquired in the supine position at rest (Figure 1.a) using a 3T scanner (Magnetom® Tim Trio, Siemens Medical Solutions, Erlangen, Germany), along with mid-sagittal *cine* images acquired at maximal Valsalva manoeuvre (Figure 1.b). Women were instructed on how to properly perform the Valsalva manoeuvre for the dynamic acquisitions.

During the Valsalva manoeuvre, there is some degree of hiatal widening, due to the relaxation of the *puborectalis* muscle, and also verticalization of the *levator plate*, immediately anterior to the coccyx (Raizada and Mittal, 2008). The antero-posterior diameter of the *levator hiatus* was measured from the postero-inferior border of the *symphysis pubis* to the *puborectalis* muscle (straight yellow line) (S. Brandão et al., 2015; Tumbarello et al., 2010). To estimate the antero-posterior displacement, the differences between the diameters obtained at rest and at Valsalva manoeuvre were computed.

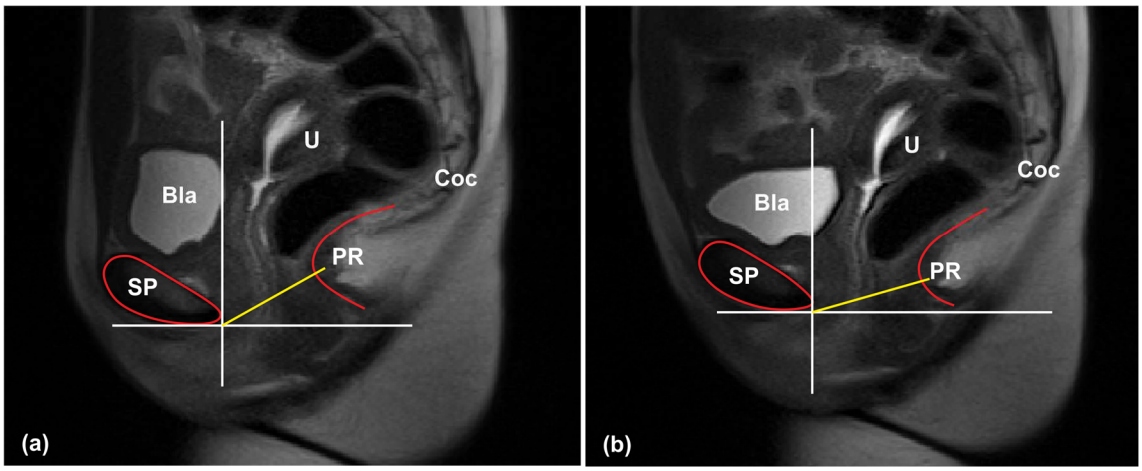

Figure 1. MR images in the mid-sagittal plane acquired at rest (a) and at maximal Valsalva manoeuvre (b). The main pelvic structures are identified (Bla - bladder; Coc - coccyx; PR - *puborectali*s muscle; SP - *symphysis pubis*).

Numerical models

The 3D geometrical models were created through semi-automatic segmentation of the T2w axial images, where the contours of the coccyx, *obturator internus* muscle (OIM), PVM and *symphysis pubis* were defined using the Mimics software v. 17 (Software and Services for Biomedical Engineering, Materialise HQ, Belgium) (see

Figure 2.a). To generate the 3D triangulated surface models from the voxel volume, the Mimics 3D default smoothing algorithm - based on the Laplacian first-order function - was applied. The finite element meshes of the five PVMs were created after importation of the triangulated 3D surface model into the Abaqus v. 6.12 software (Dassault Systmes Simulia Corp., Providence, RI, USA) - using hybrid linear tetrahedral elements (Abaqus C3D4H) (Figure 2.b). The number of the elements and nodes varied according to the morphology of the muscle.

The 3D geometric models of the surrounding structures were included in the model for visualization purposes and to correctly define the boundary conditions, i.e., the nodes corresponding to the insertion points of the PVM in the coccyx, *obturator internus* muscle and *symphysis pubis*, visualized in the MR images, were considered fixed (Parente et al., 2008, 2009; Rubod et al., 2012).

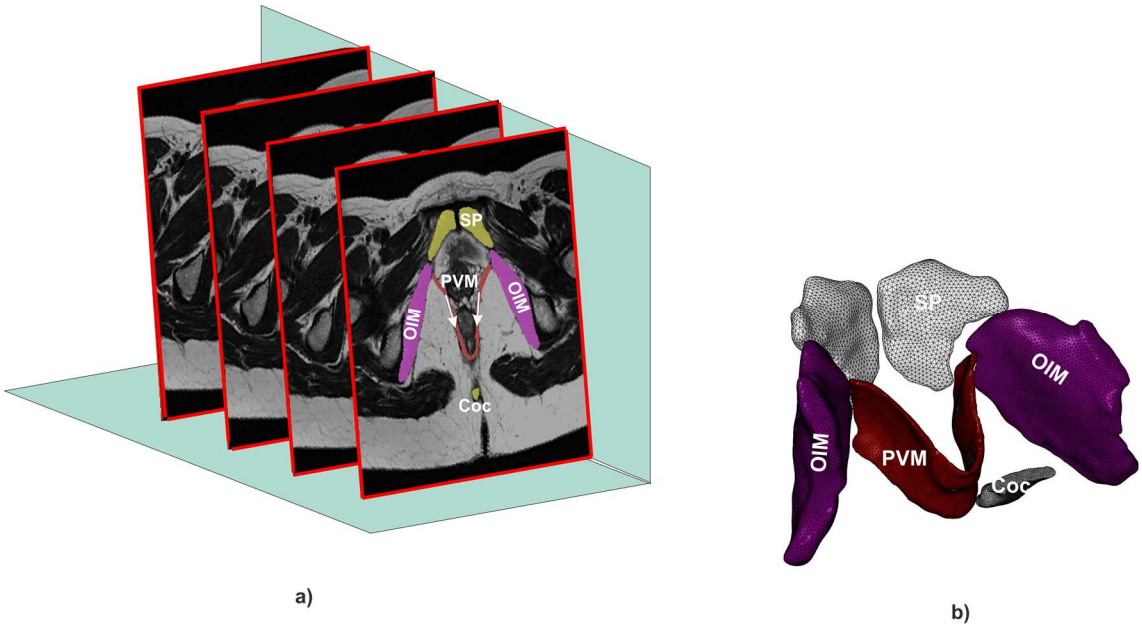

Figure 2. T2w axial images segmented through semi-automatic segmentation (a) and finite element mesh created in the Abaqus Software (b). (Coc - coccyx; OIM - *obturator internus* muscle; PVM - *puboviscerali*s muscle; SP - *symphysis pubis*).

The pressure for simulating the Valsalva manoeuvre was 4 kPa, applied in the inner surface of the PVM, following the methodology described by (Noakes et al., 2008).

As in previous works (Lee et al., 2005; Noakes et al., 2008), the PVM was assumed as isotropic, and the hyperelastic Mooney-Rivlin constitutive material model (Eq. 1) was applied. This material model employs a nonlinear relationship between stress and strain to describe the nonlinear material behaviour, defined by:

$$W = c_1(I_1 - 3) + c_2(I_2 - 3) \tag{1}$$

where W is the strain energy function, formulated to capture the nonlinear nature of the stress-strain curve at high strains, and c_1 and c_2 are material constants that must be determined from experiments on the particular material being modelled, and I_1 and I_2 are principal strain invariants (Eq. 2) of the right Cauchy-Green tensor (Eq. 3) (Noakes et al., 2008).

$$\begin{aligned} I_1 &= \lambda_1^2 + \lambda_2^2 + \lambda_3^2 \\ I_2 &= \lambda_1^2\lambda_2^2 + \lambda_2^2\lambda_3^2 + \lambda_3^2\lambda_1^2 \end{aligned} \tag{2}$$

$$\mathbf{C} = \mathbf{F}^T\mathbf{F} \tag{3}$$

where **F** (Eq. 4) is the deformation gradient and λ is the maximum principal stretch.

$$\mathbf{F} = \begin{bmatrix} \frac{\partial x}{\partial X} & \frac{\partial x}{\partial Y} & \frac{\partial x}{\partial Z} \\ \frac{\partial y}{\partial X} & \frac{\partial y}{\partial Y} & \frac{\partial y}{\partial Z} \\ \frac{\partial z}{\partial X} & \frac{\partial z}{\partial Y} & \frac{\partial z}{\partial Z} \end{bmatrix} \tag{4}$$

In the case of uniaxial stretching, the Cauchy stress σ , a function of the invariants (Eq. 5), can be described by the following equation (Martins et al., 2006):

$$\sigma = 2\left(\lambda^2 - \frac{1}{\lambda}\right)\left(\frac{\partial W}{\partial I_1} + \frac{1}{\lambda}\frac{\partial W}{\partial I_2}\right) \tag{5}$$

The inverse Finite Element Analysis

The inverse FEA implemented by (Silva et al., 2016) was used to optimize the material constants for the Mooney-Rivlin constitutive model, using the Powell's algorithm (Gao et al., 2013; Powell, 1977). The Powell's algorithm is based on the conjugated directions $\mathbf{D}^{n+1}$, and uses the components of the hessian matrix as unidirectional search vectors. The optimum set of materials constants $\mathbf{X}^{n+1}$ is obtained according to Eq. 6.

$$\mathbf{X}^{n+1} = \mathbf{X}^n + \beta^*_{n+1}\mathbf{D}^{n+1} \tag{6}$$

The objective function corresponds to the distance between two curves being compared (the first represents the *puborectalis* muscle - the inferior portion of the PVM

- in the numerical model, and the second curve represents its position in the dynamic mid-sagittal image acquired during Valsalva manoeuvre) (see Figure 3).

The Python scripting language was used to couple the MATLAB MathWorks v. R2016a (Mathematical Computing Software, Natick, Massachusetts, USA) and the Abaqus software v. 6.12 (Dassault Systmes Simulia Corp., Providence, RI, USA), and to update the displacements of all the nodes representing the *puborectalis* muscle in the numerical model.

In this work, the inverse FEA was used to search for the most suited set of material constants for each woman using two distinct optimization algorithms: the GA and Powell's algorithm.

The *Error* measure represents the sum of all the distances between the two curves,

$$Error = \sum_{i=1}^{np} \left\| d_{MRI_i} - d_{FEA_i} \right\| \tag{7}$$

where *np* is the number of points used to define the curve on the numerical model and d_{FEA_i} is the closest point projection of d_{MRI_i} on the second curve. The *Final Error* is described as follows:

$$Final\ Error = \frac{Error}{np} \tag{8}$$

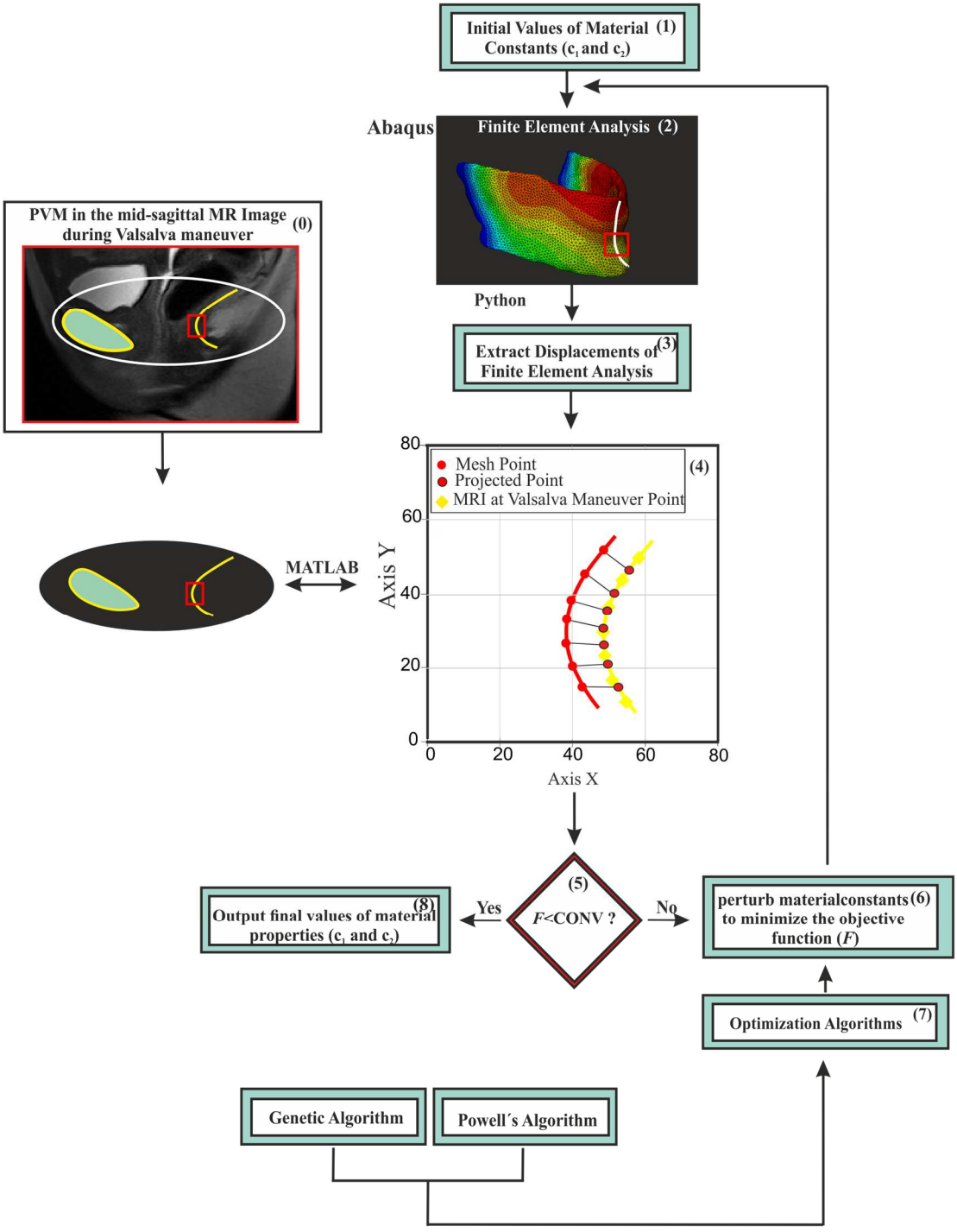

Figure 3. Flowchart of the inverse FEA. Several steps were executed in order to obtain the optimized material constants (c_1 and c_2) for the Mooney-Rivlin constitutive model.

The objective function (Eq. 9) corresponds to the normalized *Final Error*. For this normalization, the *levator hiatus* length (L_{lh}) was used (see Figure 4). The stopping criteria was set to $f < 5\%$.

$$f = \frac{Final\ Error}{L_{lh}} \times 100 \tag{9}$$

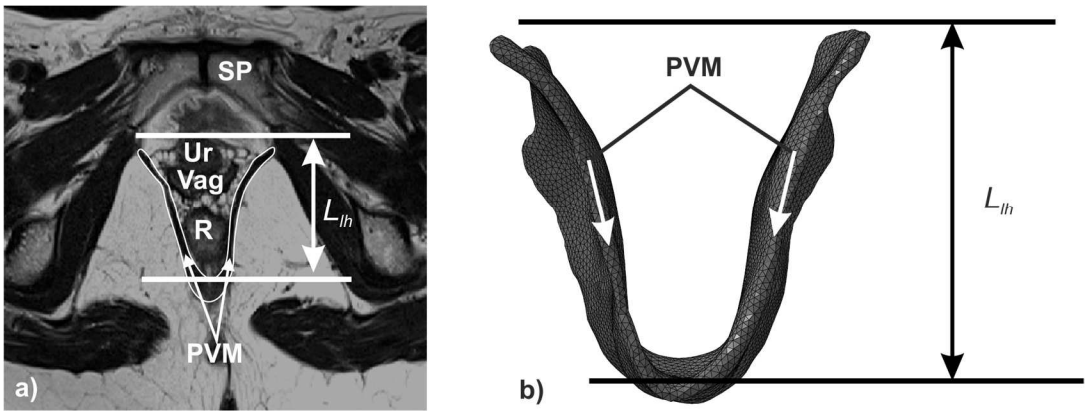

Figure 4. The *levator hiatus* length (L_{lh}) measured in the MR image acquired in the axial plane (a) and in the numerical model (b). L_{lh}: length of the *levator hiatus*; PVM: *puboviscerali*s muscle; R: rectum; SP: *symphysis pubis*; Vag: vagina: Ur: urethra.

Genetic Algorithm

The GA is a general-purpose search algorithm inspired by the natural population genetics, used to evolve the solution to problems. This algorithm is based on the global convergence (McCall, 2005), and operates on a population of several individual solutions, designed chromosomes, improving this population towards a better solution. This algorithm includes different operations: evaluation, selection, crossover and mutation.

In the present application case, we search the optimal material constants (c_1 and c_2) associated with the passive mechanical behaviour of the pelvic floor muscles by using the well-known Mooney-Rivlin material model in the simulation of the Valsalva manoeuvre. Each candidate solution is represented by an array of two material constants, for the case of the Money-Rivlin constitutive model. To initialize the GA, we start by selecting the population size. We assume that the population has a constant size (n_{pop}) and that each candidate i of the population (i=1…n_{pop}) is represented by a chromosome of length n_{ch}. The chromosome is used to encode, in binary form, the values of the parameters for each candidate i is stored in the row i of an array $P(i, j)$, $j=1…n_{ch}$.

$$n_{pop} = 10$$
$$n_{ch} = 30$$

A large population will result in higher computational costs, and a higher number of chromosomes will result in a higher resolution for the material parameters. A chromosome with a size of 15 will result in a total of 32768 possible values for a given parameter. Since we are optimizing two parameters, a total of 30 chromosomes were used.

For the optimization space, it was assumed that both material constants (c_1 and c_2) could vary between 0 and 1. When using chromosomes with a size of 15 for each material constant, a minimum variation (resolution) of 3.1E-05 was obtained.

To initialize the population, for each $P(i,j)$ a random number generator r was used, which generates random numbers following a normal distribution. The generation of the population is obtained as follows, for i varying from 1 to n_{pop} and j varying from 1 to n_{ch}:

$$\begin{cases} if \;\; r \le 0.5 \quad then \quad P(i,j) = 0.0 \\ if \;\; r > 0.5 \quad then \quad P(i,j) = 1.0 \end{cases} \tag{10}$$

To each candidate solution in the population a fitness value is then computed, and this quantifies how "fit" a candidate (chromosome) is as compared with others, that is, it checks if this candidate is liable to survive and reproduce, as a solution to a specific problem. In biology, the chromosome is referred to as the genotype, whereas the solution it represents is known as the phenotype. In this study, the material constants (c_1 and c_2 of the hyperelastic Mooney-Rivlin model) result from the decoding of the binary number to minimize a problem (minimize the distance between the two curves), the fitness function *FIT* is obtained directly through the objective function *f* given by Eq. 9:

$$FIT_i = \frac{1}{1 + f_i^2} \tag{11}$$

where *i* represents a particular candidate.

In order to obtain a new and improved generation from the original population, the GA starts by selecting pairs of parents and creates a new child for the next population. To select the first parent, two candidates are chosen at random and from these two, the fittest is select as the first parent, and the process is repeated to select the second parent. Of the two parents, the fittest is the parent one (P_1) and the other is the parent two (P_2). This operation is finished when all the pairs of parents are created. The offspring are obtained via a crossover operation. The crossover children are created by combining each pair of parents.

Two crossovers types with probability of occurrence (p_c=*0.5*) were used: the one point and two points crossover. Each pair of parents was allowed to generate one or two children. But the crossover of a gene only continues if the random number generated is greater than the p_c. In the one point crossover, a random position in the chromosome (x_1) is chosen ($x_1 \in [1, n_{ch}]$), and the crossover occurs as follows:

$$\begin{cases} if \quad j \le x_1 \quad and \quad r > p_c \quad then \quad P(i, j) = P_1 \\ if \quad j > x_1 \quad and \quad r > p_c \quad then \quad P(i, j) = P_2 \end{cases} \tag{12}$$

In the two points crossover, two positions (x_1, x_2) of the chromosomes are randomly selected ($x_1, x_2 \in [1, n_{ch}]$ *and* $x_2 > x_1$), and it is presented as follows:

$$\begin{cases} if \quad j \le x_1 \quad and \quad r > p_c \quad then \quad P(i, j) = P_1 \\ if \quad x_1 < j \le x_2 \quad and \quad r > p_c \quad then \quad P(i, j) = P_2 \\ if \quad j > x_2 \quad and \quad r > p_c \quad then \quad P(i, j) = P_1 \end{cases} \tag{13}$$

In the case of a pair of parents generating two children, the second child has the complementary genes of the first, i.e., the genes of the first child that comes from P_1, for the second child comes from P_2.

During the selection process, if the new generation has a fitness lower than the previous generation, the fittest individual of the previous generation is inserted in the current generation.

The GA terminates when the maximum number of iterations (Max_{Iter}=50) is reached, or the problem requirements are satisfied. In this case, each iteration is equivalent to a generation. The Figure 5 shows the flowchart of the genetic algorithm.

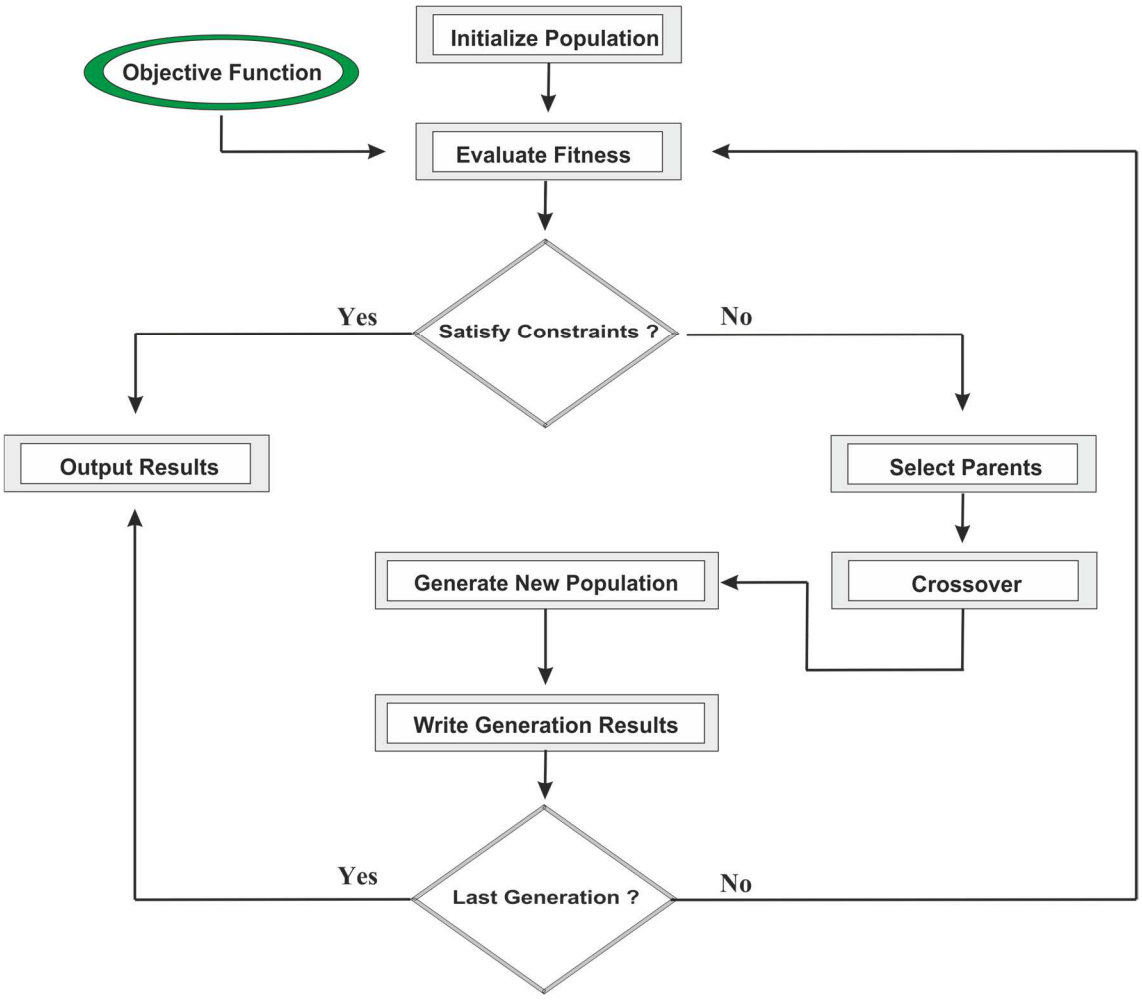

Figure 5. Flowchart of the Genetic Algorithm.

3. Results

Table 1 presents the material constants for the Mooney-Rivlin applied to the PVM using a GA and Powell's algorithm. The material constants were similar for the two algorithms. Despite the values of the objective function percentage for the different subjects were higher for the GA, the range of the difference between the two algorithms was approximately [1.5 - 58.1] %.

Table 1. Values of the material constants (c_1 and c_2) between the Genetic algorithm and Powell's algorithm, for the five women.

variables	*Genetic algorithm*				*Powell's algorithm*			
	$c_{1(MPa)}$	**$c_{2(MPa)}$**	**Func (%)**	**Nº Simul**	**$c_{1(MPa)}$**	**$c_{2(MPa)}$**	**Func (%)**	**Nº Simul**
Subj. 1	0.019	0.014	1.85	70	0.019	0.011	1.71	95
Subj. 2	0.056	0.023	2.63	30	0.044	0.030	2.59	53
Subj. 3	0.018	0.002	2.28	140	0.019	0.003	2.19	149
Subj. 4	0.019	0.014	3.15	70	0.019	0.012	2.09	131
Subj. 5	0.033	0.014	1.36	60	0.026	0.018	0.57	105

Func: objective function percentage; Nº Simul: number of simulations; Subj.: subject.

The graph of Figure 6a shows the evolution of the objective function (Eq. 9) with the number of simulations, for all the subjects. In Figure 6b, the average curves are shown, comparing the results for the GA and Powell' algorithm.

Figure 7 shows the magnitude of the displacements (1) and the principal logarithmic strain (2) of the PVM of subject 4, as an example. The higher displacements were observed for the posterior area of the *puborectalis* muscle using the material constants obtained through the GA (a) and the Powell's algorithm (b), ranging from [11.98 - 13.07] mm and [12.67 - 13.82] mm, respectively. When comparing the numerical results between the two algorithms, the difference was approximately 5% for the displacement and 4% for the logarithmic strain. The principal logarithmic strain shows

that the elements representing the insertion points display the highest values.

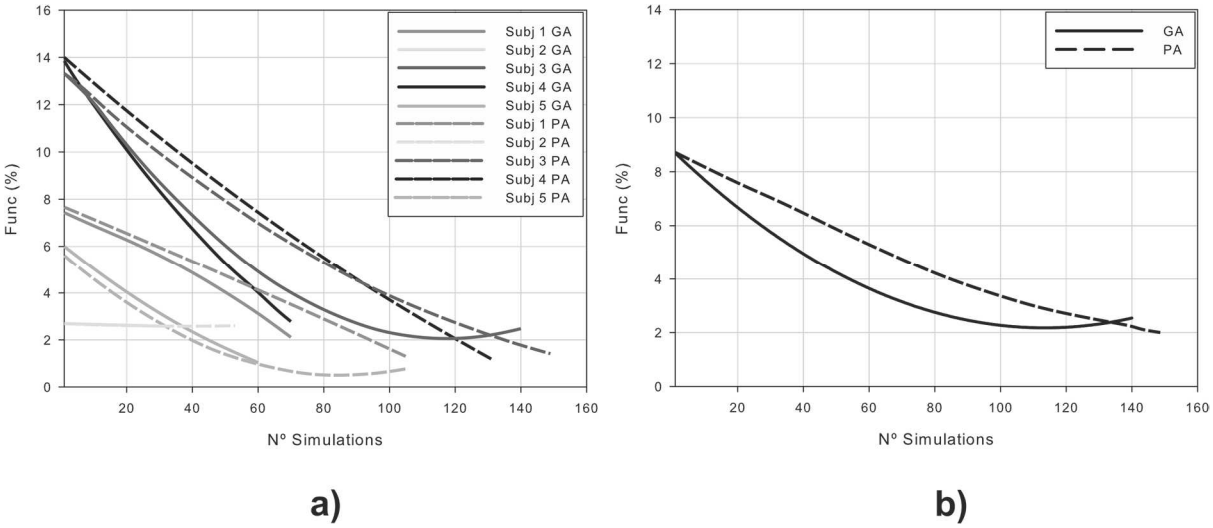

Figure 6. Function behaviour along the number of simulations for all the subjects (a) and average function behaviour curves (b), using the Genetic and Powell's algorithms.

Table 2 presents the antero-posterior displacement of the *puborectalis* muscle obtained in the dynamic MR acquisition *vs.* the ones from the numerical modelling, which were similar. When comparing the values of antero-posterior displacement from MRI *vs.* GA, the range of difference of the displacements was approximately [3.8 - 22.5] %, while for the Powell's algorithm *vs.* MRI the range was approximately [1.1 - 21.4] %.

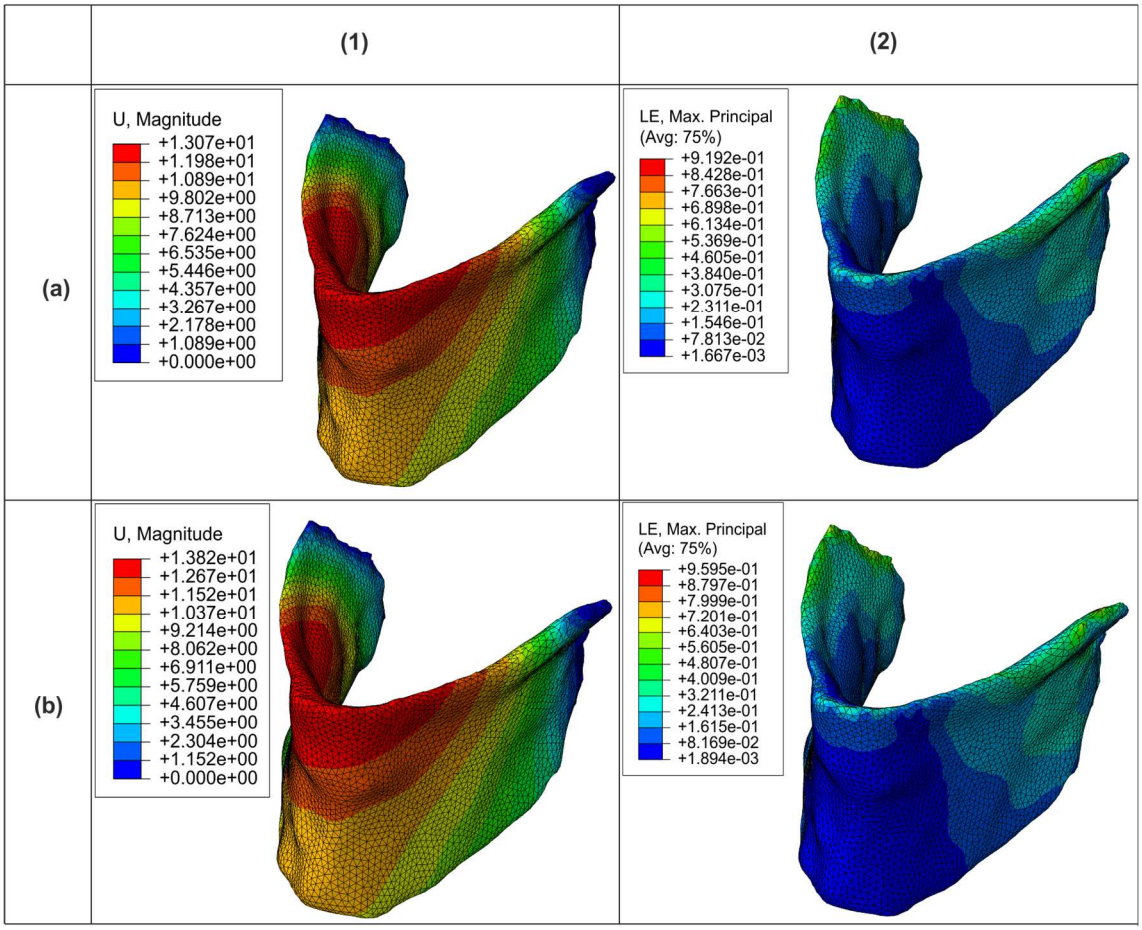

Figure 7. PVM displacement (1) and maximum principal logarithmic strain (2) for Valsalva manoeuvre, using the material constants obtained through the GA (a) and Powell's algorithm (b).

Table 2. Antero-posterior displacement of the *puborectalis* muscle (rest *vs.* Valsalva) of the dynamic MR images compared with the FE models, for the Genetic and Powell's algorithms.

variables	***AP displ. MRI (mm)***	***AP displ. NM using GA (mm)***	***AP displ. NM using PA (mm)***
Subj. 1	5.35	4.88	5.29
Subj. 2	4.35	3.37	3.42

AP: antero-posterior; displ.: displacement; GA: Genetic algorithm; NM: numerical model; PA: Powell's algorithm; Subj.: subject.

Table 2. (cont.) Antero-posterior displacement of the *puborectalis* muscle (rest *vs.* Valsalva) of the dynamic MR images compared with the FE models, for the Genetic and Powell's algorithms.

variables	*AP displ. MRI (mm)*	*AP displ. NM using GA (mm)*	*AP displ. NM using PA (mm)*
Subj. 3	3.68	3.25	3.31
Subj. 4	7.45	7.17	7.24
Subj. 5	2.41	1.89	2.23

AP: antero-posterior; displ.: displacement; GA: Genetic algorithm; NM: numerical model; PA: Powell's algorithm; Subj.: subject.

The graphs of Figure 8 present the behaviour pattern of the antero-posterior displacement of the numerical models for subjects 1 (a) and 4 (b), along the number of simulations. The results are compared with the ones from the dynamic MR images.

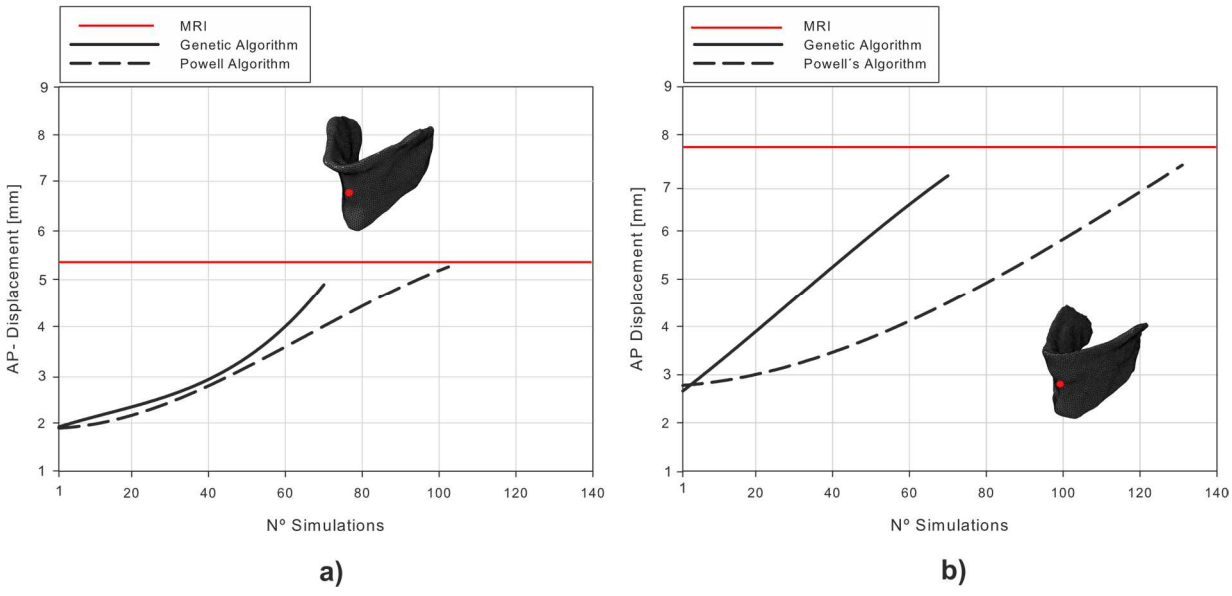

Figure 8. Antero-posterior displacement obtained for subjects 1 (a) and 4 (b), using the GA and Powell' algorithm.

4. Discussion

The *in vivo* biomechanical properties of the soft tissues (e.g., the breast, thyroid, gastro-intestinal tract and the skeletal muscle) can be analysed through MR or ultrasound elastography (Garra, 2015; Glaser et al., 2012). These techniques allow non-invasive estimation of the strain, stiffness and Young's modulus (Gennisson et al., 2010; Mariappan et al., 2010; Wells and Liang, 2011). Nonetheless, their validation is still an ongoing process (Oudry et al., 2009).

The main aim of this work was to estimate the *in vivo* biomechanical properties of the PVM using an inverse FEA, which consisted of two stages: (1) implementing the GA and (2) comparing the GA with the Powell's algorithm. The results of the inverse FEA with the GA confirm that such an approach has potential to accurately quantify the material properties without explicitly approximating a gradient search direction, which requires considerable computational time (i.e., a higher number of numerical simulations). Table 1 shows that the GA requires fewer numerical simulations to estimate c_1 and c_2, minimizing the objective function, when compared to the Powell's algorithm. Nevertheless, the Powell's algorithm presents lower function values, which in this case is associated with lower value of the material constants and a better approximation of the numerical model to the dynamic mid-sagittal image acquired at maximal Valsalva manoeuvre. In the case of subject 4, the difference between the two algorithms for the function value was approximately 34%, and for the material constants c_1 and c_2 were 0% and 14%, respectively. We can thus suggest that the difference in the function value has little influence in the numerical results, as show the Figure 7, i.e., the differences of the displacement [mm] and principal logarithmic strain were only 5% and 4%, respectively.

The mean values of the material constants (c_1=2.9E-02 MPa and c_2=1.3E-02 MPa)

obtained in this work were different from the ones applied by (Lee et al., 2005) c_1=2.5E-03 MPa and c_1=6.25E-04 MPa, and (Noakes et al., 2008) c_1=4.5E-03.MPa and c_1=2.0E-03 MPa, but this difference of magnitude can be associated with the subject-specific thickness and morphology of the PVM. Nevertheless, to validate this methodology we compared the antero-posterior displacement of the MRI *vs.* the displacements obtained in the numerical simulations, and the values were concordant (Table 2). One of the main findings of this work is the fact that the GA was capable of achieving similar displacement to the one of the dynamic MRI with fewer simulations.

The difference of the numerical results and material constants can be associated with the particular characteristics of each algorithm. The GA is a search technique particularly suited for the search spaces with an irregular structure (McCall, 2005; Meier et al., 2007), while the Powell's algorithm does not calculate the gradient, rather searches in conjugate directions (Gao et al., 2013). An advantage of utilizing a GA is its insistence on finding a global minimum.

The inverse FEA with the GA or Powell's algorithm lends itself easily to future adaptations; it is versatile to estimate a broad range of material properties, not only those characterising the passive behaviour of the PVM to assess muscle's viscoelastic properties. In a near future, we intend to use this technique to reproduce an active behaviour, using a quasi-incompressible transversely isotropic hyperelastic model (Martins et al., 1998). The use of a hyperelastic model implies greater computational time due to a larger number of constants.

In conclusion, the focus of this paper was the implementation of the GA to complement the inverse FEA with the aim of determining *in vivo* subject-specific properties of the PVM. The presented results confirm that the GA - due to it robustness -

has potential to estimate accurately the material constants of the Mooney-Rivlin constitutive model, performing fewer simulations than the Powell's algorithm.

Conflict of interest statement

The authors declare that there is no financial, professional or other personal interest of any nature or kind in any product, service and/or company that could be constructed as influencing the position.

Acknowledgments

The authors gratefully acknowledge the funding by Ministério da Ciência Tecnologia, e Ensino Superior, FCT, Portugal, under grants SFRH/BD/89519/2012 and IF/00159/2014, and the project UID/EMS/50022/2013. The fifth author acknowledge the funding of Project NORTE-01-0145-FEDER-000022 - SciTech - Science and Technology for Competitive and Sustainable Industries, cofinanced by Programa Operacional Regional do Norte (NORTE2020), through Fundo Europeu de Desenvolvimento Regional (FEDER).

References

Brandão, F.S., Parente, M.P., Rocha, P.A., Saraiva, M.T., Ramos, I.M., Natal Jorge, R.M., 2015.

Modeling the contraction of the pelvic floor muscles. Comput Methods Biomech Biomed Engin. 8, 1–10.

Brandão, S., Parente, M., Mascarenhas, T., da Silva, A.R.G., Ramos, I., Jorge, R.N., 2015. Biomechanical study on the bladder neck and urethral positions: Simulation of impairment of the pelvic ligaments. J. Biomech. 48, 217–223.

Chen, L., Ashton-Miller, J.A., DeLancey, J.O.L., 2009. A 3D finite element model of anterior vaginal wall support to evaluate mechanisms underlying cystocele formation. J. Biomech. 42, 1371–1377.

Gao, W., Liu, S., Huang, L., 2013. A novel artificial bee colony algorithm with Powell's method. Appl. Soft Comput. 13, 3763–3775.

Garra, B.S., 2015. Elastography: history, principles, and technique comparison. Abdom. Imaging 40, 680–697.

Gennisson, J., Deffieux, T., Macé, E., Montaldo, G., Fink, M., Tanter, M., 2010. Viscoelastic and anisotropic mechanical properties of in vivo muscle tissue assessed by supersonic shear imaging. Ultrasound Med Biol 35, 789–801.

Glaser, K.J., Manduca, A., Ehman, R.L., 2012. Review of MR elastography applications and recent developments. J. Magn. Reson. Imaging 36, 757–774.

Herschorn, S., 2004. Female pelvic floor anatomy: the pelvic floor, supporting structures, and pelvic organs. Rev. Urol. 6 Suppl 5, S2–S10.

Jean-Charles, C., Rubod, C., Brieu, M., Boukerrou, M., Fasel, J., Cosson, M., Clay, J.-C., Rubod, C., Brieu, M., Boukerrou, M., Fasel, J., Cosson, M., 2010. Biomechanical properties of prolapsed or non-prolapsed vaginal tissue: impact on genital prolapse surgery. Int. Urogynecol. J. 21, 1535–1538.

Kauer, M., Vuskovic, V., Dual, J., Szekely, G., Bajka, M., 2002. Inverse finite element characterization of soft tissues. Med. Image Anal. 6, 275–87.

Khalil, A.S., Bouma, B.E., Kaazempur Mofrad, M.R., 2006. A combined FEM/genetic algorithm for vascular soft tissue elasticity estimation. Cardiovasc. Eng. 6, 93–102.

Lee, S., Darzi, A., Yang, G., 2005. Subject Specific Finite Element Modelling of the Levator Ani. Med. Image Comput. Comput. Interv. 3749, 360–367.

Lei, L., Song, Y., Chen, R., 2007. Biomechanical properties of prolapsed vaginal tissue in pre-

and postmenopausal women. Int. Urogynecol. J. Pelvic Floor Dysfunct. 18, 603–607.

Lenjan-Nejadian, S., Rostami, M., 2010. Genetic Algorithm Optimization Applied to a Biomechanical Model of Snatch Lift. Int. J. Comput. Sci. Sport 9, 45–60.

Mariappan, Y.K., Glaser, K.J., Ehman, R.L., 2010. Magnetic resonance elastography: A review. Clin. Anat. 23, 497–511.

Martins, J.A.C., Pires, E.B., Salvado, R., Dinis, P.B., 1998. A numerical model of passive and active behavior of skeletal muscles. Comput. Methods Appl. Mech. Eng. 151, 419–433.

Martins, P., Jorge, R.N., Ferreira, A., 2006. A Comparative Study of Several Material Models for Prediction of Hyperelastic Properties: Application to Silicone-Rubber and Soft Tissues. Strain 42, 135–147.

McCall, J., 2005. Genetic algorithms for modelling and optimisation. J. Comput. Appl. Math. 184, 205–222.

Meier, C., Yassine, A. a., Browning, T.R., 2007. Design Process Sequencing With Competent Genetic Algorithms. J. Mech. Des. 129, 566.

Noakes, K.F., Pullan, A.J., Bissett, I.P., Cheng, L.K., 2008. Subject specific finite elasticity simulations of the pelvic floor. J. Biomech. 41, 3060–3065.

Oudry, J., Chen, J., Glaser, K., Miette, V., Sandrin, L., Ehman, R., 2009. Cross-validation of magnetic resonance elastography and ultrasound-based transient elastography: a preliminary phantom study. J Magn Reson Imaging 30, 1145–50.

Parente, M., Natal Jorge, R., Mascarenhas, T., Fernandes, A., Martins, J., 2008. Deformation of the pelvic floor muscles during a vaginal delivery. Int. Urogynecol. J. Pelvic Floor Dysfunct. 19, 65–71.

Parente, M.P., Natal Jorge, R.M., Mascarenhas, T., Fernandes, A. a., Silva-Filho, A.L., 2010. Computational modeling approach to study the effects of fetal head flexion during vaginal delivery. Am. J. Obstet. Gynecol. 203, 217.e1-217.e6.

Parente, M.P.L., Jorge, R.M.N., Mascarenhas, T., Fernandes, A.A., Martins, J.A.C., 2009. The influence of an occipito-posterior malposition on the biomechanical behavior of the pelvic floor. Eur. J. Obstet. Gynecol. Reprod. Biol. 144, S166–S169.

Powell, M.J.D., 1977. Restart procedures for the conjugate gradient method. Math. Program. 12, 241–254.

Raizada, V., Mittal, R.K., 2008. Pelvic Floor Anatomy and Applied Physiology. Gastroenterol Clin North Am 37, 493–497.

Roza, T. Da, Brandão, S., Oliveira, D., Mascarenhas, T., Parente, M., Duarte, J.A., Jorge, R.N., 2015. Football practice and urinary incontinence: Relation between morphology, function and biomechanics. J. Biomech. 48, 1587–1592.

Rubod, C., Boukerrou, M., Brieu, M., Jean-Charles, C., Dubois, P., Cosson, M., 2008. Biomechanical properties of vaginal tissue: Preliminary results. Int. Urogynecol. J. Pelvic Floor Dysfunct. 19, 811–816.

Rubod, C., Brieu, M., Cosson, M., Rivaux, G., Clay, J.C., De Landsheere, L., Gabriel, B., 2012. Biomechanical properties of human pelvic organs. Urology 79, 968.e17-968.e22.

Silva, M., Brandao, S., Parente, M., Mascarenhas, T., Natal Jorge, R., 2016. Establishing the biomechanical properties of the pelvic soft tissues through an inverse finite element analysis using magnetic resonance imaging. Proc. Inst. Mech. Eng. Part H J. Eng. Med. 230, 298–309.

Silva, M.E.T., Oliveira, D. a., Roza, T.H., Brandão, S., Parente, M.P.L., Mascarenhas, T., Natal Jorge, R.M., 2015. Study on the influence of the fetus head molding on the biomechanical behavior of the pelvic floor muscles, during vaginal delivery. J. Biomech. 48, 1600–1605.

Tumbarello, J.A., Hsu, Y., Lewicky-Gaupp, C., Rohrer, S., DeLancey, J.O.L., 2010. Do repetitive Valsalva maneuvers change maximum prolapse on dynamic MRI? Int. Urogynecol. J. Pelvic Floor Dysfunct. 21, 1247–1251.

Wells, P.N., Liang, H.D., 2011. Medical ultrasound: imaging of soft tissue strain and elasticity. J R Soc Interface 7;8, 1521–49.

APPENDIX

Autorização de compilação

Fernanda Sofia Quintela da Silva Brandão, Marco Paulo Lages Parente, Maria Teresa da Quinta e Costa de Mascarenhas Saraiva e Renato Manuel Natal Jorge na qualidade de co-autores do artigo "Establishing the Biomechanical Properties of the Pelvic Soft Tissues through an inverse Finite Element Analysis using Magnetic Resonance Imaging" publicado na revista *Proceedings of the Institution of Mechanical Engineers, Part H: Journal of Engineering in Medicine*, declaram que autorizam a inclusão do mesmo na dissertação de doutoramento da candidata Maria Elisabete Teixeira da Silva, intitulada "Evaluating the mechanical properties of biological soft tissues using inverse methods: application to the pelvic floor muscles".

Porto e FEUP, 20 de Novembro 2017,

.....	.....
(Fernanda Sofia Quintela da Silva Brandão)	*(Maria Teresa da Quinta e Costa de Mascarenhas Saraiva)*
.....	.....
(Marco Paulo Lages Parente)	*(Renato Manuel Natal Jorge)*

Autorização de compilação

Fernanda Sofia Quintela da Silva Brandão, Marco Paulo Lages Parente, Maria Teresa da Quinta e Costa de Mascarenhas Saraiva e Renato Manuel Natal Jorge na qualidade de co-autores do artigo "Biomechanical properties of the pelvic floor muscles of continent and incontinent women using an inverse finite element analysis" publicado na revista *Computer Methods in Biomechanics and biomedical Engineering Journal*, declaram que autorizam a inclusão do mesmo na dissertação de doutoramento da candidata Maria Elisabete Teixeira da Silva, intitulada "Evaluating the mechanical properties of biological soft tissues using inverse methods: application to the pelvic floor muscles".

Porto e FEUP, 20 de Novembro2017,

(Fernanda Sofia Quintela da Silva Brandão)

(Maria Teresa da Quinta e Costa de Mascarenhas Saraiva)

(Marco Paulo Lages Parente)

(Renato Manuel Natal Jorge)

Autorização de compilação

Fernanda Sofia Quintela da Silva Brandão, Marco Paulo Lages Parente, Maria Teresa da Quinta e Costa de Mascarenhas Saraiva e Renato Manuel Natal Jorge na qualidade de co-autores do artigo "The influence of pelvic organ prolapse on the passive biomechanical properties of pelvic floor muscles" publicado na revista *Journal of Mechanics in Medicine and Biology*, declaram que autorizam a inclusão do mesmo na dissertação de doutoramento da candidata Maria Elisabete Teixeira da Silva, intitulada "Evaluating the mechanical properties of biological soft tissues using inverse methods: application to the pelvic floor muscles".

Porto e FEUP, 20 de Novembro 2017,

(Fernanda Sofia Quintela da Silva Brandão)

(Maria Teresa da Quinta e Costa de Mascarenhas Saraiva)

(Marco Paulo Lages Parente)

(Renato Manuel Natal Jorge)

Autorização de compilação

Fernanda Sofia Quintela da Silva Brandão, Marco Paulo Lages Parente, Maria Teresa da Quinta e Costa de Mascarenhas Saraiva e Renato Manuel Natal Jorge na qualidade de co-autores do artigo "Characterization of the Passive and Active Material Parameters of the *Puboviscerali*s Muscle using an Inverse Numerical Method" submetido para publicação na revista *Journal of Biomechanics*, declaram que autorizam a inclusão do mesmo na dissertação de doutoramento da candidata Maria Elisabete Teixeira da Silva, intitulada "Evaluating the mechanical properties of biological soft tissues using inverse methods: application to the pelvic floor muscles".

Porto e FEUP, 20 de Novembro 2017,

(Fernanda Sofia Quintela da Silva Brandão)	*(Maria Teresa da Quinta e Costa de Mascarenhas Saraiva)*
(Marco Paulo Lages Parente)	*(Renato Manuel Natal Jorge)*

Autorização de compilação

Fernanda Sofia Quintela da Silva Brandão, Marco Paulo Lages Parente, Maria Teresa da Quinta e Costa de Mascarenhas Saraiva e Renato Manuel Natal Jorge na qualidade de co-autores do artigo "Characterising the Biomechanical Properties of the *Puboviscerali*s Muscle using a Genetic Algorithm and Finite Element Method" submetido para publicação na revista *Journal of Inverse Problems in Science and Engineering*, declaram que autorizam a inclusão do mesmo na dissertação de doutoramento da candidata Maria Elisabete Teixeira da Silva, intitulada "Evaluating the mechanical properties of biological soft tissues using inverse methods: application to the pelvic floor muscles".

Porto e FEUP, 20 de Novembro 2017,

(Fernanda Sofia Quintela da Silva Brandão)

(Maria Teresa da Quinta e Costa de Mascarenhas Saraiva)

(Marco Paulo Lages Parente)

(Renato Manuel Natal Jorge)